Natural and artificial ligands of cereblon and their therapeutic potential

Dissertation

der Mathematisch-Naturwissenschaftlichen Fakultät
der Eberhard Karls Universität Tübingen
zur Erlangung des Grades eines
Doktors der Naturwissenschaften
(Dr. rer. nat.)

vorgelegt von
Christopher Heim
aus Reutlingen

Tübingen
2020

Gedruckt mit Genehmigung der Mathematisch-Naturwissenschaftlichen Fakultät der Eberhard Karls Universität Tübingen.

Tag der mündlichen Qualifikation:	06. Oktober 2020
Stellvertretender Dekan:	Prof. Dr. József Fortágh
1. Berichterstatter:	Prof. Dr. Andrei N. Lupas
2. Berichterstatter:	Prof. Dr. Karl Forchhammer

Abstract

The infamous teratogenic small molecule thalidomide, previously used as a sedative and to relieve morning sickness during pregnancy, caused many miscarriages and led to the birth of thousands of children with abnormalities. However, owing to their pleiotropic properties, thalidomide and its analogues, called immunomodulatory drugs (IMiDs), are indispensable today in the treatment of various forms of cancer and autoimmune diseases. Generally, IMiDs are capable of binding to cereblon (CRBN), the substrate receptor of the $CRL4^{CRBN}$ ligase complex. The natural substrates and functions of this ligase complex in absence of IMiDs and its natural substrates remain largely elusive. However, binding of IMiDs was found to modulate the substrate recognition interface of CRBN to recruit neo-substrates to the E3 complex, which leads to ubiquitination and proteasomal degradation of the latter. This mode of action dictates part of their efficacy in multiple diseases and has also been linked to their teratogenic effects. E3 binders, which are moieties that are capable of binding to E3 ligases, gained even more attention with the development of a directed proteolysis approach. In so-called PROTACs, an E3 binder and a warhead that binds to a protein of interest (POI) are connected via a flexible linker, which leads to the formation of a ternary complex. Close proximity within this ternary complex consisting of PROTAC, E3 ligase and POI can then lead to the ubiquitination and subsequent degradation of the latter. Current constraints of this approach include the limited availability of E3-recruiting moieties.

To address this limitation, we have developed crystallographic and affinity-based assays for the characterization of CRBN ligands. Constructs of the human CRBN protein and of a single-domain bacterial homologue from *Magnetospirillum gryphiswaldense* were designed and used to establish affinity assays based on Microscale

Thermophoresis, which showed superior sensitivity and are orthogonal to previously established assays. In these assays and in angiogenesis assays, we investigate the importance of CRBN binding on the anti-angiogenic effects of fluorinated and un-fluorinated thalidomide analogues.

We have probed the chemical space of CRBN binding by using a high-throughput screen and specifically designed *de novo* CRBN effectors. The latter was guided by hydrolysis products of thalidomide and analogs, which we used to design more compact CRBN-binders based on amido-succinimide as a scaffold. In affinity assays and X-ray crystal structures, we show that this scaffold allows the attachment of almost arbitrary chemistry, while still retaining high affinity to CRBN. Without further chemical optimization, several of these compounds already showed neosubstrate degradation in cell culture.

In the high-throughput screen, we identified novel, chemically distant binding moieties, showing that the substrate spectrum of CRBN is much bigger than previously thought. Validation in affinity assays and crystal structures showed that some of the newly identified moieties have superior affinities and revealed previously unexplored regions of the ligand space, which can be used to expand the geometrical and chemical space of CRBN binders. These results may guide the design of more effective and selective protein degraders in the future.

Additionally, we characterized the binding of endogenous CRBN substrates in affinity assays and in a high-resolution crystal structure with a substrate-derived peptide. We identified a modification of this peptide, which points at a possible connection between artificial small-molecule CRBN effectors and a degron that might be recognized by CRBN in vivo.

Zusammenfassung

Der für seine teratogene Wirkung berüchtigte Wirkstoff Thalidomid wurde früher als Schlafmittel und zur Behandlung von Schwangerschaftsübelkeit eingesetzt, was zu vielen Fehlgeburten und embryofetalen Fehlbildungen führte. Heute sind Thalidomid und seine Analoga, die auch „immunomodulatory drugs“ (IMiDe) genannt werden, aufgrund vielfältiger Wirkungsweisen jedoch unverzichtbar in der Behandlung verschiedener Krebsarten und Autoimmunerkrankungen. Zumindest einen Teil ihrer Wirkung entfalten sie durch die Bindung an das Protein Cereblon (CRBN), den Substratrezeptor des $CRL4^{CRBN}$ E3 Ubiquitin-Ligase-Komplexes. Die natürlichen Substrate und Funktionen dieses Ligase Komplexes in Abwesenheit der IMiDe sind weitgehend unbekannt. Es wurde jedoch gezeigt, dass die Binding von IMiDen die Substraterkennung so moduliert, dass sogenannte „Neo-Substrate“ an die E3-Ligase rekrutiert werden. Neo-Substrate werden dann ubiquitiniert und anschließend durch das Proteasom abgebaut. Dies erklärt zumindest teilweise die Wirksamkeit dieser Moleküle bei verschiedenen Erkrankungen und wurde auch in Verbindung mit ihren teratogenen Eigenschaften gebracht.

IMiDe und andere Liganden für E3-Ligasen (E3-Binder) erhielten in den letzten Jahren besondere Aufmerksamkeit mit der Entwicklung eines zielgerichteten Ansatzes zum Abbau von Proteinen: Der Ansatz beruht auf sogenannten „PROTAC“ Molekülen, welche auf einer Seite über einen E3-Binder eine E3-Ligase, und auf der anderen Seite über einen Liganden oder Inhibitor an ein abzubauendes Zielprotein binden. In dem herbeigeführten Komplex aus E3-Ligase, PROTAC und Zielprotein wird letzteres aufgrund der räumlichen Nähe durch die E3-Ligase ubiquitiniert und anschließend durch das Proteasom abgebaut. Eingeschränkt wird dieser Ansatz aktuell vor allem durch die geringe Anzahl an verfügbaren E3-Bindern.

Um diesen Mangel zu lindern haben wir kristallographische und affinitätsbasierte Assays für die Charakterisierung von E3-Bindern entwickelt. Hierzu wurden Konstrukte des humanen CRBN und eines homologen bakteriellen Proteins aus *Magnetospirillum gryphiswaldense* entworfen und für die Entwicklung von auf Microscale Thermophoresis (MST) basierenden Assays verwendet. Diese sind orthogonal zu bereits bestehenden Assays und überzeugen teils durch hervorragende Sensitivität. In diesen und in Angiogenese-Assays haben wir untersucht, wie bedeutsam die Bindung an CRBN für fluorierte und un fluorierte Thalidomidanaloga für deren antiangiogenetischen Eigenschaften ist.
Zudem haben wir den chemischen Raum der CRBN-Bindung in einem Hochdurchsatz-Screen untersucht und zielgerichtet neue CRBN-Effektoren entworfen. Bei Letzterem haben wir uns von Hydrolyseprodukten von Thalidomid und dessen Analoga inspirieren lassen, was uns zu deutlich kompakteren CRBN-Bindern basierend auf Amido-Succinimid führte. In Affinitätsassays und Kristallstrukturen zeigen wir, dass diese Binder mit fast willkürlichen chemischen Gruppen verknüpft werden können, ohne wesentlich an Affinität zu CRBN zu verlieren. Ohne weitere chemische Optimierungen zeigten einige dieser Verbindungen bereits einen Abbau von Neo-Substraten in Zellkultur.
Darüber hinaus identifizierten wir im Hochdurchsatz-Screen neue und chemisch nicht mit Thalidomid verwandte Motive, was darauf hinweist, dass das Substratspektrum von CRBN deutlich größer ist als bisher gedacht. Die Validierung in Affinitätsassays und Kristallstrukturen zeigte bei einigen Motiven herausragende Affinitäten und unerwartete Bindemodi, was dazu genutzt werden kann, den geometrischen und chemischen Raum für CRBN-Binder zu erweitern. All diese Ergebnisse können dazu beitragen, zukünftig effektivere und selektivere Verbindungen für den Abbau von krankheitsrelevanten Proteinen zu entwickeln.
Schließlich charakterisierten wir die Bindung eines endogenen Substrates mittels Affinitätsassays und in einer Kristallstruktur in Komplex mit einem Peptid, das einem Teil des endogenen Substrates entsprach. Dieses Peptid wies eine Modifikation auf, die auf einen möglichen Zusammenhang zwischen künstlichen CRBN-Effektoren und natürlichen Erkennungsmotiven, die *in vivo* erkannt werden, hindeutet.

Contents

Abstract i

Zusammenfassung iii

List of Figures viii

List of Tables x

1 Introduction 1
- 1.1 Small Molecule Drugs . . . 1
- 1.2 Thalidomide and IMiDs . . . 3
  - 1.2.1 History . . . 3
  - 1.2.2 The renaissance of thalidomide and its primary target . . . 3
- 1.3 The ubiquitin-proteasome pathway . . . 5
  - 1.3.1 E3 ligases . . . 6
- 1.4 Cereblon . . . 7
  - 1.4.1 Structure of human cereblon . . . 7
  - 1.4.2 *Magnetospirillum gryphiswaldense* cereblon isoform 4 . . . 8
- 1.5 Molecular glues, neo-substrates and proteolysis targeting chimeras (PROTACs) . . . 9
  - 1.5.1 Molecular glues . . . 9
  - 1.5.2 Neo-substrates . . . 10
  - 1.5.3 PROTACs . . . 11
- 1.6 Endogenous substrates of $CRL4^{CRBN}$ . . . 12
  - 1.6.1 5′ AMP-activated protein kinase . . . 13
  - 1.6.2 Myeloid Ecotropic Insertion Site 2 . . . 13
  - 1.6.3 Glutamine Synthetase . . . 13
  - 1.6.4 Amyloid Precursor Protein . . . 14
- 1.7 Cereblon-mediated teratogenicity . . . 14
- 1.8 Aim of this thesis . . . 16

2 Materials and Methods 17
- 2.1 Materials . . . 17
  - 2.1.1 Chemicals . . . 17
  - 2.1.2 Enzymes . . . 18
  - 2.1.3 Cell culture . . . 19

2.1.4 Antibodies . . . 20
2.1.5 Bacteria . . . 20
2.2 Methods . . . 21
2.2.1 Cloning, expression, purification of cereblon (CRBN) constructs and mutants . . . 21
2.2.1.1 MSCI4 and mutants . . . 21
2.2.1.2 hthalidomide binding domain (TBD) . . . 22
2.2.1.3 DNA damage binding protein 1 (DDB1)-CRBN . . . 22
2.2.2 NanoDSF . . . 23
2.2.3 FRET assay . . . 23
2.2.4 MST assays . . . 24
2.2.4.1 Labeled MST assay . . . 25
2.2.4.2 Competitive MST assay . . . 25
2.2.5 Crystallography . . . 26
2.2.6 Cell culture . . . 27
2.2.6.1 Mammalian cell culture . . . 28
2.2.6.2 Insect cell culture . . . 28
2.2.7 Endothelial cell tube formation assay . . . 29
2.2.8 Rat aortic ring angiogenesis assay . . . 29
2.2.9 Western Blotting . . . 30

3 Design and characterization of bacterial and human CRBN constructs 31
3.1 Introduction . . . 31
3.2 Mutations of *Magnetospirillum gryphiswaldense* cereblon isoform 4 (MsCI4) . . . 33
3.2.1 Truncation of MsCI4 . . . 34
3.2.2 Humanization of MsCI4 . . . 35
3.2.3 Stability of MsCI4 and mutants . . . 37
3.3 Structural characterization of novel immunomodulatory drugs . . . 40
3.4 hCRBN . . . 43
3.5 Conclusions . . . 45

4 *De-novo* design of cereblon (CRBN) effectors guided by natural hydrolysis products of thalidomide derivatives 47
4.1 Introduction . . . 47
4.2 Biophysical and structural characterization of immunomodulatory drug (IMiD) analogs and their hydrolysis products . . . 50
4.3 Binding mode of CBG, a major hydrolysis product of thalidomide 54
4.4 Rational design of novel succinimide effectors guided by hydrolyzed metabolites . . . 57
4.5 Displacement of endogenous substrates . . . 65
4.6 Degradation of neo-substrates . . . 68
4.7 Conclusions . . . 70

5 On the anti-angiogenic properties of thalidomide and its analogs 72

5.1 Introduction . . . 72
5.2 Design of compounds . . . 74
5.3 Development of an MST based assay . . . 74
5.4 Characterization of Gu compounds . . . 77
5.5 Conclusions . . . 82

6 Novel binding motifs for cereblon and assays for their characterization 85
6.1 Introduction . . . 85
6.2 Affinities and structural characterization of high throughput screening (HTS) hits . . . 86
6.3 Development of a competitive MST assay for CRBN variants . . . 94
6.3.1 Establishment of the competitive MST assay based on MsCI4 94
6.4 Establishing the competitive MST assay based on human CRBN . . 97
6.5 Affinities of HTS hits to hCRBN . . . 99
6.6 Conclusions . . . 101

7 Investigation of possible endogenous substrates and recognition motifs 103
7.1 Introduction . . . 103
7.2 Structure and functions of amyloid precursor protein . . . 105
7.3 Affinities and structural characterization of truncated amyloid precursor protein (APP) peptides . . . 107
7.4 A degron for CRBN-recognition? . . . 110
7.5 Conclusions . . . 114

8 Concluding Remarks 116

9 Contributions 119

Acknowledgments 121

Bibliography 122

List of Figures

1 Boundaries for physicochemical properties of small molecule drugs (SMDs) . . . 2
2 Chemical structures of classical IMiDs . . . 4
3 Overview of the ubiqutin-proteasome pathway (UPP) . . . 5
4 Domain architecture and structure of human CRBN . . . 8
5 Degradation of endogenous substrates and IMiD-mediated remodulation of CRBN . . . 10
6 PROTAC scheme . . . 11
7 Structure of MANT-Uracil . . . 24
8 Chemical structure of uracil BODIPY 493/503 reporter (BU) . . . 26
9 Sequence alignment of MsCI4 and TBD . . . 33
10 Sequence alignment of MsCI4 constructs . . . 34
11 Structural superposition of MsCI4 and hCRBN in complex with casein kinase 1a (CK1α) and zinc-finger transcription factor Ikaros (IKZF1) ZF2 . . . 36
12 Melting curves of MsCI4 . . . 39
13 Interactions of CC-122 and CC-220 with MsCI4 . . . 42
14 Melting temperatures of DDB1-CRBN . . . 44
15 Reagents and conditions for the synthesis of 1a-5b . . . 50
16 five- and six-ring based thalidomide analogs . . . 52
17 Overview of the thalidomide binding mode and electron densities of thalidomide analogs and their hydrolysis products bound to MsCI4. . . . 54
18 The binding mode of the initial compounds and their hydrolysis products inside the binding pocket . . . 56
19 Reagents and conditions for the synthesis of 6a-7h . . . 57
20 Compounds inspired by hydrolysis products of thalidomide analogs and their affinity data . . . 58
21 Binding modes of compounds from the second and third panel. . . . 59
22 Reagents and conditions for the synthesis of 10a-20b . . . 60
23 $F_O - F_C$ maps of bound compounds shown in Figure 21 . . . 62
24 Densiometric analysis of endogenous Myeloid Ecotropic Insertion Site 2 (MEIS2) levels . . . 66
25 Relative MEIS2 levels upon compound treatment . . . 67
26 Compound-mediated IKFZ3 degradation in vitro. . . . 69

27 MST dose-response curves for water-soluble compounds and reference compounds 75
28 MST binding curves for thalidomide analogues 78
29 Results for endothelial cell tube formation assay 79
30 Results for rat aortic ring assay 81
31 Previously established pharmacophore-based nomenclature for CRBN-binding 86
32 Chemical structures of HTS hits 87
33 Labeled MST experiments of identified compounds in the HTS . . 88
34 $F_O - F_C$ omit maps of HTS hits 91
35 Binding mode of HTS hits 92
36 Fluorescence and Microscale Thermophoresis (MST) data of competitive MsCI4 assay 96
37 Binding curves for competitive MST assays with hTBD 98
38 Binding curves of HTS hits with hTBD 101
39 Domain organization and overall structure of APP protein 106
40 MST binding curves of N-terminally truncated APP COOH-terminal petides 108
41 Crystal structure of MsCI4 in complex with tetra peptide (QMQN) containing a C-terminally cyclized Asn 109
42 Schematic mechanisms leading to C-terminal succinimide motifs . 112
43 Initial glutamine synthetase (GS) pull-down 113

List of Tables

1 Chemicals . . . 17
2 Enzymes . . . 18
3 Cell culture media . . . 19
4 Cell lines . . . 19
5 Antibodies . . . 20
6 Bacteria . . . 20
7 T_m of MsCI4 constructs . . . 38
8 Data collection and refinement statistics of novel IMiDs . . . 43
9 Melting temperatures for human CRBN-constructs measured by nano differential scanning fluorimetry (NanoDSF) (n=3) . . . 45
10 Data Collection and Refinement Statistics of crystal structures with novel succinimide effectors and thalidomide hydrolysis product . 63
11 Binding affinities of reference compounds measured by labeled MST 76
14 Markush structures of thalidomide analogues, their affinities to MsCI4 and anti-angiogenic potential . . . 82
15 Affinities determined by labeled MST assay for BS1-5 and glucocorticoids and their respective K_i^* values . . . 89
16 Data collection and refinement statistics of crystal structures of MsCI4 and HTS hits . . . 93
17 Competitive MST assay results for MsCI4 . . . 95
18 Affinities of commercially available IMiDs and minimal binders to hTBD . . . 99
20 Affinities determined by competitive MST assay for BS1-5 and glucocorticoids and their respective K_i values to hTBD. . . . 101
21 Sequences of peptides resembling the C-terminus of APP . . . 107
22 Data collection and refinement statistics for MsCI4 · $QMQN_{cyc}$ . . 110
23 Sequence comparison of endogenous CRBN substrates . . . 113

Acronyms and Abbreviations

ADME absorption, distribution, metabolism, and elimination.

AICD amyloid precursor protein intracellular domain.

ALPL2 amyloid-precursor like protein 2.

AMPK 5′ AMP-activated protein kinase.

APP amyloid precursor protein.

ASU asymmetric unit.

BK(Ca) large-conductance Ca^{2+}-activated K^{+}.

bRo5 beyond rule-of-five.

CK1α casein kinase 1a.

COX Cyclooxygenase.

CRBN cereblon.

CRL4$^{\mathbf{CRBN}}$ CUL4–RBX1–DDB1–CRBN E3 ubiquitin ligase.

CULT Cereblon domain of Unknown activity, binding cellular Ligands and Thalidomide.

CYP Cytochrome P450.

DCAF DDB1-CUL4 Associated Factor.

DDB1 DNA damage binding protein 1.

DMPK drug metabolism and pharmacokinetics.

DUB deubiquitinating enzyme.

ENL erythema nodosum leprosum.

FDA U. S. Food and Drug Administration.

FRET förster resonance energy transfer.

GS glutamine synthetase.

HECT homologous to the E6AP carboxyl terminus.

HPLC-MS high-performance liquid chromatography coupled to mass spectrometry.

HTS high throughput screening.

IKZF1 zinc-finger transcription factor Ikaros.

IKZF3 zinc-finger transcription factor Aiolos.

IMiD immunomodulatory drug.

MDS myelodysplastic syndrome.

MEIS2 Myeloid Ecotropic Insertion Site 2.

MM multiple myeloma.

MOA mechanism of action.

MsCI4 *Magnetospirillum gryphiswaldense* cereblon isoform 4.

MST Microscale Thermophoresis.

NanoDSF nano differential scanning fluorimetry.

NME new molecular entity.

NSAID non-steroidal anti-inflammatory drug.

POI protein of interest.

PROTAC proteolysis targeting chimera.

PTM post-translational modification.

RBR RING-between-RING.

RING really interesting new gene.

Ro5 Rule-of-five.

RP regulatory particle.

SALL4 spalt-like transcription factor 4.

SMD small molecule drug.

SPPS solid-phase peptide synthesis.

TBD thalidomide binding domain.

TRIC temperature related intensity change.

UPP ubiqutin-proteasome pathway.

VEGF vascular endothelial growth factor.

VHL von Hippel-Lindau E3 ligase.

Chapter 1

Introduction

1.1 Small Molecule Drugs

A fundamental class of agents in pharmaceutical research are small molecule drugs (SMDs). SMDs are organic compounds with typically less than 900 Da molecular weight. This stands in contrast to large molecule drugs like nanobodies or antibodies with molecular weights of typically 15 kDa and 150 kDa (IgG), respectively. In addition to the low molecular weight, which facilitates their diffusion across membranes [184] and usually allows for oral administration, several other key properties have been identified which help in making a compound "drug-like". Several rules have been established that aim to predict the drug-likeness of a compound, based on a few physicochemical features. For SMDs, the Lipinski´s Rule of Five [105] has been considered the standard. This rule describes that relatively small and moderately lipophilic molecules, which have no more than 5 H-bond donors, 10 H-bond acceptors, a mass of less than 500 Da, and an octanol-water partition coefficient (log P) of less than 5, are likely to be orally active in humans. However, assessing small molecules that have been developed in recent years shows that the drug-likeliness extends further, referred to as beyond rule-of-five (bRo5). The average physicochemical properties of a set of such bRo5 compounds is shown in Figure 1. Compounds from the preclinical

drug metabolism and pharmacokinetics (DMPK) database of AbbVie [32] show higher values than previously suggested for orally active agents.

Prior to 1980, SMDs were mostly selected by in vitro potency and in vivo efficacy in animal studies. Since then, efforts have been made in understanding and building of models for the absorption, distribution, metabolism, and elimination (ADME) of small molecules. Especially the development of xenobiotic-inducible transcription of Cytochrome P450 (CYP) genes [34] has led to a paradigm shift. About 75% of drug metabolism occurs through CYPs, which leads to bioactivation or deactivation and excretion of the drug [57, 140]. Since CYPs play such a pivotal role in drug metabolism, they are increasingly important even in early drug development. Effects of new molecular entitys (NMEs) on CYP could be studied using high-performance liquid chromatography coupled to mass spectrometry (HPLC-MS), leading to a better understanding of DMPK. Until today, DMPK and ADME build the foundation of small molecule drug discovery [82, 104]. The importance of SMD development is highlighted by the fact that of 48 FDA-approved NMEs in 2019 [47], 70% were SMDs.

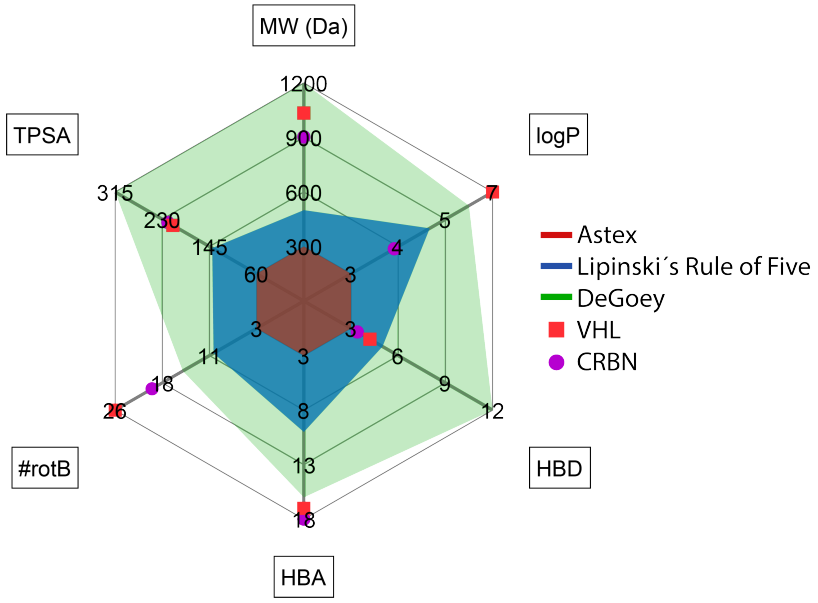

FIGURE 1: Established boundaries for physicochemical properties of SMDs. Boundaries of the rule of 3 established by Astex and the Lipinski´s Rule of Five limits are plotted, as well as average values for a preclinical DMPK dataset from AbbVie (DeGoey [32]). Average values calculated for previously reported PROTACs using von Hippel-Lindau E3 ligase (VHL) and CRBN [41] are highlighted.

1.2 Thalidomide and IMiDs

1.2.1 History

Immunomodulatory drugs (IMiDs) are a class of SMDs termed after their structural basis, which is an imid group, as well as abbreviation for immunomodulatory drugs. The latter term is coined by their pleiotropic effects including immunomodulatory, anti-inflammatory, anti-proliferative and anti-angiogenic. The class of IMiDs started with the development of thalidomide. The company "Chemie Grünenthal GmbH" sought after novel and cheaply synthesizable sedatives and soon patented the SMD thalidomide [α-(N-phthalimido)glutarimide]. Treatment with thalidomide showed strong sedative and hypnotic effects on mice and humans. Dosing experiments performed on several animal species had no considerable side effects and the drug was therefore determined to be safe [83, 180], even as an over-the-counter drug [118]. Thalidomide was marketed starting 1957 under the brand names Contergan and Softenon. Appreciated by its ability to relieve morning sickness, thalidomide was also recommended to pregnant woman. It was this widespread use of thalidomide during pregnancy that led to the birth of $\sim$ 15.000 children [197] with malformations of limbs, inner organs, inner and outer ears [119], and other abnormalities. These defects depended largely on the time of thalidomide intake [179], while it also caused unknown numbers of miscarriages. Animal trials at the time were not performed on pregnant animals and teratogenic effects of thalidomide were missed. After linking thalidomide to these severe birth defects, it was retracted from the market in 1961 [197].

1.2.2 The renaissance of thalidomide and its primary target

Although being retracted from the market and banned in several countries, researchers and physicians continued to work with thalidomide. It was in 1965 when an Israeli physician serendipitously discovered that thalidomide quickly relieves patients of the immune-mediated erythema nodosum leprosum (ENL)

[172], a complication of leprosy. It also showed efficacy in multiple myeloma (MM) [66, 78, 87, 88, 96, 98, 176, 198]. Over the years, the analogs lenalidomide (CC-5013) [8, 10, 39, 149, 188], pomalidomide (CC-4047) [71, 213], iberdomide (CC-220) [4, 18, 162] and avadomide (CC-122) [24, 151] (Figure 2) have been developed and approved for the treatment of various diseases and clinical trials. They are patented by Cellgene, which is why some effectors are still being referred to by their code names starting with "CC". Apart from apremilast, all current IMiDs are based on glutarimide and typically a phtaloyl-based second moiety (2).
Thalidomide and its analogs have gained approval by the U. S. Food and Drug Administration (FDA) and other agencies undeterred by the lack of understanding for their mechanism of action (MOA). The molecular targets and MOA of IMiDs remained completely unclear until 2010 when Ito et al. [72] were able to pull down two proteins out of HeLa cell extract by tethering thalidomide to ferrite-glycidyl methacrylate beads. The two proteins identified by mass spectrometry were DDB1 and CRBN. DDB1 and CRBN are part of an E3 ligase complex. Within this CUL4–RBX1–DDB1–CRBN E3 ubiquitin ligase ($CRL4^{CRBN}$) ligase complex consisting of CRBN, Roc1, Cul4a and DDB1, CRBN serves as the substrate receptor. Molecular functions of E3 ligases and their potential for therapeutic drug development are discussed in the next sections.

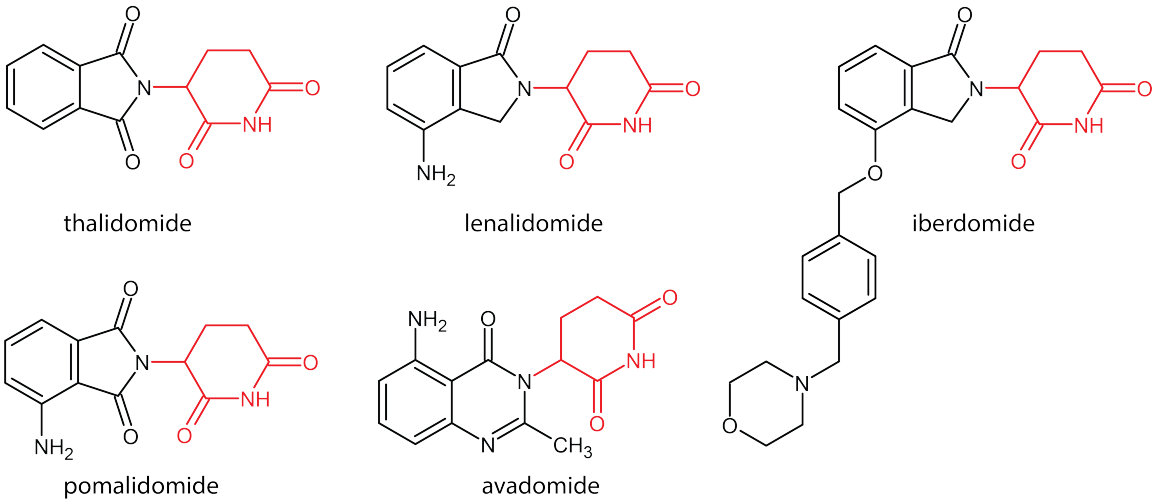

FIGURE 2: Chemical structures of thalidomide, lenalidomide, pomalidomide, avadomide and iberdomide with their glutarimide moiety shown in red.

1.3 The ubiquitin-proteasome pathway

The ubiqutin-proteasome pathway (UPP) is one of the major pathways for protein catabolism in eukaryotes. Within the mammalian cytosol and nucleus, the UPP affects and regulates almost all cellular processes. The UPP ensures degradation of misfolded and regulatory proteins involved in cell cycle and division [107, 152, 192], immune response, stress response, an apoptosis [36, 106, 112]. The UPP is divided in two distinct events: the conjugation of a substrate with ubiquitin molecules, and the recognition of the ubiquitin signal and subsequent degradation of the tagged protein by the 26S proteasome (Figure 3).

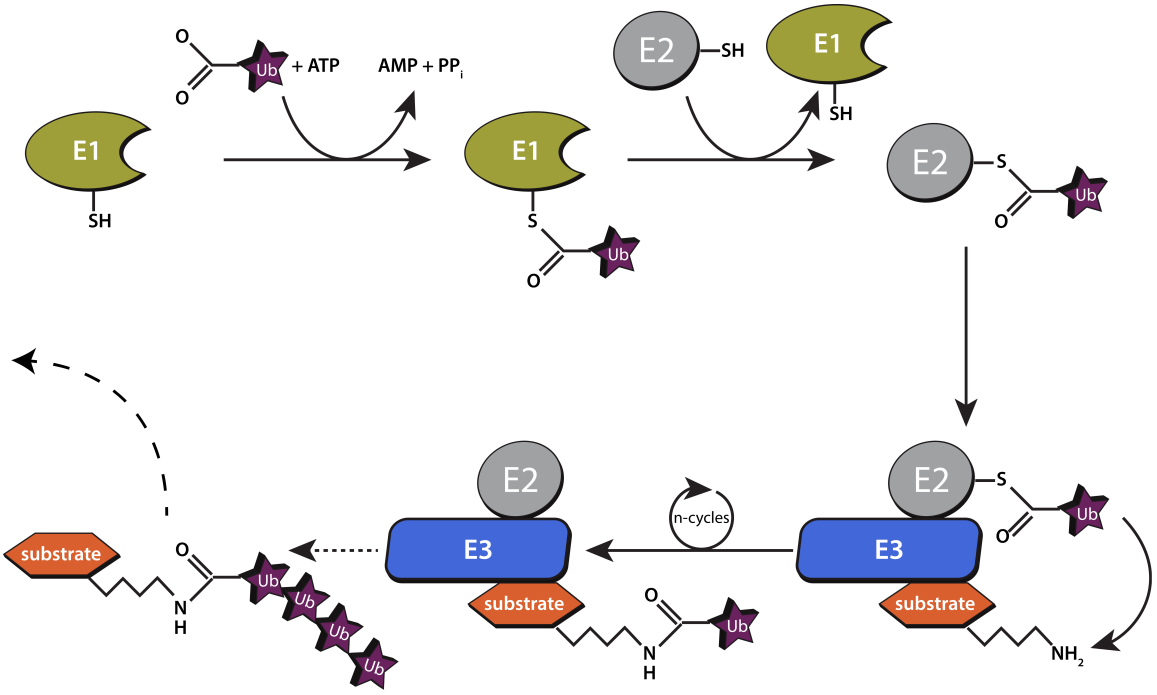

FIGURE 3: Overview of the UPP. After activation and transfer of ubiquitin from an E1 to E2 enzyme, the ubiquitin-carrying E2 joins the E3-ligase complex. Bound substrates are then mono-,di-,or polyubiquitinated and subjected to proteasomal degradation

The conjugation of a substrate occurs via a three-way enzyme cascade. An E1, the ubiquitin activating enzyme activates ubiquitin via its active site cysteine

residue, before transferring it to a cysteine of one of over 35 ubiquitin conjugating enzymes, or E2. Finally, in one of over 600 E3 ligase complexes in human, a ubiquitin-loaded E2 and a substrate protein are brought together and ubiquitin is transferred to a surface lysine of the substrate. Conjugation of additional ubiquitins onto the ε-amine of lysine residues on ubiquitin itself leads to polyubiquitin chains of the substrate. This conjugation can also be reversed by specific deubiquitinating enzymes (DUBs) [31, 74, 106, 120, 139]. Intact polyubiquitin chain linkage, however, directs the conjugated substrate to the 26S proteasome, which is composed of the catalytic 20S proteasome and the 19S regulatory particles (RPs) (Figure 5). Here, the substrate is subjected to proteolysis by the β-subunits of the 20S core particle, which results in typically 2 – 24 residue long degradation products [161].

1.3.1 E3 ligases

E3 ligases are the most heterogeneous class of enzymes in the UPP, as they are responsible for substrate recognition. More than 600 E3s have been identified in humans so far [35, 163]. Besides the smaller classes of homologous to the E6AP carboxyl terminus (HECT) E3s [177, 202, 205] (around 30 in humans) and RING-between-RING (RBR) E3s [38, 183, 193] (around 12 in humans), the family of really interesting new gene (RING) E3s is the most abundant type of ubiquitin ligase [21, 35, 38, 154, 183]. Members of this family are characterized by the presence of a zinc-binding RING domain or by a U-box domain. The RING and U-box domains bind the ubiquitin-charged E2 and stimulate ubiquitin transfer. The spectrum of substrate recognition differs between the E3 ligases and is determined by the substrate recognition subunit. In the subgroup of CUL4-DDB1-based E3 ligases, the substrate recognition is mediated by one of about 60 DDB1-CUL4 Associated Factors (DCAFs) [21, 99]. One such DCAF is the protein cereblon.

1.4 Cereblon

The gene encoding for the human protein CRBN was initially found while studying genes related to memory and learning [67]. Because of its apparent involvement in brain development and the classification as a member of the Lon containing protein family, it was termed "cerebral protein containing a Lon domain" (cereblon). However, it has been shown that the 442 residue long protein is ubiquitously expressed (in over 225 organs) in human [67, 208], and its orthologs are highly conserved in bacteria and eukaryotes [111]. CRBN localizes in the cytoplasm, nucleus, and the peripheral membranes [72].

1.4.1 Structure of human cereblon

Human CRBN consists of an N-terminal LON-like domain and a C-terminal domain. The 236 residue long LON domain, contains an N- and C-terminal subdomain, separated by a helical-bundle domain, which is responsible for DDB1 binding [25, 50, 72] (Figure 4). The C-terminal domain of CRBN is referred to as thalidomide binding domain, or Cereblon domain of Unknown activity, binding cellular Ligands and Thalidomide (CULT). It consists of two four-stranded, anti parallel beta-sheets and contains a structurally bound zinc, coordinated by the cysteins 323, 326, 391 and 394. Moreover, it features a highly conserved aromatic cage (W380, W386, W400, F402), that is responsible for IMiD binding [25, 50, 111]. The conserved glutarimide moiety of IMiDs (Figure 2) is able to bind to this aromatic cage, while the phtaloyl moiety is solvent exposed. Depending on the solvent exposed moiety, that differs between IMiDs, the substrate spectrum of the ligase complex changes [91–93, 116] upon binding of IMiDs. The high sequence conservation of CRBN and especially of the TBD across species was shown in bioinformatical analyses and high resolution structures [2, 111].

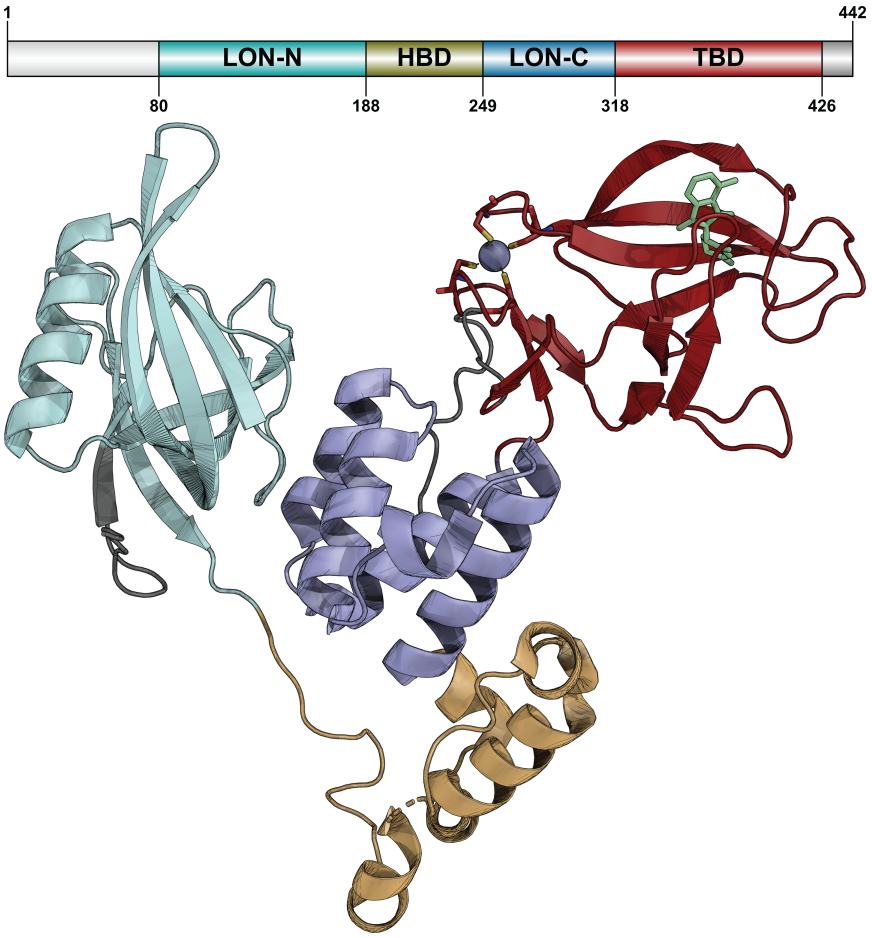

FIGURE 4: Domain architecture and structure of human CRBN (PDB 6H0F). The LON-N, HBD, LON-C and TBD are colored individually. The C-terminal TBD is shown with the bound structural zinc ion and a pomalidomide molecule.

1.4.2 *Magnetospirillum gryphiswaldense* cereblon isoform 4

Amongst TBDs from different eukaryotes, the bacterial Magnetospirillum gryphiswaldense cereblon isoform 4 (MsCI4) from *Magnetospirillum gryphiswaldense* was found to be the most accessible in our lab. It is well expressed in *Escherichia coli* (*E. coli*), soluble and can be purified to satisfactory levels. We used this protein to produce crystals in complex with several small molecules. Co-crystallization with thalidomide was found to be very reproducible, and was used to subsequently soak in compounds to be studied into MsCI4 [20, 62, 63]. Extended soaking in ground solution also showed that the binding pocket partially unfolds upon wash-out of the ligand [62].

We have also prepared mutants of MsCI4. The double mutant MsCI4$^{YW/AA}$ (Y83A, W85A) is deficient in IMiD binding, which is analogous to the respective hCRBN$^{YW/AA}$ (Y384A,W386A) mutant [108]. The protein was also used to construct a mutant MsCI4$^{WW/FF}$, in which all tryptophans outside of the binding pocket were replaced by phenylalanines. These mutations (W-F) lead to a minimized intrinsic fluorescence, which was used in a förster resonance energy transfer (FRET) assay for the determination of binding affinities. Based on the success of these mutations, we will use this protein for several mutated constructs throughout this thesis.

1.5 Molecular glues, neo-substrates and PROTACs

1.5.1 Molecular glues

SMDs like thalidomide, that are capable of binding to E3-ligases and thereby altering their substrate recognition interface, are called molecular glues. They allow for the association of two proteins that have not evolved to interact with each other. In the case of thalidomide and other IMiDs, this can lead to the formation of a ternary complex, bringing non-endogenous substrates, or neo-substrates into close proximity (Figure 5) of the E3 ligase complex. Available lysine residues on the neo-substrate surface can get ubiquitinated, poly-ubiquitinated, and the neo-substrate then gets shuttled to the 26S proteasome, where it gets degraded. While current IMiDs rely on glutarimide as CRBN binding-moiety (Figure 2), we have identified succinimide as a minimal binding moiety in our FRET-assay [19].

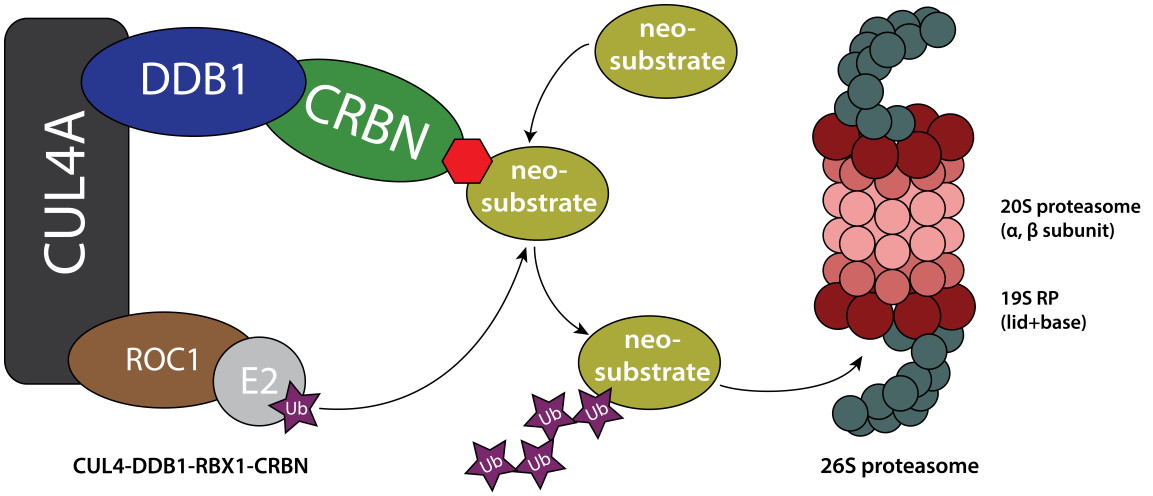

FIGURE 5: Binding of IMiDs (red hexagon) leads to a remodulation of the substrate recognition interface of CRBN, which results in the binding, ubiquitination and proteasomal degradation of neo-substrates. Binding of IMiDs and endogenous substrates are exclusive of each other.

1.5.2 Neo-substrates

The serendipitously discovered phenomenon of molecular glues explains at least parts of the MOAs of IMiDs. Binding of thalidomide provides a binding interface on CRBN for the zinc finger transcription factors IKZF1 and IKZF3 [93, 109]. Binding to $CRL4^{CRBN}$ leads to their ubiquitination and degradation. This possibly triggers multiple responses, including up-regulation of IL-2 expression in T cells, which is detrimental for MM-cell survival. Lenalidomide, the only IMiD effective in treating myelodysplastic syndrome (5q-), was shown to be able to target and degrade the neo-substrate CK1α [91]. In this subtype of myelodysplastic syndrome (MDS), a deletion in the long arm of chromosome 5 results in removal of regions including CSNK1A1 gene which encodes for CK1α, leading to a haploinsufficiency. Structural analysis showed, that only lenalidomide, which lacks a ketophtaloyl group, allows the protruding moiety to move about 2.5 Å towards E377. This movement is necessary to accommodate a β-hairpin of CK1α (residues 35-41) onto the surface of CRBN [143]. Another critical residue is a glycine at the base of the β-hairpin. It contributes to binding interactions and is in close contact with CRBN. Consequently, mutations of glycine to bulkier residues completely

abolished binding.

Such β-hairpin motifs with key glycine residues have subsequently been found to be important structural elements, that are common for several neo-substrates. The modified IMiD CC-885 shows anti-tumor activity that is mediated by recruitment to $CRL4^{CRBN}$ and subsequent degradation of translation termination factor GSPT1. Binding of GSPT1 is facilitated by a similar β-hairpin, and key interactions are largely conserved [116]. Moreover, crystal structures with the zinc fingers ZFP91 and spalt-like transcription factor 4 (SALL4) show the same degron containing a key glycine. Considering that most interactions are only formed by the backbone of the neo-substrate, it seems possible that a wide range of neo-substrates can be recruited, as long as the structural feature is present.

1.5.3 PROTACs

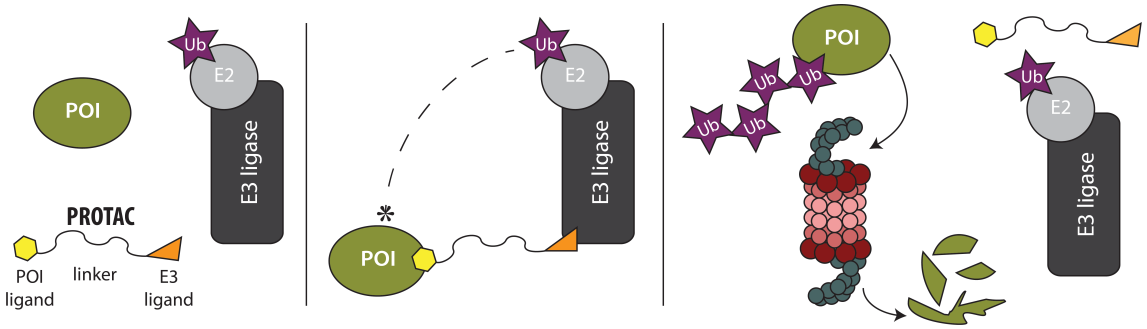

FIGURE 6: PROTAC scheme. Overview of the PROTAC principle Ub, ubiquitin; POI, protein of interest; E3, E3 ubiquitin ligase complex; E2,E2 ubiquitin transfer enzyme

In the 21st century, the strategy of bringing neo-substrates into close proximity to an E3 ligase for their ubiquitination and subsequent degradation was advanced in a more directed manner. This was realized in an approach called proteolysis targeting chimera, where virtually any protein of interest (POI) can be targeted for proteasomal degradation by linking an E3-recruiting moiety and a binder of the POI by a linker (Figure 6). The term PROTAC was coined by Craig Crews and

coworkers who started using peptide ligands coupled to a VHL-recruiting moiety. Since these first proof-of-concept PROTACs were reported in 2001, ligands for a variety of targets have been developed into PROTACs in order to deplete endogenous proteins. From BET bromodomains [145, 173, 206, 211], estrogen [69, 80, 103, 141, 157, 160] and androgen receptor [60, 148, 174], various kinases like CDK9 [16, 155] and even tau proteins [28, 81, 110]. Notably, the functionality and efficiency of a PROTAC not only depends on the choice of the E3 ligase, but also on the linker length and the exit vector of the ligand for the POI [178]. These factors pose an enormous challenge in the development of new PROTACs, as small changes in PROTAC-structure can completely abolish degradation effects. Current efforts are focused on understanding and predicting the affinity of PROTACs, the formation of ternary complexes, ubiquitination of the POI, and the depletion of the POI by proteasomal degradation. The goal is to move away from serendipity by combination of linker, E3-recruiting moiety and ligand for the POI to targeted PROTAC-design. Figure 1 shows the average physicochemical properties of recently published PROTACs that utilize VHL and CRBN [41]. Because of their chimeric origin, PROTACs are large in size and do not adhere to the classical Rule-of-five (Ro5).

1.6 Endogenous substrates of CRL4^{CRBN}

In the absence of IMiDs, CRBN exerts multiple functions in different cells and organs. It has been shown to play a role in the modulation of 5' AMP-activated protein kinase (AMPK), and acetylation-dependent recognition of glutamine synthetase (GS). CRBN was further suggested to interact directly with the cytosolic C-terminus of the alpha-subunit of large-conductance Ca^{2+}-activated K^{+} (BK(Ca)) channels. The transcription factor MEIS2 and amyloid precursor protein (APP) have also been found to be recognized by the human TBD, hTBD. However, the mechanism by which CRBN recognizes these proteins remains largely elusive so far.

1.6.1 5' AMP-activated protein kinase

CRBN plays a role in the regulation of proteins and signal pathways as well as having impact on cell proliferation and apoptosis. CRBN knockdown in MM cells showed decreased cell viability [214], whereas CRBN overexpression promoted cell proliferation [6]. One enzyme that plays essential roles in cell energy homeostasis is AMPK. The AMPK enzyme is a heterotrimeric $\alpha\beta\gamma$-complex [210]. It is expressed in multiple tissues and conserved from yeast to humans. It plays a role in multiple pathways related to fatty acid oxidation, glucose uptake and adipocyte lipolysis [30, 61]. As such, inactivation of AMPK caused by CRBN has been found in different cardiovascular diseases and obesity. In contrast, high AMPK activity can potentially protect cells from disorders of lipometabolism and alcoholic liver damage [86, 185].

1.6.2 Myeloid Ecotropic Insertion Site 2

The transcription factor (TF) Myeloid Ecotropic Insertion Site 2 (MEIS2) belongs to the highly conserved three-amino acid extension loop (TALE) homeobox protein superfamily [1]. TALE TFs have been shown to play essential roles in transcription regulation, embryogenesis and other developmental programs [166, 201]. MEIS2 has been identified as an endogenous CRBN substrate in an on-chip ubiquitination assay. It is assumed that IMiDs and MEIS2 compete for the same binding site. Therefore, the prevention of ubiquitination of MEIS2 has been proposed as a major MOA of IMiDs anti-MM activity [1].

1.6.3 Glutamine Synthetase

CRBN was also found to be involved in the glutamine metabolism, which is dysregulated in many diseases. The essential glutamine-regulating protein GS was found to interact with CRBN directly. This binding leads to the ubiquitination and degradation of GS [129, 130]. It was shown that this functions as a negative

feedback when high glutamine concentrations are present in the cell. Responsible for the recognition through CRBN seems to be the acetylation of two lysine residues, K11 and K14. In contrast to other substrates such as MEIS2, where small molecule and endogenous substrate binding are mutually exclusive, IMiDs were reported to enhance the binding of CRBN and GS [85].

1.6.4 Amyloid Precursor Protein

Amyloid-beta precursor protein APP is an integral membrane protein that has been shown to play a role in neurite growth, adhesion and axiogenesis, neural plasticity, antimicrobial activity, and iron export [17, 64, 68, 182]. Most prominently, APP has been shown to be the precursor of beta amyloid (Aβ), which is the most abundant component of amyloid plaques found in Alzheimer´s disease [3, 14, 53, 70, 84]. Alternative cleavage of APP leads to the release of Aβ (containing 37 to 49 amino acids). Accumulation of Aβ can lead to the formation of oligomers which are neural toxic [58] and can ultimately lead to Alzheimer [136, 171, 199]. It was shown in pull-down experiments that the intracellular domain of APP (AID) directly interacts with CRBN, DDB1 and Cul4a [33, 94], however no mechanism has been shown. A detailed description of the domain organization of APP is shown in Chapter 7.

1.7 Cereblon-mediated teratogenicity

Albeit being the first IMiD and first-line therapy for MM [131], thalidomide is most prominently known for its teratogenic side effects. The use of thalidomide showed the biggest risk of miscarriage and malformations when used especially in the early stage of pregnancy, with no apparent damages after 36-42 days of gestation [126, 179, 196]. Malformations include absence and shortening of limbs, called phocomelia and other defects to heart, ear, eyes, and other internal organs. Treatment with thalidomide today is conditioned to tight regulations in

order to prevent exposure during pregnancy. However, even 22 years after the re-approval of thalidomide for ENL, the underlying mechanisms of teratogenicity are still not fully uncovered. Early hypotheses suspected reactive oxygen species that damage DNA [204], and inhibition of angiogenesis, because it was found that antiangiogenic derivatives of thalidomide also showed teratogenic effects [134, 187]. Thalidomide itself also undergoes spontaneous hydrolysis into more than 12 products, which potentially mediate side effects [45, 167]. However, it was the discovery of CRBN as the main target of thalidomide, that sparked structural investigations. Notably, it was shown that mouse and rat CRBN, which are 95% homologous to the human protein [42, 72], do also bind thalidomide, but thalidomide does not exert teratogenic effects in these rodents. Crystal structures of CRBN in complex with neo-substrates (zinc fingers, GSPT1) showed that the interaction between the two proteins is mediated through a common β-hairpin structure with a glycine residue at the base [37]. A key residue of murine CRBN, I391, blocks this structural motif from binding to the CRBN surface. Mutation to valine, which is present in the human protein, induced degradation of neo-substrate, and also showed thalidomide-induced fetal loss in mice [49]. This led to the hypothesis, that a neosubstrate is likely to be responsible for the teratogenic effects. Like IKZF1 and zinc-finger transcription factor Aiolos (IKZF3), SALL4 belongs to the same class of C2H2 zinc finger transcription factors. SALL4 is enriched in embryonic stem cells, and loss-of-function mutations result in phenotypes similar to thalidomide. Paradoxically, some patients with mutations in SALL4 genes have even been misdiagnosed for thalidomide embryopathy. Further studies have shown that mice, that were expressing human CRBN, were still resistant to teratogenic effects of thalidomide. However, it was also shown that mouse SALL4 cannot be degraded through human CRBN, while humanized SALL4, with mutations in the zinc finger domain can. This observation led to the conclusion, that the degradation of SALL4 through CRBN is the main driver of thalidomide teratogenicity [37, 115].

1.8 Aim of this thesis

We have previously shown that CRBN is able to accommodate more chemically diverse moieties than glutarimide, which is the basis for thalidomide and its analogues. This raises the question of what the molecular determinants of CRBN-binding are, and what mediates the interactions of effectors and non-endogenous substrates? An important goal of this study was therefore the identification of binding moieties that might be chemically distant from known binders. To this end, we planned to use high-throughput screening and chemical modifications of identified binders. Their characterization was enabled by structural and biophysical assays, that we planned to establish based on CRBN constructs from bacterial and human origin. Here, the aim was to identify novel and potentially more potent binders that can aid in the design of future generation therapeutics. Moreover, fluorinated analogues of thalidomide have been shown to exert antiangiogenic properties, possibly independent from CRBN-binding. We aimed to characterize such analogues for their antiangiogenic properties and determine their affinities to CRBN.

Finally, we aimed to understand the binding of natural ligands. The role of CRBN in the absence of drugs remains largely elusive so far, however given the high sequence conservation of the C-terminal domain of CRBN and its homologues, common natural ligands seem plausible. We therefore set out to characterize the binding of suspected natural ligands and proteins, which could give additional clues about conserved functions of the thalidomide-binding domain.

Chapter 2

Materials and Methods

2.1 Materials

2.1.1 Chemicals

Table 1: Chemicals

Chemical	Manufacturer
Ammonium persulfate (APS)	Roth
Beta (β)-mercaptoethanol	Merck
Bromphenol blue	Sigma-Aldrich
Bovine serum albumin (BSA) fraction V	Roth
Coomassie brilliant blue G-250	Serva
4-(2-hydroxyethyl)-1-piperazineethanesulfonic acid (HEPES)	Roth
Dimethyl sulfoxide (DMSO)	Sigma-Aldrich
Disodium hydrogen phosphate, Na_2HPO_4	Roth
Ethanol absolute	Sigma-Aldrich
Glycerol	Roth
Glycine	Roth
Hydrochloric acid, HCl	Roth
Isopropyl β-d-1-thiogalactopyranoside (IPTG)	Roth

Magnesium chloride, $MgCl_2$	Sigma-Aldrich
Methanol absolute	Sigma-Aldrich
Monosodium phosphate, NaH_2PO_4	Roth
Non-fat dry milk	Roth
Potassium chloride, KCl	Roth
Potassium dihydrogen phosphate, KH_2PO_4	Roth
Potassium hydroxide, KOH	Roth
Protease inhibitor cocktail	Thermo Scientific
RIPA buffer	Thermo Scientific
RNase A	Sigma-Aldrich
Rotiphorese Gel 30 (37,5:1), 30% acrylamide/bis-acrylamide solution	Roth
Sodium chloride, NaCl	Roth
Sodium hydroxide, NaOH	Roth
Sodium dodecyl sulfate (SDS)	Roth
Tris(2-carboxyethyl)phosphine (TCEP)	Sigma-Aldrich
Tetramethylethylanediamine (TEMED)	Fluka
Tris(hydroxymethyl)aminomethane (Tris)	Roth
Triton X-100	Roth
Tween-20 (polysorbate 20)	Roth

2.1.2 Enzymes

Table 2: Enzymes

Enzyme	Manufacturer
BamHI (FD)	Thermo Scientific
Benzonase® Nuclease	Sigma-Aldrich
DNase I	Sigma-Aldrich
Phusion (HF) DNA Polymerase	Thermo Scientific
T4 DNA Ligase	Roche Diagnostics GmbH

Taq DNA Polymerase	New England Biolabs
XhoI (FD)	Thermo ScientificTM

2.1.3 Cell culture

Table 3: Cell culture media

Media or supplement	Manufacturer
Dulbecco's Modified Eagle Medium (DMEM)	Sigma-Aldrich
RPMI 1640	Gibco Life Sciences
DMEM: F-12 Medium (ATCC 30-2006)	LGC Standards GmbH
Fetal bovine serum (FBS)	Gibco Life Sciences
ExpiSf CD Medium	Gibco Life Sciences
ExpiFectamine Sf Transfection Reagent	Gibco Life Sciences
ExpiSf Enhancer	Gibco Life Sciences
Opti-MEM	Gibco Life Sciences
Penicillin	Sigma-Aldrich
Phosphate-buffered saline (PBS)	in-house media kitchen
Penicillin - Streptomycin	Sigma-Aldrich
Trypsin-EDTA (0.05 %)	Gibco Life Sciences

Table 4: Cell lines

Cell line	Description	Supplier
OPM-2	human MM cell line	DSMZ (ACC 50)
M059J	human malignant glioblastoma cell line	ATCC (CRL-2366)

NAMALWA.CSN/70	human Burkitt lymphoma cell line	DSMZ (ACC 70) LOT 2
HEK293T	human embryonal kidney cell line	stock
ExpiSf9 Cells	high density Sf9 insect cells	gibco LOT 2010958

2.1.4 Antibodies

Table 5: Antibodies

Antibody	Species	Manufacturer
anti-CK1α ab108296	rabbit	Abcam
anti-FLAG F7425	rabbit	Sigma-Aldrich
anti-His DIA-900-200	mouse	dianova
anti-IKZF3 15103S	rabbit	Cell Signaling Technology
anti-MEIS2 H00004212-M01	mouse	Abnova
HRP conjugate 111-035-144	goat anti-rabbit	Jackson Immuno Research
HRP conjugate 115-035-003	goat anti-mouse	Jackson Immuno Research
IRDye 680LT	Donkey anti-Mouse	LI-COR
IRDye 800CW	Goat anti-Mouse	LI-COR

2.1.5 Bacteria

Table 6: Bacteria

Cells		Origin
DH10EMBacY	chemically competent cells	generous gift from Weir group

C41 (DE3)	chemically competent cells	stock
Rosetta 2 pLysS	chemically competent cells	stock
TOP10	chemically competent cells	stock

2.2 Methods

2.2.1 Cloning, expression, purification of CRBN constructs and mutants

2.2.1.1 MSCI4 and mutants

Proteins were expressed in *E. coli* C41 (DE3) cells grown in LB media unless otherwise specified. Protein expression was induced with isopropyl β-D-1- thio-galactopyranoside (IPTG) at log phase A_{600} ~0.6 for 4 to 6 h at 37 °C. Cells were pelleted, resuspended in 20 mM Tris, pH 7.5, 100 mM NaCl, 5 mM β-Mercaptoethanol, 4 mM $MgCl_2$, DNase I and Protease Inhibitor Cocktail. After lysis with ultrasonication, soluble protein was separated via ultracentrifugation and loaded onto NiNTA affinity column. Column was washed with 20 mM Tris, pH 7.9, 300 mM NaCl, 5 mM β-Mercaptoethanol and protein was eluted with a gradient of 0 - 0.5 M imidazole. Fractions containing target protein were pooled, TEV protease was added and dialyzed overnight against 20 mM Tris, pH 7.5, 150 mM NaCl, 5 mM β-Mercaptoethanol. The HIS-tag was removed via a second NiNTA column and flow through was collected and concentrated to 17 mg/mL. For the MsCI4 humanized construct, with the mutations A52H, M54Y, F56H, R68N, A72R, I87V and L89Q, codons were optimized for expression in *E. coli* and synthesized (Eurofins). From the commercial carrier vector, humanized $MsCI_4$ was then subcloned via BamHI and XhoI restriction sites into pETHis_1a leading to GFP-MsCI4 humanized construct. Round-the-horn PCR was used to remove GFP and the final MsCI4 humanized construct was expressed and purified as described for WT $MsCI_4$.

2.2.1.2 hTBD

Gene encoding for hTBD (residues 319–425) [2] was synthesized and subcloned via BamHI and XhoI into pGEX4T1. Vector was used to transform chemically competent *E. coli* Rosetta 2 pLysS cells. A 5 mL pre-culture that was grown for 16 h at 37 °C was then used to inoculate 25 mL TB media for 16 h at 37 °C. Finally, this starter culture was transferred to 1.5 L TB media that was supplemented with 50 µM $ZnCl_2$. Protein expression was induced with 0.5 mM IPTG at 16 °C for 20 h. Cells were pelleted by centrifugation and stored at -80 °C. Cell pellet was resuspended in lysis buffer (50 mM Tris pH 8.0, 500 mM NaCl, 1 mM Tris(2-carboxyethyl)phosphine (TCEP), 0.1% Triton X-100, 10 µM $ZnCl_2$, DNase I, Protease Inhibitor Cocktail). After homogenization by ultrasonication and separation of soluble protein by ultracentrifugation, protein was loaded onto a GSTrap FF column (25 mL), and washed with several column volumes of 50 mM Tris pH 8.0, 500 mM NaCl, 1 mM TCEP, 10 uM $ZnCl_2$ until a stable baseline was reached. Protein was eluted with wash buffer supplemented with 10 mM reduced glutathion and pooled. After cleavage with thrombin for 4 h at 4 °C, hTBD and GST tag were separated via SEC (Superdex 75). Protein was pooled, concentrated and stored at -80 °C.

2.2.1.3 DDB1-CRBN

Based on previously published structures [114, 143, 175], genes encoding for His-DDB1$^{\Delta BPB}$ and Twin-Strep-CRBN were synthesized and cloned into a pFastBac dual vector. With the aim to further stabilize the protein, PCR reactions were used to delete the first 40 residues of CRBN, which are predicted to be unstructured. The final construct pFastBac dual His-DDB1$^{\Delta BPB}$-Twin-Strep-CRBN$^{\Delta N40}$ was used to transform DH10EMBacY cells. Blue/white screening was used for selection, and baculovirus shuttle vector (bacmid) was purified from these cells. Transposition occurs through the mini-Tn7 element on the pFastBac vector and the mini-Tn7 site on the bacmid. Recombinant bacmid further included a YFP gene, which was used to follow the subsequent transfection of ExpiSf9 cells via

cell fluorescence detection. Transfection was performed using the manufacturer´s protocol. The high density of ExpiSf9 cells led to high virus titer, and P1/P2 were used for recombinant protein expression. Protein was expressed for 72h before pelleting of the cells at storage at -80 °C. Cell pellet was resuspended in buffer XT (100 mM potassium phosphate buffer (pH 7.8), containing 150 mM sodium chloride) and subjected to ultrasonication (3 x 30s). Soluble protein was extracted by ultracentrifugation (40.000 g, 45 min, 4 °C) and subject to Strep-Tactin XT affinity chromatography. Bound protein was eluted with buffer XT containing additional 50 mM biotin. Fractions containing protein were pooled and flash frozen.

2.2.2 NanoDSF

For stability measurements, a modified technology based on differential scanning fluorimetry was used. NanoDSF relies on intrinsic fluorescence of tryptophan and tyrosin. These amino acids are excited at 280 nm and emission is recorded at 330 and 350 nm. Upon heating the sample, the protein undergoes structural rearrangements which change the local conformation and environment around the fluorophore. This leads to a change in the emission maximum and intensity, which can be used to determine the temperature at which 50% of the protein is denatured [T_m]. These data were recorded on a Prometheus NT.48 (Nanotemper Technology), with heat ramps <2 °C/min. Initial experiments (Table 7) were performed on a Tycho NT.6 (Nanotemper Technology), where the heating rate was 20 °C/min. These fast heating rates lead to inflection temperatures [T_i], rather than melting temperatures.

2.2.3 FRET assay

In order to identify possible CRBN ligands, we have developed a FRET-based binding assay. This relies on a reporter ligand, 1-(N-2-MANT-imidoethyl)-uracil (MANT) (Figure 7), that binds specifically to the thalidomide-binding pocket and builds a FRET pair with the tryptophans inside the binding pocket [19]. For

this assay, the MsCI4$^{WW/FF}$ mutant was used, in which tryptophans outside the binding pocket are replaced by phenylalanines, which led to a lower inner filter effect. Stock solutions for MANT-uracil (1 M), and test compounds (400 and 200 mM) were prepared in DMSO. Master dilution series were performed in DMSO and diluted in assay buffer (20 mM Tris, pH 7.5, 150 mM NaCl, and 0.5 mM β-mercaptoethanol), in order to keep final DMSO concentration below 0.02%. Measurements were performed in black 96-well plates. Upon excitation at 295 nm, the MsCI4-MANT complex showed high fluorescence at 440 nm (recorded via top optics, read height 8 mm), which declined upon displaced of the reporter by compound. Measurements were done in triplicates and fluorescence as a function of compound concentration was fitted as one-binding site model (SigmaPlot 12.3). Obtained IC_{50} from these curves were calculated to K_i values using Cheng-Prusoff equation.

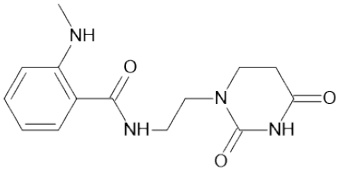

FIGURE 7: Chemical structure of MANT-Uracil reporter

2.2.4 MST assays

Microscale Thermophoresis relies on the principle, that a fluorescently labeled molecule moves along a temperature gradient based on its molecular properties like size, hydration, charge and conformation [75]. Therefore, induced changes by binding to small molecules or protein alters the movement significantly. Measurements are performed by inducing a temperature change with an IR-laser and recording variations of fluorescence in dependence of ligand concentration. Two main drivers of these variations can be used to determine affinities: One is the temperature related intensity change (TRIC), which only occurs in the first few seconds after a temperature gradient is applied. And the second effect, thermophoresis, which usually reaches its equilibrium after around 20s, describes

the physical movement of a fluorescent molecule along the applied temperature gradient. The influence of individual effects has to be determined empirically.

2.2.4.1 Labeled MST assay

MsCI4 protein was covalently labeled using the Labeling Kit RED-NHS 2nd Generation (Nanotemper Technology) according to the manufacturer´s protocol with a few optimizations. Buffer exchange into labeling buffer was performed using 30 µM protein and diluted to 10 µM for labeling. TCEP was included in the buffer at a final concentration of 0.1 mM in order to minimize oxidation of the protein. Since it was known that DMSO also binds to the protein, the labeling dye was reconstituted in labeling buffer immediately before mixing with diluted protein. Fractions after a SEC column were collected and concentration/degree of labeling were measured using a microvolume spectrophotometer NP-80 (Implen). Aliquots were flash frozen in LN_2 and diluted 1:100 in MST buffer before measurements, which resulted in assay concentrations of ~20 nM.
Evaluation of binding data was performed by plotting concentrations against either initial fluorescence or difference in MST behavior (Δ Fnorm ‰). Nonlinear Regressions were calculated using the variable slope model (4PL) integrated into Prism (Graphpad). Data was calculated using asymmetrical (profile-likelihood) models at a confidence level of 95%. Data is reported throughout this thesis as mean ± sem, unless otherwise stated.

2.2.4.2 Competitive MST assay

A BODIPY-uracil coupled reporter (Figure 8) was designed and synthesized for the development of a competitive MST assay. The BODIPY 493/503 fluorophore is coupled to the known binder of MsCI4, uracil. BODIPY 493/503 absorbs at 493 nm and emits at 503 nm, and this fluorescence is recorded in the blue channel of the Monolith NT.115 (Nanotemper). The two moieties are coupled via an amide bond to form the reporter ligand (BU). BU powder was dissolved and diluted to

2 mM in DMSO and further to 2 µM in MST buffer. Native protein was diluted to 14 µM in protein buffer and mixed 1:1 with 2 µM BODIPY-uracil to generate final assay concentrations of 3.5 µM protein and 500 nM BODIPY-uracil. For the hTBD, BU was used at final concentrations of 200 nM and 10 µM protein. Upon displacement of the fluorescent reporter by compounds, a shift in the thermophoretic behavior is observed which was used to determine affinities.
For the competitive MsCI4 assay, quantitative evaluation of K_i is difficult, and data is reported as IC_{50} values only.
For the competitive hTBD assay, IC_{50} values are reported, as well as their respective K_i values. Calculation is based on previously reported correlations shown in equation 1 [132].

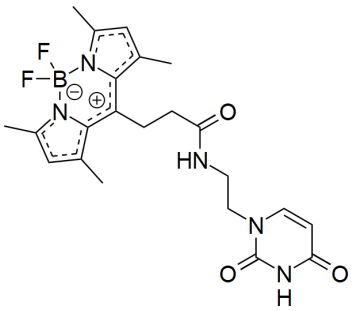

FIGURE 8: Chemical structure of uracil BODIPY 493/503 reporter (BU)

$$K_i = \frac{K_d}{2-\gamma} \cdot \left(\frac{EC_{50}}{\frac{[T]_t}{\gamma} - \frac{K_d}{2-\gamma} - \frac{[C]t}{2}} - \gamma \right) \tag{1}$$

with

$$\gamma = \frac{[T]_t + [C]_t + K_d - \sqrt{([T]_t + [C]_t + K_d)^2 - 4[T]_t[C]_t}}{2[C]_t} \tag{2}$$

2.2.5 Crystallography

For crystallization, $MsCI_4$ and humanized $MsCI_4$ protein solution generally was concentrated to 17 mg/mL and mixed with 3 mM of effectors (thalidomide, or

7d in Chapter 4). Crystallization trials for humanized $MsCI_4$·thalidomide, which turned out to be humanized $MsCI_4$·CBG, and $MsCI_4$ ·7d were performed via the vapor diffusion technique at 20 °C in sitting-drops. 400 nL of protein solution were mixed with 400 nL of reservoir solution with the Honeybee 963 robot (Genomic Solutions Ltd). Diffraction-quality crystals of humanized $MsCI_4$·CBG were obtained in a condition containing 20 % PEG 3350 and 0.2 M ammonium acetate, and crystals of $MsCI_4$·7d were obtained using 15 % PEG 6K and 5 % glycerol.
For all other compounds that were studied via soaking experiments, crystals were prepared in sitting drop experiments by mixing 0.4 µL 0.4 M $(NH_4)_2HPO_4$ ground solution with 0.4 µL $MsCI_4$·thalidomide solution. Crystals grown in this set-up were transferred to 3 µL ground solution spiked with individual compounds for soaking. After 36 - 72 h, crystals were cryoprotected by the addition of 20 % PEG 3350 solution. Crystals were flash-cooled in liquid nitrogen and diffraction data was collected at 100 K and a wavelength of 1 Å on beamline X10SA at the Swiss Light Source using a PILATUS 6M-F, or Eiger2 16M (Dectris Ltd.). Data was processed and scaled using XDS [77]. Structures were solved based on the $MsCI_4$·thalidomide coordinates (PDB 4v2y). The co-crystal structures of the complexes with CBG and 7d were of other crystal forms and were solved using molrep [194] with 4v2y as a search model, locating four and two chains in the asymmetric unit (ASU), respectively. All structures were rebuilt using Coot [44] and the integrated suite Lidia for chemical structures and generation of restraints. The models were finalized via cyclic modeling in Coot and refinement using REFMAC5 [123]. Molecular figures were generated using PyMOL [165]. Data collection and refinement statistics are summarized in Tables 8, 10, 22 which are shown in the respective chapters.

2.2.6 Cell culture

All experiments conducted on/with cell cultures were done using aseptic techniques. Cell counting was performed using a Neubauer chamber or automated cell counter, and cell viability was determined by trypan blue exclusion.

2.2.6.1 Mammalian cell culture

The suspension cell lines OPM-2, M059J and the adherent cell line HEK293T were cultured in a humidified incubator with a constant atmosphere of 37 °C and 5% CO_2. All cell lines were passaged to a maximum of 20 cycles to avoid genetic drift. Cells of the MM-cell line OPM-2 were cultured in RMPI 1640 media supplemented with 10% h.i. FBS and 1% penicillin - streptomycin. Cells were passaged every 2 - 3 days by splitting 1:2 – 1:4, depending on cell growth to maintain a cell density of 0.5 x 10^6 cells/mL. Adherent M059J cells were routinely cultivated in a 1:1 mixture of DMEM:F-12 Media supplemented with 2.5 mM L-glutamine and 10% h.i. FBS. For passaging and harvesting, media was removed, and cells were washed once with PBS. Cell monolayer was incubated with Trypsin-EDTA for a few minutes at 37 °C to remove adherent cells. Trypsin was inactivated by the addition of fresh media and resuspended in 1:6 – 1:8 ratios depending on cell growth. NAMALWA.CSN/70 cells were cultivated in RMPI 1640 media, supplemented with 10% h.i. FBS. Cells were split 1:3 – 1:4 every 2 - 3 days, keeping them at a density of 0.5 x 10^6 cells/mL. OPM-2 cells 4 mL of culture per well were pipetted in a sterile environment. Stock solutions of lenalidomide were prepared at concentrations of 80 mM and 400 mM, stock solutions of test compounds were prepared at a concentration of 400 mM. For the assay, 10 µL of stock solutions were added to 4 mL cell culture. DMSO controls were prepared in the same manner, leading to a final DMSO concentration of 0.25%. After 24 h of incubation, cell solution was centrifuged at 500 g. After one washing step with ice cold PBS, cell pellets were resuspended in 35 µL of lysis buffer (20 mM Hepes, 175 mM NaCl, 1 % NP40, 2mM $MgCl_2$) on ice and supplemented with 0.5 µL benzonase.

2.2.6.2 Insect cell culture

ExpiSf cells (a high density cell line based on Sf9 cells) were initially seeded in 25 mL CD media and grown at 27 °C until a density of >5 x 10^6 cells/mL. Cells were split to approx. 0.6 - 1.0 x 10^6 cells/mL for routine cell culture. For cryopreservation, cell suspension was centrifuged at 300 g for 5 min and adjusted

to 1 x 10^7 cell/mL using conditioned media (supernatant). DMSO was added to a final concentration of 7.5% and cooled down at - 80 °C for 24 h before transferring to liquid nitrogen vapor phase.

2.2.7 Endothelial cell tube formation assay

The endothelial cell tube formation assays were conducted in the lab of William D. Figg, NIH, USA and in principle work as following [127]. Human umbilical vein endothelial cells were seeded at 30,000 cells/well in EGM-II, containing DMSO or compounds, in eight-well slide chambers layered with 150 µL Matrigel. After 16 h at 37 °C, slides were washed with PBS and fixed in 100% Methanol for 10s. DiffQuick solution II (Dade Behring, Inc.) was used to stain samples and images were recorded. Area was measured as the number of pixels using the MetaMorph software (Universal Imaging, Downingtown, PA).

2.2.8 Rat aortic ring angiogenesis assay

The rat aortic ring angiogenesis assay was conducted in the lab of William D. Figg, NIH, USA and follows the previously published protocol [101]. Twelve-well plates were covered with 250 µL Matrigel and incubated at a constant atmosphere of 37°C and 5% CO_2. Thoracic aortas from male Sprague Dawley rats (6- to 8 weeks old) were excised and fibroadipose tissue was used for further experiments. 1 mm cross-sections were placed into wells and coated with Matrigel. Tissue was cultured for 24 h in 1 mL EGM-II (EBM-II + EGM-II Bulletkit, Clonetics). Media was removed and 1 mL fresh EBM-II, supplemented with FBS (2%), amphotericin B, 10 µg/mL gentamicin, and DMSO or compound dissolved in DMSO was added. Media was renewed daily for 4 days, before quantifying vascular outgrowth (growth in pixels of treated ring/growth in pixels of control ring) on day 5 based on digital photographs.

2.2.9 Western Blotting

Proteins were separated by using SDS PAGE gels (Life Technologies) or Mini-PROTEAN TGX gels (BIO-RAD) and transferred to low-fluorescence PVDF membranes. Additionally, TGX gels were activated under UV light before transfer and imaged before blocking. Depending on the primary antibody, either 5 % milk in PBS-T or 4 % BSA in PBS-T were used to block membranes for at least 2 h before incubating with primary antibody overnight. For chemiluminescence detection, horseradish peroxidase conjugated secondary antibodies were used at 1:20.000 dilutions for detection of bands by chemiluminescence (ECL Vilbert). Protein bands were detected and integrated using FUSION Xpress (Peqlab) or the BioRad analysis suite. Protein levels were normalized using either housekeeping proteins (actin) or Stain-Free Technology and analyzed by one-way ANOVA according to Holm-Sidak method integrated into SigmaPlot. For IR-detection, membrane blocking and final washing steps were performed without the addition of detergent. Fluorescently labeled antibodies were used to image protein bands via 700 nm/800 nm channel directly.

Chapter 3

Design and characterization of bacterial and human CRBN constructs

3.1 Introduction

The identification of CRBN as the primary target of thalidomide sparked strong interest into its three-dimensional structure. As such, multiple labs have since worked with CRBN variants from human, mouse and chicken, and determined their structure. In our lab, we have predominantly been using the single domain bacterial homologue *Magnetospirillum gryphiswaldense* cereblon isoform 4 from *Magnetospirillum gryphiswaldense* [19, 20, 62, 63, 65]. Human and bacterial protein are highly similar with 35% sequence identity and < 1Å over 100 Cα in structure. Sequence alignment and structural superposition (Figure 9) visualize this high conservation. The thalidomide binding pocket within MsCI4 is formed by the three conserved tryptophan residues W79, W85 and W99, which correspond to W380, W386 and W400 in the human protein. Binding of compounds based on glutarimide form the following canonical interactions: The glutarimide ring forms two hydrogen bonds, one between the amino group and F77 (H378

hCRBN) and the other between the distal keto group and W79 (W380 hCRBN). A third hydrogen bond is specific for organisms carrying a mutation at the base of the aromatic cage. The distal keto group of glutarimide and the hydroxyl group of the tyrosine Y101 form this interaction which is absent in the human protein as the corresponding residue is F402.

Besides MsCI4, we are also working with the isolated C-terminal domain of human CRBN, which will be referred to as hTBD. The much larger construct of human CRBN (ΔN40) in complex with DDB1 (ΔBPB) will be referred to as DDB1-CRBN. Each protein construct holds several advantages and disadvantages.

The bacterial protein MsCI4 has extensively been used in our lab. It tolerates mutations like Y101F, by which an aromatic cage that is chemically equivalent to hCRBN is created. Moreover, a mutant with W36F and W59F was used in a FRET assay, in order to reduce intrinsic protein fluorescence. Besides biophysical assays, MsCI4 was used to establish a crystal soaking system. Crystals grown in complex with thalidomide were used to soak multiple dozen compounds and characterize their binding at a molecular level. However, differences between human and bacterial protein become prominent as compounds get bigger and extend further out of the binding pocket [20]. Here, interaction can potentially deviate between species. To this end, several humanized MsCI4 constructs were designed and will be shown in the next sections.

The human construct, DDB1-CRBN could only be expressed in insect cells and is therefore more laborious than constructs that can be expressed in *E. coli*. Moreover, due to its size and flexible regions, crystal structures with DDB1-CRBN are of lower resolution than MsCI4 (>2.45 Å PDB 5FQD vs. 1 Å PDB 6R1D, respectively). Binding affinities of IMiDs and other small molecules to DDB1-CRBN were found to be up to 100 fold higher than to single domain CRBN constructs [2]. This is possibly due to N-terminal stabilization of compound interactions [2], and has to be kept in mind when comparing affinities shown throughout this thesis. In contrast, the hTBD is similar in size to MsCI4 and could be expressed in *E. coli*. It was also found to have similar affinities to IMiDs as MsCI4 [2, 20]. However, no crystal structure with hTBD has been released so far.

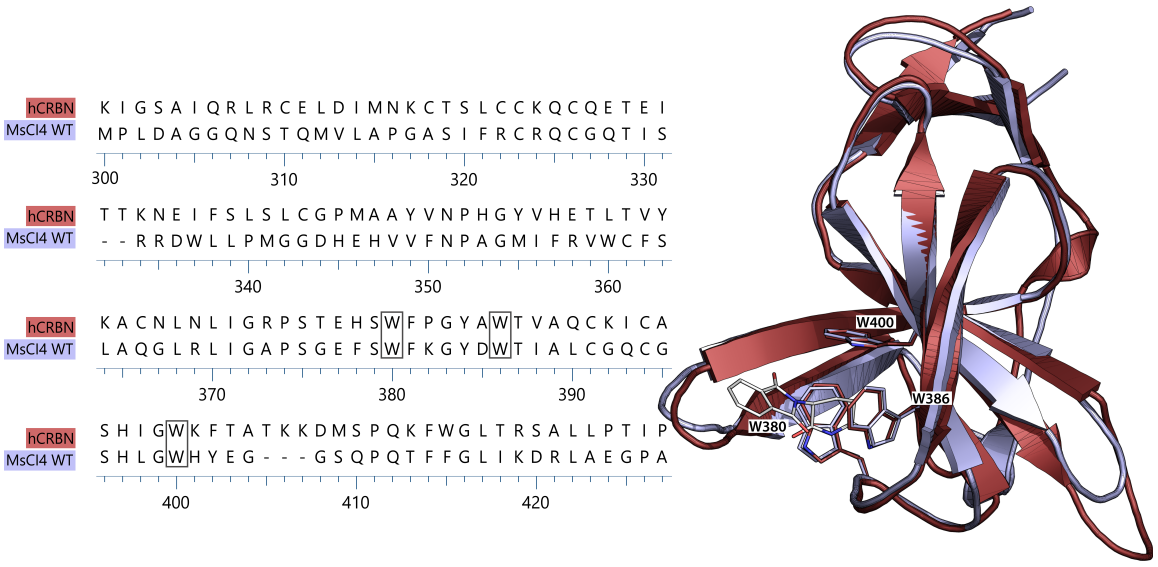

FIGURE 9: Sequence alignment of MsCI4 and hTBD (left) and a structural superposition of both proteins. Shown in stick representation is the tri-Trp cage and a bound thalidomide molecule. Numbering refers to amino acids of hCRBN

3.2 Mutations of MsCI4

MsCI4 has been used in our lab to study the binding of small molecules to CRBN. Crystal structures in complex with these compounds allowed us to delineate not only minimal moieties but also rules for avoiding unintended cereblon binding. However, during these studies it became also apparent that the MsCI4 binding pocket had its limitations in regard to compound length. While MsCI4 represented an ideal model system for studying minimal moieties, extended compounds can potentially interact with residues that are not conserved between human and bacterial protein. Therefore, several mutants of MsCI4 were designed during the course of this thesis. An overview of the designed constructs is shown in Figure 10. Colored amino acids show residues that are different from the wild-type construct.

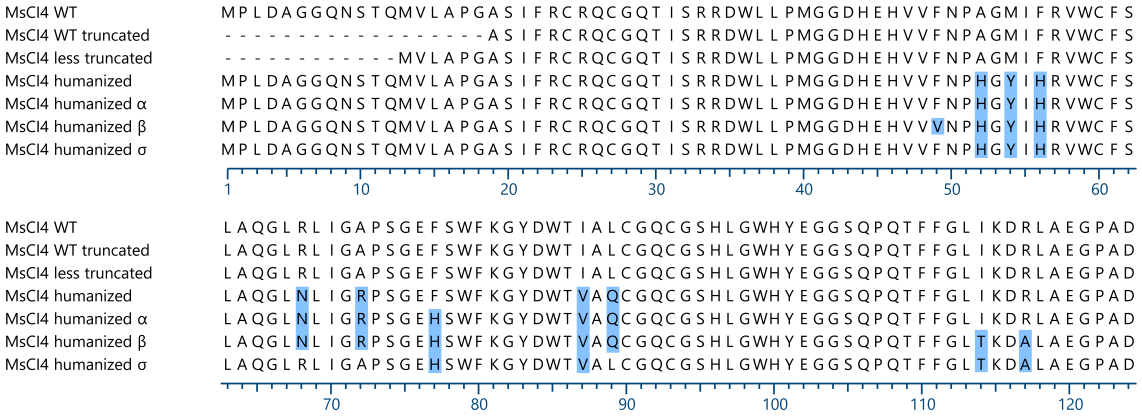

FIGURE 10: Sequence alignment of MsCI4 constructs designed during this project. Colored amino acids show residues that are different from the wild-type construct

3.2.1 Truncation of MsCI4

For the majority of crystal structures that our lab has obtained since working with MsCI4, the first 19 residues were usually not resolved in the electron density map. This is also in agreement with secondary structure predictions where the N-terminus is expected to be unstructured. Unstructured residues or even domains are generally a hindrance when attempting to crystallize a protein. In an effort to aid crystallization, we designed a construct in which the first 18 N-terminal residues were truncated. Expression and purification yields were in the expected range, however the protein was very unstable in solution and crystallization attempts could not be performed. Therefore, we designed a less truncated construct in which only the 12 N-terminal residues were omitted. We saw high yields for this construct and used previously established purification protocols to obtain highly pure protein, which also crystallized in a variety of commercially available crystal screens. It can therefore be concluded that this truncated construct can be used for further structural characterizations where the full-length construct does not lead to adequately diffracting crystals.

3.2.2 Humanization of MsCI4

During the early phases of this project, a crystal structure of hCRBN in complex with lenalidomide and CK1α was published, which showed that CRBN and lenalidomide jointly provide an interface for the binding of CK1α [143]. This interface is in direct proximity of the binding pocket on the CRBN surface and allows a β-hairpin-loop to bind. Moreover, binding experiments and structural alignment suggested that other neo-substrates like IKZF1 and IKZF3 could show a similar binding mode. Based on this data, we set out to construct "humanized" MsCI4 mutants based on structural superposition (Figure 11). Mutations of several surface exposed residues should allow for neo-substrate binding to MsCI4 in a related mode as seen for hCRBN. A construct carrying seven mutations was synthesized, cloned and expressed in *E. coli*. This humanized MsCI4 was well expressed, soluble, and could be purified to high levels by affinity chromatography. After His-tag cleavage, the mutant was also set up for co-crystallization with thalidomide which led to a high resolution structure. Interestingly, during crystallization, this construct apparently selectively bound a hydrolysis product of thalidomide that is of high pharmacological interest. This finding inspired additional experiments which build the basis of the work shown in Chapter 4, in which the crystal structure of this humanized version is described.

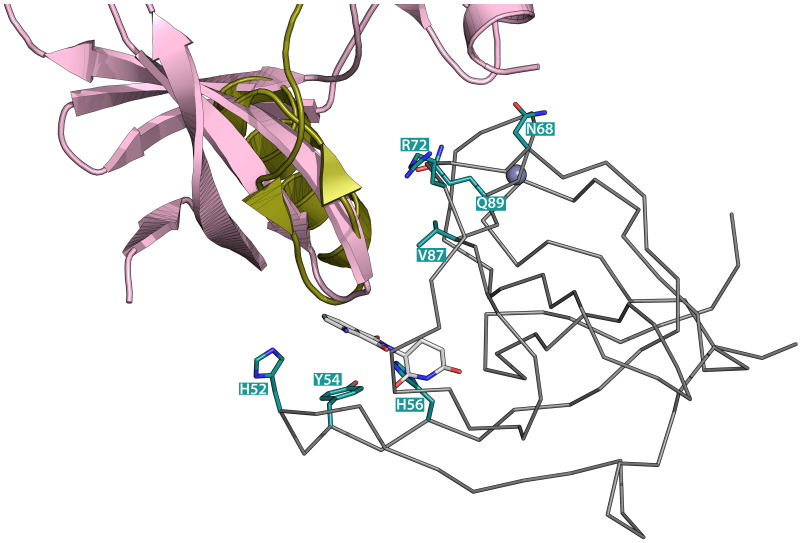

FIGURE 11: Structural superposition of MsCI4 (shown as ribbon) and hCRBN (omitted for clarity) in complex with CK1α (pink, PDB 5FQD) and IKZF1 ZF2 (brown, PDB 6H0F), both shown as cartoon. Highlighted residues show mutations of humanized MsCI4 versus WT

As all side-chains were clearly resolved within the complex, we could verify that mutated residues adopted a similar orientation as seen in hCRBN structures. Therefore, this construct can be used to study not only IMiD binding, but possibly also canonical neo-substrate recruitment. With this "humanized" protein at hand, the goal was to further characterize the binding of neosubstrates via X-ray crystallography. Based on superposition of the available structure of CRBN· lenalidomide · CK1α, we designed a short peptide motif of zinc finger 2 from IKZF1. Initial attempts to crystallize complexes of humanized MsCI4· IMiD· IKZF1 (ZF2) yielded crystals diffracting to 1.3 Å. Their structure was solved via molecular replacement using previous MsCI4 structures as a search model, however no electron density was seen for the zinc finger peptide. Further crystallization trials were not attempted after the publication of the DDB1· CRBN· pomalidomide· IKZF1(ZF2) /ZNF692(ZF4) structures [175]. These structures confirmed the related binding mode of the neosubstrates CK1α and zinc fingers IKZF1 and IKZF3 (included in the superpostion in Figure 11).

The invariability of the core aromatic cage allowed us to use MsCI4 as a model system for small molecule binding to CRBN. We have established biophysical assays for small molecule binding [19], established purification and crystallization protocols for MsCI4 [19, 20, 62, 63], which allowed us to delineate the chemical space of CRBN binding. However, with the expansion of chemical space and elongation of protruding moieties, the need arose for additional mutations of distant residues that differ between bacterial and human protein. Further analysis of these species-specific differences in complex with small molecules led us to design an additional construct, MsCI4 α with a F77H mutation. In some instances, this histidine in the human protein was involved in additional interaction with the proximal keto group of glutarimide and was therefore also included in our model system. Evaluation of surface-exposed residues surrounding the binding pocket showed F49, I114 and R117 as residues that could potentially be in close distance of elongated compounds such as PROTACs. Round the horn PCR was used to mutate these residues for MsCI4 humanized β construct (Figure 10). The last construct, MsCI4 humanized σ, was designed to improve stability by keeping mutations to a minimum. Here, mutations are focused on surface-exposed and potentially compound-accessible residues around the IMiD-binding site, without regards to neo-substrate binding.

3.2.3 Stability of MsCI4 and mutants

In addition to purity analysis by SDS-PAGE, constructs mentioned above were also characterized by their apparent melting points via NanoDSF. In general, all constructs with the exception of "MsCI4 WT truncated" were highly expressed, soluble and showed high melting temperatures. Melting temperatures are indicative for the stability of a protein and confirms that MsCI4 tolerates the mutations introduced in the humanized versions. Interestingly, His-tagged MsCI4 constructs generally showed a lower T_m and are hence less stable. Resulting from

these measurements, cleavage of the His-tag was henceforth performed in parallel with dialysis and improved overall protein yields.

TABLE 7: Inflection temperature [T_i] and melting temperatures [T_m] of MsCI4 WT, mutants and the influence of ligands

Construct		Inflection temperature T_i [°C]
MsCI4 WT HIS		71.3
MsCI4 WT		82.7
	+ pomalidomide	86.8
	+ succinimide	85.9
	+ 0.5% DMSO	85.2
Construct		**T_m [°C]**
MsCI4 WT	1x freeze-thaw	76.2 ± 0.04
	2x freeze-thaw	75.9 ± 0.73
	+ thalidomide	74.0 ± 0.17
	+ avadomide	74.8 ± 0.02
	+ 0.1% DMSO	71.9 ± 0.03
	+ 0.5% DMSO	73.7 ± 0.08
	+ 1% DMSO	74.5 ± 0.26
	+ 5% DMSO	77.2 ± 0.11
MsCI4 humanized HIS		63.1 ± 0.53
MsCI4 humanized		67.9 ± 0.05
MsCI4 Y101F		65.2 ± 0.24

Furthermore, NanoDSF measurements were also used to detect and confirm ligand binding. Binding within the aromatic cage stabilizes the protein and hence raises its inflection temperature T_i [°C], and melting temperature T_m [°C]. Both of these temperatures are indicative of the stability of a protein. However, the fast temperature ramps performed via the Tycho NT.6 (NanoTemper Technologies) lead to inflection points rather than melting temperatures. As expected, these stabilizing effects were seen for the classical IMiDs thalidomide, pomalidomide and avadomide. It was also apparent that the second and third generation IMiDs pomalidomide and avadomide have a bigger impact on the T_m, most likely due to their superior affinity. These measurements were performed via the Prometheus NT.48 (NanoTemper Technologies) with heat ramps <2°C/min, from which melting temperatures T_m [°C] were fitted using a 2-state model integrated

into MO.Affinity Analysis (NanoTemper Technologies). A similar stabilizing effect was seen for increasing concentrations of DMSO, which confirms our previous observations that DMSO can bind to MsCI4 WT, and to a much lower extent to Y101F mutants. Generally, we found that humanization of MsCI4 did clearly affect the stability of the protein, however the melting temperatures were still above 65°C and still higher than the previously used [63] single point mutation Y101F (65.2°C).

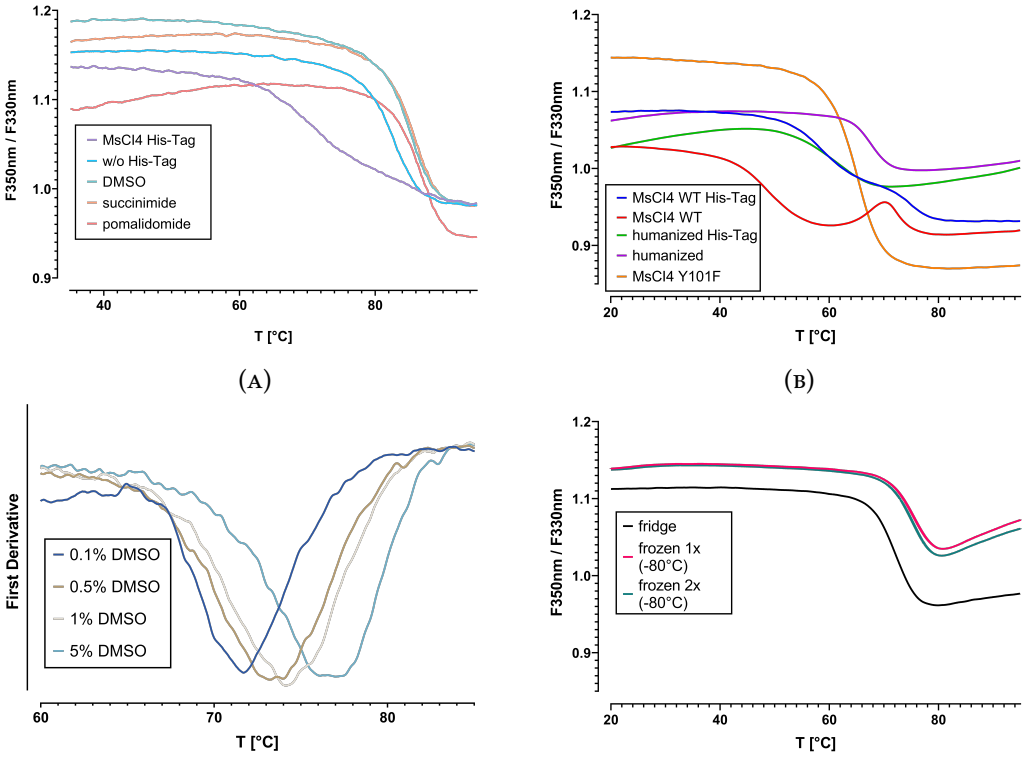

FIGURE 12: Thermal unfolding curves as functions of F350nm/F330nm plotted against temperature gradient from which T_i and T_m values were derived. (A) Melting curves at a thermal ramp of 30°C/min from which T_i values were derived. (B) Melting curves for MsCI4 WT and humanized constructs, with and without His-Tag, and the previously used Y101F mutant. (C) First derivative of melting curves for MsCI4 WT and increasing concentrations of DMSO. (D) Melting curves for MsCI4 WT at different storage conditions.

3.3 Structural characterization of novel immunomodulatory drugs

It has been shown that treatment with thalidomide and its second generation analogues, lenalidomide and pomalidomide in diseases such as MM can lead to resistances, which can be caused by CRBN mutations, chromosomal deletion, and low CRBN expression [215]. For these cases, new generations of IMiDs have been developed that show a much higher potency for neo-substrate degradation. Two such effectors that modulate cereblon E3 ligase activity and exhibits potent anti-tumor and immunomodulatory activities are avadomide (CC-122) and iberdomide (CC-220). Both are currently in clinical trials against advanced solid tumors, non-Hodgkin lymphoma (NHL), and multiple myeloma [4, 18, 24, 151]. Like the canonical binders thalidomide, lenalidomide and pomalidomide, iberdomide and avadomide also rely on glutarimide as the E3 binding moiety, however, their protruding moieties are fundamentally different. Avadomide (CC-122) has a compact 5-Amino-2-methyl-4-oxoquinazolin group solvent exposed, whereas iberdomide (CC-220) extends far out of the binding pocket with its morpholin and phenyl group that are connected via a methoxy linker to isoindol (Figure 2). One of the goals of this study was to determine their binding modes at a molecular level. As co-crystallization trials were unsuccessful, we quickly resorted to our previously established MsCI4-soaking system. This led to a 1.5 Å structure with CC-122 and a 1.9 Å structure with CC-220.

Avadomide (CC-122) was found to be present in chain C, while thalidomide molecules remained in chain A and B of the ASU. The glutarimide moiety of avadomide shows the conserved IMiD interactions, whereas the geometry of the protruding quinazolinone leads to a slight shift towards the tri-Trp cage compared to the phtaloyl moiety in thalidomide. No additional interactions of the protruding moiety with MsCI4 were seen for this compound. The high potency reported for the degradation of IKZF1 and IKZF3 [59] is therefore likely due to

additional interactions with the neo-substrate, potentially mediated by the solvent exposed primary and secondary amine group (Figure 13A).

Iberdomide (CC-220) was found to be present in all three chains. However, the orientation of the protruding moiety in chain A was different from chains B and C. Electron density in all chains was clearly defined (Figure 13 D). The ligand in chain A is oriented similar to that in the human complex (Figure 13 B). While the glutarimide moiety shows the canonical interactions with the tri-Trp pocket, the phenyl ring is harbored in a channel formed by E76, F77, and P51 of MsCI4. The human CRBN possesses an additional H353 which contributes to this groove. This corresponds to A52 in MsCI4, which cannot contribute to this interaction. In chain B and C, the ligand is oriented such that the protruding moiety, including the phenyl ring connected to the isoindolinone also collapses onto the MsCI4 surface, however, upwards towards W99. It was previously concluded that increase in potency for neo-substrate degradation of CC-220 is most likely due to the increase in affinity to CRBN [113]. The additional binding mode of CC-220 observed here, could either be an alternative conformation that was not present in the human crystal structure (PDB 5V3O), or species-specific amino acid substitutions did not allow for the same interactions.

These results clearly highlight the advantages and disadvantages of using MsCI4 as a soaking system. MsCI4 crystals can be grown reproducibly in a variety of conditions and generally diffract to high resolutions, even after extensive soaking trials. Furthermore, the solvent accessible binding pockets of three subunits per ASU allow us to potentially capture alternative binding modes in one crystal structure, such as seen for iberdomide. However, species-specific amino acid differences can interfere with their binding modes. This becomes prominent for elongated compounds and can be circumvented by using the presented humanized versions of MsCI4.

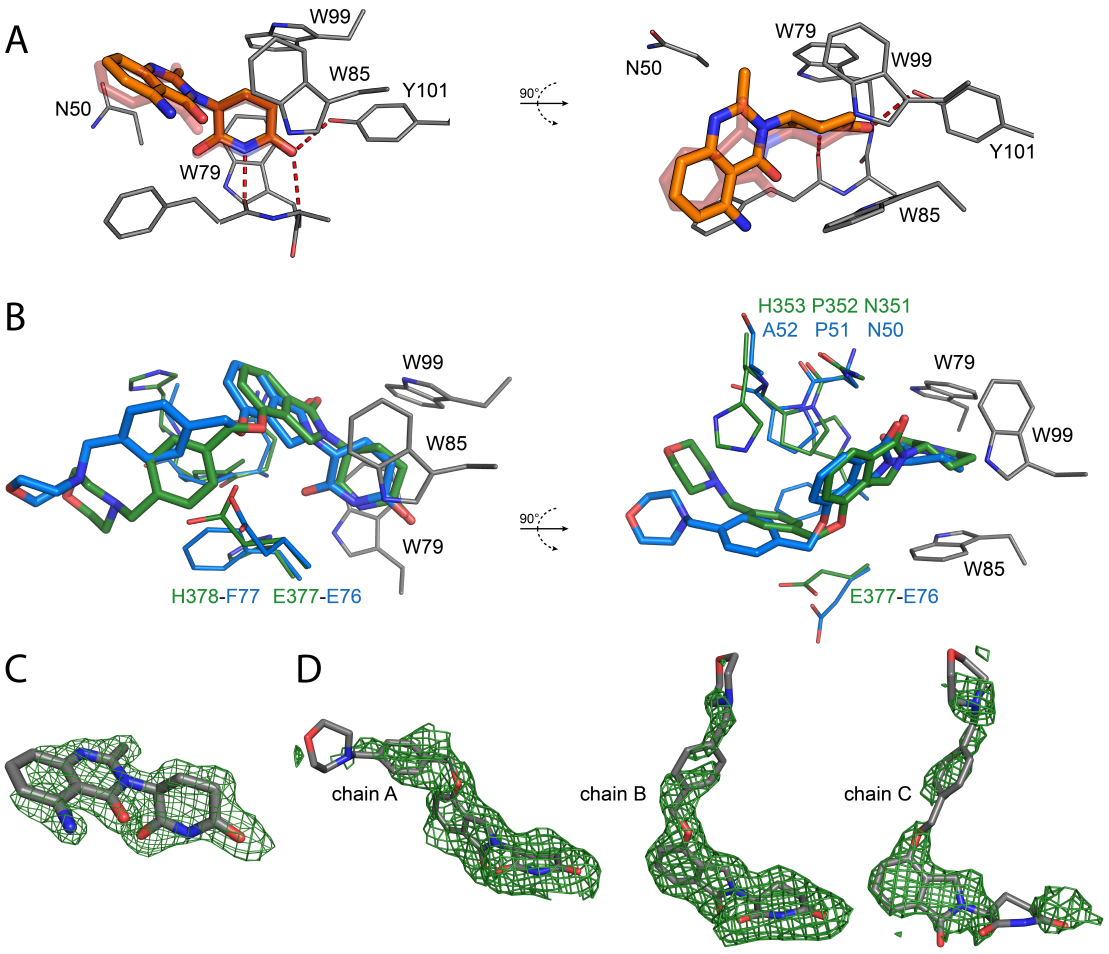

FIGURE 13: Interactions of CC-122 and CC-220 with MsCI4. (A) CC-122 (orange) inside the aromatic cage of MsCI4. For reference, a thalidomide molecule (purple) is superimposed transparently. (B) Superposition of CC-220 in complex with MsCI4 (shown in blue) and hCRBN (shown in green, PDB 5V3O). (C) $F_O - F_C$ omit map of CC-122 at 2 σ. (D) $F_O - F_C$ omit map of CC-220 at 1.5 σ in chain A, 2 σ in chain B and 1.5 σ in chain C

TABLE 8: Data collection and refinement statistics of novel IMiDs avadomide and iberdomide in complex with MsCI4.

	MsCI4 · avadomide	MsCI4 · iberdomide
Data Collection		
Space group	P212121	P212121
Unit cell		
a, b, c (Å)	56.60 60.16 88.40	56.00 58.85 88.58
α, β, γ (°)	90, 90, 90	90, 90, 90
Resolution range, Å	47.66 - 1.60 (1.70- 1.60)	44.29-1.89 (2.01-1.89)
Redundancy	12.6 (12.5)	12.6 (12.4)
Completeness %	99.9 (99.4)	98.3 (95.8)
Rmerge %	6.3 (81.3)	12.7 (91.5)
CC(1/2)	99.9 (91.1)	99.8 (89.4)
I/σ(I)	21.37 (2.48)	12.19 (1.92)
Refinement		
Number of reflections (total/test)	40519 (3990)	23545 (2197)
No. of atoms	2747	2650
Protein	2518	2375
Solvent	157	173
Ligand	72	102
Rwork%	0.18	0.20
Rfree%	0.21	0.24
Ligand in chain		
A	thalidomide	iberdomide
B	thalidomide	iberdomide
C	avadomide	iberdomide

3.4 hCRBN

Due to the species-specific differences seen for MsCI4 and the human CRBN in the previous section, it was also desirable to have the human protein available. Based on recently published data [2, 114, 143, 175], we were able to obtain the protein hTBD and the DDB1-CRBN complex. The hTBD could be expressed in

E. coli Rosetta 2(DE3)pLysS after modification of existing protocols and mild protein expression conditions. An expression protocol based on high density Sf9 cells was established for DDB1-CRBN, because this construct was unsuitable for bacterial expression. Both constructs could be expressed and purified to satisfactory levels. GST affinity, followed by size exclusion was used for the purification of hTBD. For the DDB1-CRBN complex, an N-terminal Twin-Strep-tag of CRBN was used to capture the complex via a Strep-Tactin XT column. Initial characterization of DDB1-CRBN by nanoDSF showed that the complex is folded and melts at 47.2 °C (Table 9). Stabilization upon ligand binding as seen for MsCI4 was not observed. Incubation and measurement of T_m with water-soluble succinimide showed no significant effect. Thalidomide seemed to lower the T_m of the complex, however this effect could be contributed to the co-solvent DMSO, which showed similar effects.

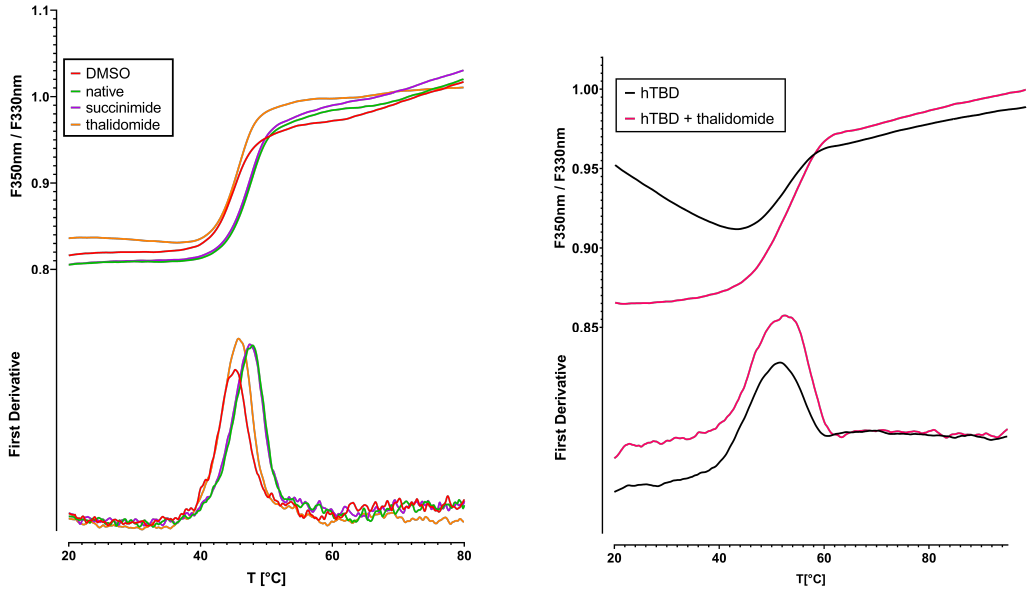

(A) (B)

FIGURE 14: F350nm/F330nm and first derivatives of DDB1-CRBN plotted against temperature gradients from which T_m values were derived. (A) Thermal unfolding curves of DDB1-CRBN. (B) Thermal unfolding curves of hTBD

Table 9: Melting temperatures for human CRBN-constructs measured by NanoDSF (n=3)

T_m [°C]	native	DMSO	thalidomide	succinimide
DDB1-CRBN	47.2 ± 0.0	44.9 ± 0.3	45.3 ± 0.3	47.0 ± 0.3
hTBD	50.2 ± 0.1	-	53.5 ± 0.3	-

As expected, the single hTBD expressed in Rosetta cells showed a higher yield than the DDB1-CRBN insect cell expression. HTBD was well folded and showed higher melting temperatures than DDB1-CRBN as measured by NanoDSF. Ligand binding to hTBD further stabilized the protein as indicated by the shift in melting temperature (Table 9). These initial data, availability and accessibility of the hTBD make this construct highly promising for further in vitro characterizations.

3.5 Conclusions

MsCI4 has proven to be a stable protein for in vitro and structural characterization of CRBN-binders. It has allowed us to characterize the chemical ligand space of CRBN and identify minimal binding moieties [19, 20] and is further used throughout this thesis. Based on MsCI4, we have designed several constructs that show advantages over the WT for specific tasks. Truncated constructs of MsCI4 show potential to be utilized in instances where the full-length protein does not lead to adequately diffracting crystals. Using subsequently humanized constructs allows us to assay for binders that rely on species-specific mutations. Residues identified to be important for neo-substrate recruitment in human CRBN have been introduced in MsCI4 and should allow for further studies of this neomorphic substrate recognition interface. Constructs carrying F77H mutation (MsCI4 α) and surface-exposed residues surrounding the binding pocket (MsCI4 humanized β) allow us to study the binding of small molecules and larger compounds such as PROTACs, with a chemically equivalent binding mode to human CRBN.

Advantages of the WT protein such as high yields in *E. coli*, stability and access to structural characterization via X-ray crystallography also apply for the mutant constructs.

Besides MsCI4, we have also designed constructs of human CRBN. For the expression of DDB1-CRBN, a high-density insect cell expression and purification protocol was established that led to well folded protein. This constructs allows for in vitro studies that are close to the native complex. One disadvantage compared to MsCI4 is the achievable resolution of x-ray crystal structures. Due to the size and flexibility of the DDB1-CRBN complex, crystal structures are usually below 3 Å resolution, while MsCI4 crystals typically diffract to high resolution (<2 Å). A possible alternative here is the use of the TBD of human CRBN. A construct for this hTBD was designed, expressed in *E. coli*, purified and used for biophysical assays. Further experiments will include the attempt to crystallize hTBD, however it must be mentioned that no crystal structure of the human TBD alone has been released yet. Together, the presented work allows us to resort to optimal constructs of CRBN, depending on the task at hand, which will be used throughout this thesis.

Chapter 4

De-novo design of cereblon (CRBN) effectors guided by natural hydrolysis products of thalidomide derivatives

This Chapter was, with small modifications, published in J. Med. Chem. 2019, 62, 14, 6615-6629, June 28, 2019 [65]. Additional experiments conducted on the displacement of endogenous substrates were added under section 4.5.

4.1 Introduction

Classical IMiDs like thalidomide and its second and third generation analogs lenalidomide, pomalidomide, avadomide (CC-122) and iberdomide (CC-220) have constantly emerged to new therapeutic areas. Originally developed as a sedative [181] and banned in 1961 for its catastrophic effects on newborns when used during pregnancy [100, 195], thalidomide and a number of newly developed analogs are approved for the treatment of MM [76], Erythema nodosum [46] and MDS [15, 79]. Because of their pleiotropic and especially anti-angiogenic properties,

IMiDs have further been reported effective in many off-label indications as for Hodgkin's lymphoma [54, 95, 207], Light chain-associated (AL) amyloidosis [168] and Acute myeloid leukemia (AML) [7, 190].

Currently, IMiDs share a common glutarimide moiety (Figure 2), which is connected to a second moiety that is typically derived from phthaloyl. Via the glutarimide moiety, they are able to bind to a tri-tryptophan pocket within the TBD [25, 62, 63] of CRBN. CRBN is the substrate receptor of the Cullin RING E3 ubiquitin ligase CUL4-RBX1-DDB1-CRBN ($CRL4^{CRBN}$) [50] and responsible for the recognition of endogenous substrates such as GS [129], MEIS2 [50] and APP [33]. In presence of IMiDs, however, its substrate specificity is changed. The solvent-exposed second moiety, the protruding moiety that is unique to each IMiD, recruits novel substrates to the CRBN surface for ubiquitination. The degradation of these neo-substrates accounts for most of the efficacy of IMiDs in multiple myeloma (IKZF1 and IKZF3) [93], 5q-deletion associated myelodysplastic syndrome (CK1α) [91] and acute myeloid leukemia (GSPT1) [113]. Recently, it could also be shown that the degradation of the neo-substrate SALL4 is linked to developmental malformations caused by thalidomide [37, 113].
Crystal structures of the neo-substrate complexes $CRBN \cdot lenalidomide \cdot CK1\alpha$, $CRBN \cdot pomalidomide \cdot IKZF1$, and $CRBN \cdot pomalidomide \cdot ZNF692$ provided first insights into the binding mode of neo-substrates [143, 175]. Many of the identified neo-substrates possess no obvious sequence homology, but they all exhibit a structurally analogous β-hairpin, which binds to the surface around the IMiD-binding site, involving interactions with both surface residues and the IMiD itself. A potential prerequisite for the recruitment is the presence of a glycine at the tip of this β-hairpin; this glycine was found to be conserved for many neo-substrates, like CK1α [143] and GSPT1 [116], and appears in the common C X(2)-C-G motif [37] in many transcription factors belonging to the C2H2 zinc finger class, including IKZF3 [143], IKZF1 [143], ZFP91 [37] and SALL4 [37]. While IMiDs seem to generally recruit several members of the C2H2 zinc finger family, only lenalidomide was proven to recruit CK1α, indicating that the protruding moiety imparts substrate specificity. The CRBN-binding ability of IMiDs

has further been exploited for targeted protein degradation in an approach called Proteolysis Targeting Chimera (PROTAC), coined in 2001 by Craig Crews and co-workers [97, 159]. PROTACs are bifunctional small molecules which possess a binding moiety for a target protein fused to a binding moiety for an E3 ubiquitin ligase, thus inducing ubiquitination and proteasomal degradation of the target protein. Recent examples of successful PROTACs target the Estrogen [69] and the Androgen receptor [60] via a VHL E3 ligase ligand, but also BET bromodomains via linkage to thalidomide as a CRBN ligand [206]. Notably, also PROTACs with a VHL ligand on one, and thalidomide as CRBN ligand on the other end have been designed, leading to unidirectional degradation of CRBN [186]. In general, the PROTAC approach has high potential to target the undruggable; a particularly illustrative example for its potential is exemplified by the recent discovery of a PROTACs targeting the Tau protein. To date, essentially all CRBN effectors, IMiDs and CRBN-based PROTACs, are derived from thalidomide and its derivatives. However, the chemical space of CRBN ligands ranges far beyond thalidomide: In a first systematic characterization we have revealed that a large range of lactams and cyclic imides are potent binders, including several marketed drugs [20]. Specifically, we have shown succinimide to exhibit higher affinity than glutarimide, using the single-domain bacterial CRBN homologue from *Magnetospirillum gryphiswaldense* (MsCI4) in a FRET assay [63]. In this study, we set out to further explore and exploit the chemical space of CRBN binding by designing effectors based on succinimide and glutarimide, which we characterize with regard to their affinity, their structural binding mode, and their ability to induce proteasomal degradation of neo-substrates. Guided by hydrolyzed metabolites of thalidomide and of three of our designs, we present novel minimalistic motifs that are able to recruit and degrade neo-substrates, and may serve as E3-recruiting ligands for future PROTACs.

4.2 Biophysical and structural characterization of IMiD analogs and their hydrolysis products

As a starting point for new effectors we chose the classical IMiD scaffold. Based on the finding that succinimide is able to bind to CRBN with a higher affinity than glutarimide (K_i values of 4.3 μM vs. 28 μM for MsCI4 [20]), we designed a first panel of derivatives based on glutarimide and succinimide, in which we probed the effect of different substitutions in the phthaloyl moiety (Figure 16). The respective compounds 2a-5b were prepared by the synthetic route shown in Figure 15. The imides 3a and 3b were synthesized from the commercially available Nα-(tert-butoxycarbonyl)-L-asparagine (1a) and Nα-(tert-butoxycarbonyl)-L-glutamine (1b) respectively via an imide formation using N,N-carbodiimidazole (CDI) and 4-dimethylaminopyridine (4-DMAP) in THF as well as a deprotection reaction in the presence of trifluoracetic acid (TFA). Compounds 4a-4d were obtained through a coupling between the imides 3a or 3b and the commercially available 3-nitrophthalic anhydride or 4-nitrophthalic anhydride. Catalytic hydrogenation of the molecules 4a and 4b using 10 wt% Pd/C in EtOAc produced the derivatives 5a and 5b.

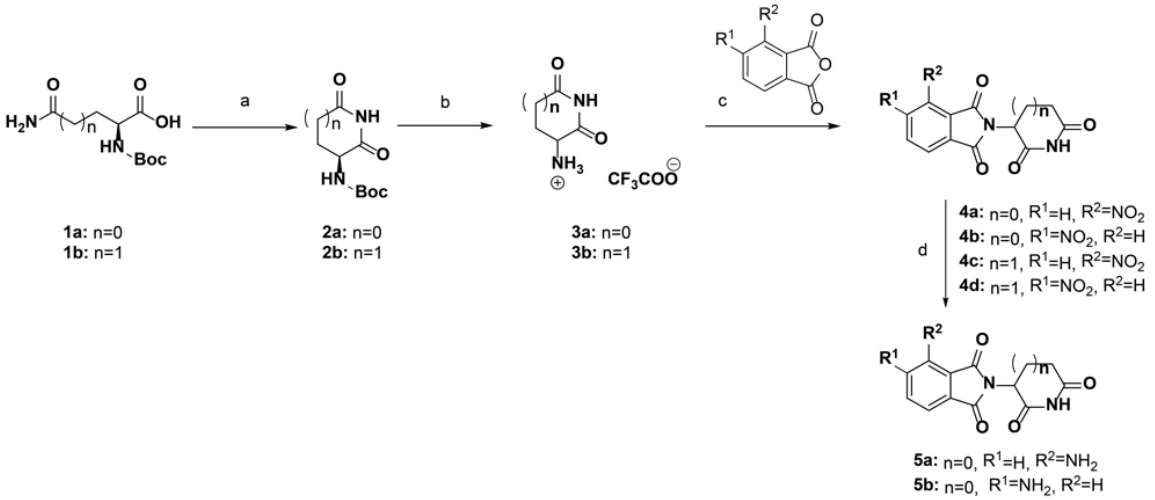

FIGURE 15: Reagents and conditions: (a) CDI, 4-DMAP, THF, reflux, 17-48 h; (b) TFA, RT, 30 min; (c) CDI, 4-DMAP, THF, reflux, 5-20 h; (d) 10 wt. % Pd/C, EtOAc, RT, 20 h

The binding affinities of these compounds for MsCI4 were assessed in the FRET assay, starting with the glutarimide-based compounds 4c and 4d in comparison to the commercial thalidomide derivatives lenalidomide and pomalidomide. Lenalidomide (K_i = 3.1 μM) and pomalidomide (K_i = 0.8 μM), both carrying an additional amino group in the R^2 position, show improved affinity to MsCI4 as compared to thalidomide (K_i = 4.4 μM). When we exchanged this amino group for a nitro group (4c), we saw a significant drop in affinity, into a range in which a precise value could not be obtained ($K_i > 40$ μM) [20]; moving this nitro group to the R^1 position (4d) had less impact on the affinity (K_i = 8.9 μM, Figure 16A). Similar effects were observed in a recent study that was published during the preparation of this manuscript [23]. As both compounds, 4c and 4d, retained affinity to MsCI4, their overall binding mode is supposedly conserved and comparable to thalidomide, which is consistent with previous studies showing that small modifications on the protruding moiety have little influence on the overall affinity to CRBN [50, 63]. The binding modes of lenalidomide and pomalidomide have previously been reported to be virtually identical to thalidomide [25, 143]. For the succinimide-based compounds 4a, 4b, 5a and 5b, we obtained a similar picture as for the glutarimide-based compounds. Although they showed overall weaker binding in the FRET assay (Figure 16 B), substitutions in the R2 position are less favorable for the affinity as substitutions in R^1. For 4a and 5a, which have a nitro or an amino group in R^2, respectively, we obtained K_i values of > 40 μM. For 4b and 5b, which have the respective groups in the R^1 position, the obtained K_i values are 11 μM and 12 μM, respectively.

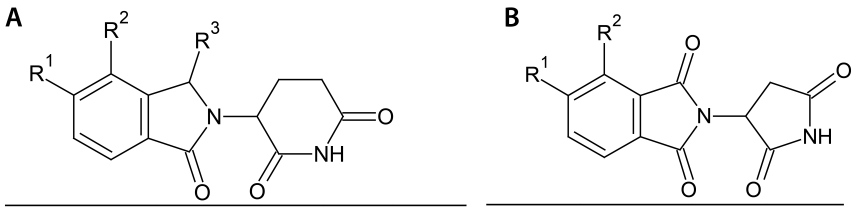

Name	K_i (μM)	R^1	R^2	R^3
thalidomide	4.4 ± 0.2	H	H	=O
pomalidomide	0.80 ± 0.2	H	NH_2	=O
lenalidomide	3.1 ± 0.7	H	NH_2	H
4c	>40	H	NO_2	=O
4d	9.0 ± 1.6	NO_2	H	=O

Name	K_i (μM)	R^1	R^2
4a	>40	H	NO_2
4b	11 ± 1.8	NO_2	H
5a	>40	H	NH_2
5b	12 ± 0.7	NH_2	H

FIGURE 16: The first panel of chemical structures, five- and six-ring based thalidomide analogs and their affinity to MsCI4 determined as K_i values in the FRET assay.

In a next step, we determined the molecular binding determinants of the succinimide-based compounds via X-ray crystallography. To this end, crystals of the MsCI4 · thalidomide complex were reproduced [20] and subsequently used for soaking experiments, in which the thalidomide molecules bound to MsCI4 may be displaced by the compound of interest. There are three chains, i.e. three MsCI4 · thalidomide complexes, in the asymmetric unit (ASU) of these crystals, in which the bound thalidomide molecules can potentially be displaced. However, as the three chains form different crystal contacts and differ slightly in their conformation, it is possible that thalidomide is only replaced in one or two chains of the ASU, depending on the particular compound [20]. These experiments yielded crystal structures for the four compounds tested, 4a, 4b, 5a and 5b, all showing the classical IMiD binding-mode with the basal main-chain interactions of the succinimide amino-group with F77 and the carbonyl group with W79 of MsCI4. Also the orientation of the protruding moieties of 4a, 5a and 5b are very similar to that of thalidomide, despite the different ring size of glutarimide and succinimide. As a result, the hydrogen bond that is typically observed between the conserved N50 and a carbonyl group of the phthaloyl moieties for the classical glutarimide-based compounds is also found for 5b.

However, the crystal structures also held surprises. They did not only reveal the binding modes of the pure compounds, but also that of hydrolysis products

of 4a, 4b and 5a with unambiguous electron density; only 5b was exclusively observed in non-hydrolyzed form (Figures 17, 18). For 4a and 5a, hydrolyzed metabolites were only observed in one chain of the ASU, with the second chain occupied with a non-hydrolyzed version and the third chain with thalidomide. For 4b, which showed the highest affinity with a K_i of 11 µM, all three binding pockets in the ASU were occupied by a hydrolyzed metabolite, so the binding mode of non-hydrolyzed 4b could not be studied. In all cases, for the hydrolysis products of 4a, 4b and 5a, ring opening of the phthaloyl group had led to the formation of a secondary amide and a carboxyl group, which are clearly resolved in F_O-F_C omit maps (Figure 17). Both of these form important interactions with the binding pocket: Firstly, the secondary amide rescues the hydrogen bond to the conserved N50, which is typically formed by a carbonyl of the phthaloyl moiety. Secondly, the additional carboxyl group replaces a conserved water molecule previously coordinated by W99 and engages in direct hydrogen bonding with the W99 side chain. In contrary, the primary amino group of hydrolyzed 5a and the solvent exposed nitro groups of hydrolyzed 4a and 4b do not show additional interactions.

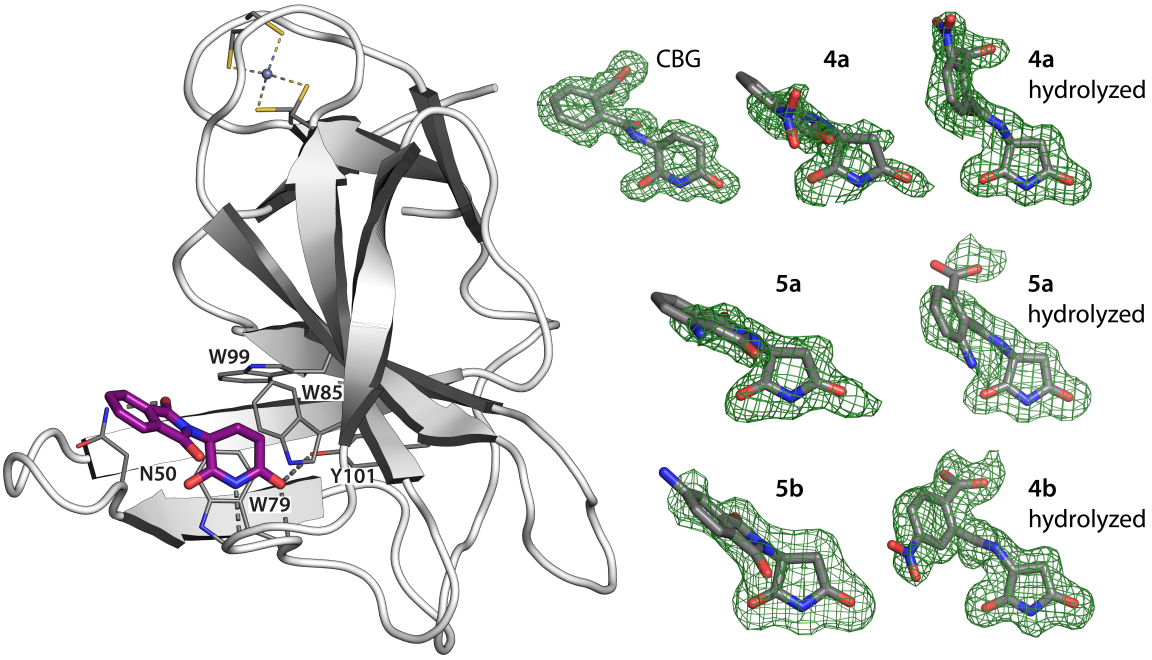

FIGURE 17: Overview of the thalidomide binding mode and electron densities of thalidomide analogs and their hydrolysis products bound to MsCI4. Left: Cartoon representation of thalidomide-bound MsCI4 with key residues of the binding pocket shown as sticks. Right: FO - FC maps of CBG (PDB 6R0Q), 4a and hydrolyzed 4a (PDB 6R0S), hydrolyzed 4b (PDB 6R0V), 5a and hydrolyzed 5a (PDB 6R0U) and 5b (PDB 6R11) in the MsCI4 binding pocket, contoured at 2σ.

4.3 Binding mode of CBG, a major hydrolysis product of thalidomide

Admittedly unintentionally, in addition to the hydrolysis products of 4a, 4b and 5a, we were able to characterize the binding mode of a major hydrolyzed thalidomide metabolite. It is known that IMiDs can rapidly racemize in bodily fluids and water [9], and spontaneously hydrolyze under physiological conditions [27, 153, 167]. For thalidomide, being eliminated mainly by spontaneous hydrolysis in blood and tissues, a half-life of about 5.5 to 7.3 h at the physiological pH of 7.4 was reported [189]. Among several proposed hydrolysis products, the two main urinary metabolites are 2-phthalimidoglutaramic acid (50%) and α(2-carboxybenzamido) glutarimide (CBG) (30%) [12]. Of these, CBG has an unmodified glutarimide moiety, and is also one of three major metabolites

in human plasma [29]. As CBG was also reported to possess higher TNF-α production-inhibitory activity (80%) than thalidomide (32%) at concentrations of 3 μM [29, 124], it is of great pharmacological interest, but its mode of interaction remained elusive so far [137]. During the course of this study, we obtained a crystal structure of CBG in complex with a humanized mutant form of MsCI4 (Figures 17, 18). This structure was the result of a co-crystallization trial of this mutant with thalidomide, which aimed at the characterization of the mutant protein. However, the mutant selectively bound CGB that was presumably present in traces in our crystallization setup with thalidomide. This mutant has a number of non-conserved residues in the direct vicinity of the thalidomide binding pocket mutated to the residues in the human protein, including the substitution F56H. While this residue is not directly involved in classical IMiD binding in MsCI4 or the human protein, it plays an important role in the binding of CBG: Together with N50, it coordinates one oxygen of the carboxyl group in the CBG protruding moiety; the other oxygen of this carboxyl coordinates the conserved water molecule bound to W99. However, in contrast to the hydrolysis products of the succinimide-based compounds 4a, 4b and 5a, the amide moiety resulting from ring-opening is not found to be involved in defined hydrogen bonding – although superposing approximately with the phthaloyl moiety of thalidomide, it does not form the canonical hydrogen bond with N50, as the latter is engaged in the hydrogen bond to the carboxyl group.

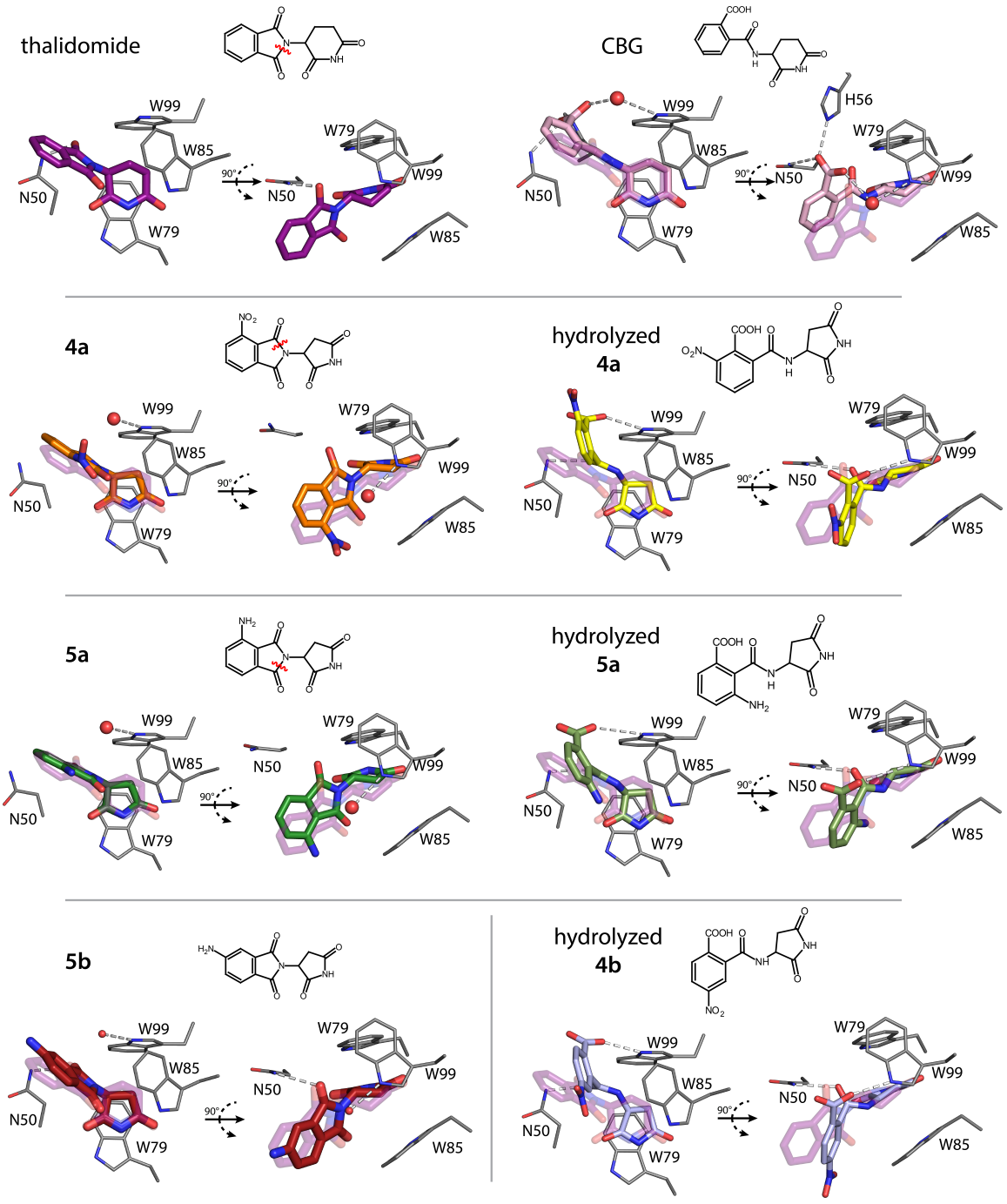

FIGURE 18: The binding mode of the initial compounds and their hydrolysis products inside the binding pocket. Thalidomide, 4a and 5a are shown with their respective hydrolysis products. Ring opening of the phtaloyl moiety that leads to the observed hydrolysis product is indicated in red in the chemical drawings. 5b was exclusively found in non-hydrolyzed form, whereas 4b was exclusively found as a hydrolysis product.

4.4 Rational design of novel succinimide effectors guided by hydrolyzed metabolites

In a next step, we aimed to exploit our knowledge on the binding mode of hydrolyzed metabolites for the design of novel effectors. The fact that the hydrolysis products were selected against their parent compounds in several co-crystallization or soaking experiments suggested that they pose binders of similar, if not superior affinity. Comparing the binding modes of CBG and hydrolyzed 4a, 4b and 5a, we further hypothesized that the difference seen for the hydrogen bonding of their amide linkers should yield increased affinity for succinimide-based effectors. Consequently, we used this amide linker to connect different functional groups as protruding moieties to succinimide as the binding moiety. To this aim, we prepared derivatives 7a-7h as shown in Figure 19, by treating imide 3a with the corresponding acyl chlorides 6a-6h and N, N-diisopropylethylamine (DIPEA) in THF.

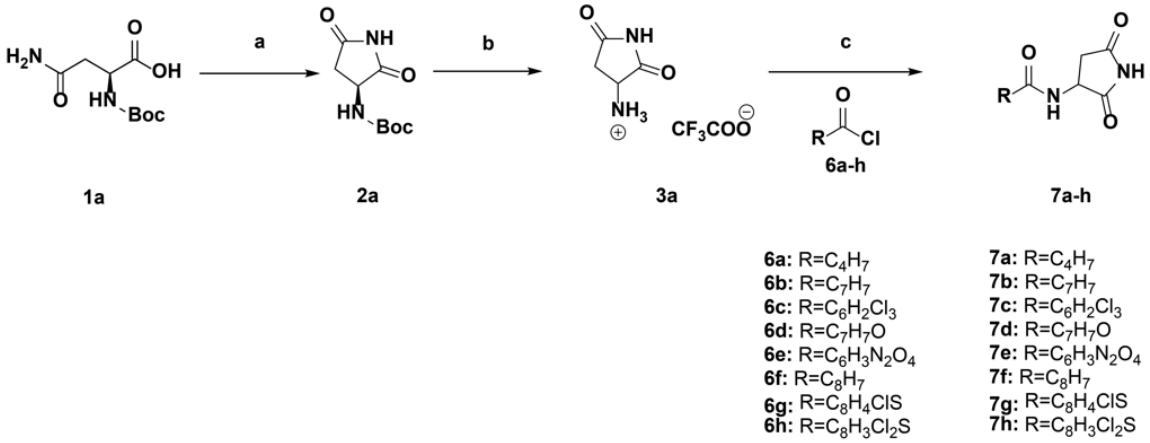

FIGURE 19: Reagents and conditions: (a) CDI, 4-DMAP, THF, reflux, 48h; (b) TFA, RT, 30 min; (c) 6a-h, DIPEA, THF, 0 °C to reflux, 2 h

All derivatives of this second panel were tested in the FRET assay. Only for compound 7e, with a 3,5-dinitrobenzol group, the affinity was decreased under the detectable levels of the FRET assay. For the compounds with an isobutylene (7a), benzyl (7b) or chlorobenzothiophene group (7g) as the protruding moiety,

binding was well detectable but could not be quantified ($K_i > 40$ μM). Better binding was observed for compounds with a styryl (7f) and dichloro-benzothiophene (7h) group, both showing K_i values of 20 μM (Figure 20 A). Finally, the highest affinities were achieved with a 2,4,6-trichlorobenzol moiety (7c, $K_i = 9$ μM) and benzyloxy group (7d, $K_i = 4$ μM), rendering 7d the highest-affinity binder in this study, with a K_i value comparable to unmodified succinimide [20] (Figure 20 A).

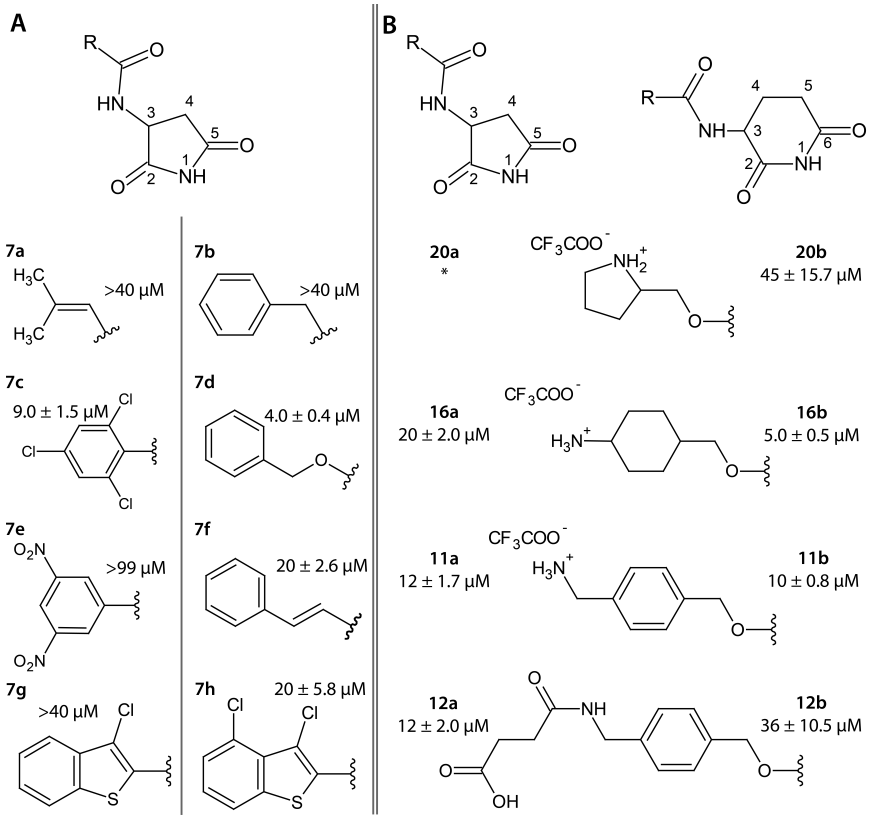

FIGURE 20: Compounds inspired by hydrolysis products of thalidomide analogs and their affinity data. (A) Second panel of compounds, based on the 3-amidosuccinimide scaffold. (B) Third panel of compounds, inspired by 7d. ∗ 20a could not be purified to satisfactory levels for affinity testing.

We continued with characterizing the binding modes of compounds 7a-c and 7f via crystallography. For the best binder 7d we performed a co-crystallization screen, which yielded a new crystal form diffracting to 1.1 Å resolution; the other compounds were successfully evaluated in soaking experiments. All compounds revealed the expected binding mode as observed for the hydrolyzed metabolites of 4a, 4b and 5a, with the succinimide moiety forming the canonical interaction

within the binding pocket, and the amide linker forming the hydrogen bond with N50. Besides these hydrogen bonds of the binding and linking moiety, no defined interactions with the protein were found for the protruding moieties of any of the five compounds, including the best binder 7d. Figure 21 shows a superposition of the compounds of this panel and their conserved binding mode in the aromatic cage.

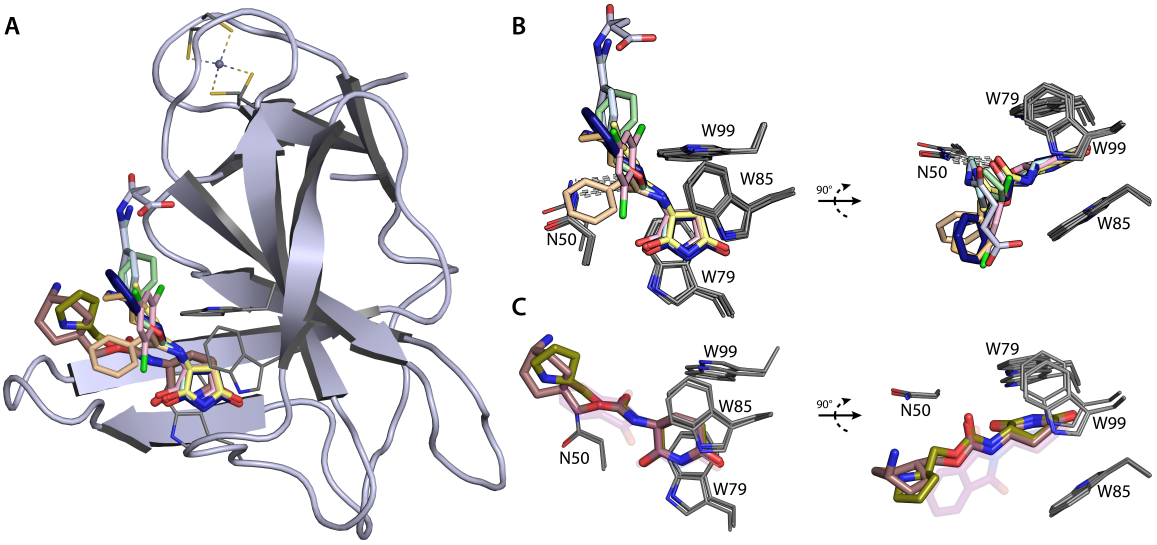

FIGURE 21: Binding modes of compounds from the second and third panel. (A) Superposition of all compounds bound to MsCI4. (B) Detailed side and top view of bound effectors based on the 3-amidosuccinimide scaffold: 7a (yellow, PDB 6R1X), 7b (sand, PDB 6R12), 7c (pink, PDB 6R1K), 7d (green, PDB 6R1D), 7f (blue, PDB 6R13) and the water soluble 11a (cyan, PDB 6R18) and 12a (light blue, PDB 6R1C), indicating interactions with N50. (C) Side and top view of compounds based on 3-amidoglutarimide, 16b (brown, PDB 6R1W) and 20b (dark green, PDB 6R1A). Although the depicted instances for this scaffold do not show the interaction with N50, this interaction was observed in one other instance for 16b.

Based on these data, we hypothesized that the planar benzene connected via an oxygen as in 7d is favorable for the affinity. Consequently, we designed a third panel of derivatives carrying this feature based on succinimide and glutarimide (Figure 20 B). In this panel, in addition to affinity improvement, we also sought to increase the solubility in water via additional polar or charged groups. As described in 22, reaction of the intermediates 8, 13 and 17 with phosgene solution (15 wt% in toluene) in THF yielded to the corresponding chloroformates

9, 14 and 18. Derivatives 11a, 11b, 16a, 16b, 20a and 20b were prepared by a coupling reaction between the imides 3a or 3b and the aforementioned chloroformates 9, 14 and 18 using N,N-diisopropylethylamine (DIPEA) in THF followed by a deprotection using trifluoracetic acid (TFA). Treatment of the derivatives 11a and 11b with succinic anhydride and triethylamine (Et3N) in DMF produced the molecules 12a and 12b, respectively.

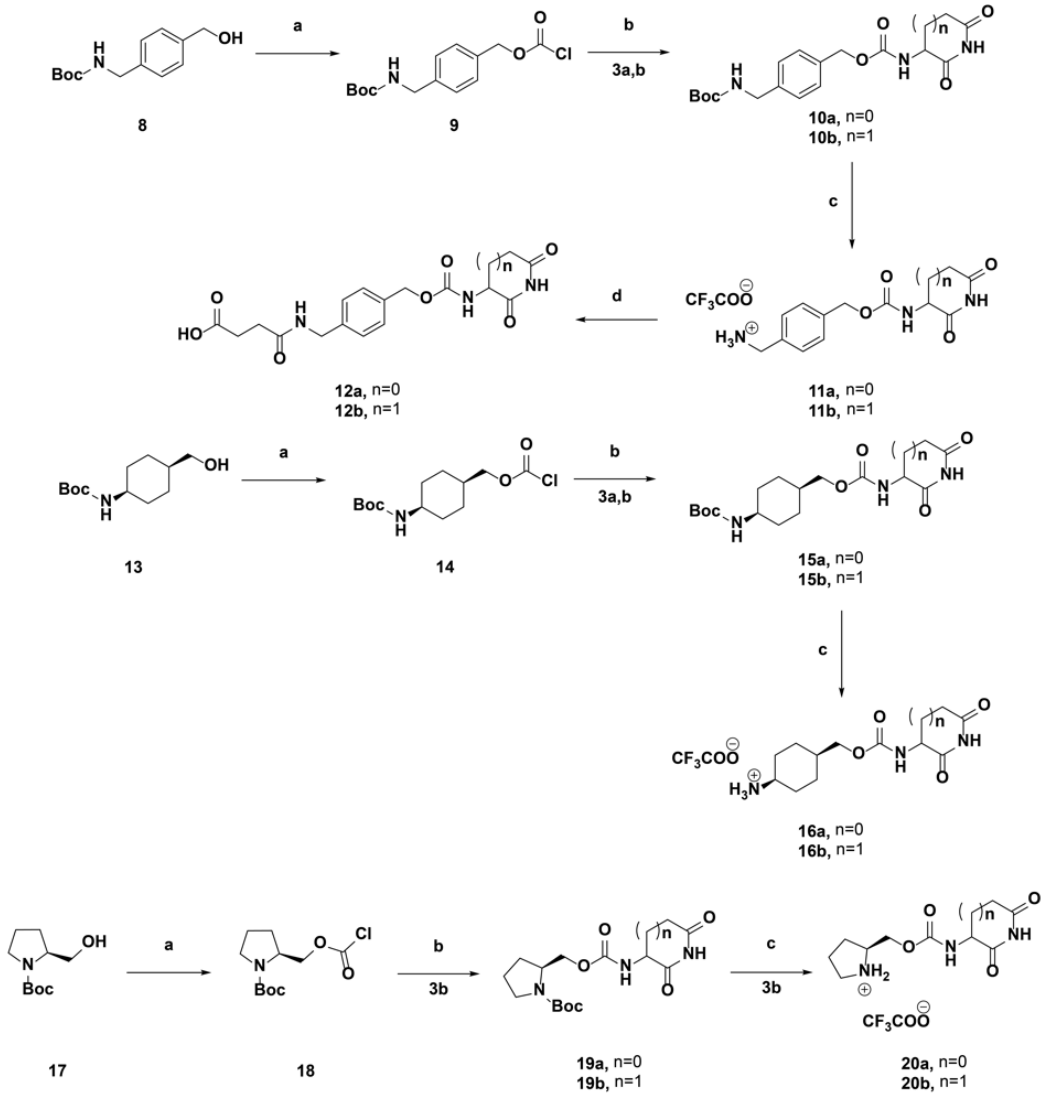

FIGURE 22: Reagents and conditions: (a) Phosgene solution 15 wt. % in toluene, THF, 0 °C to RT, 20 h; (b) 3a or 3b, DIPEA, THF, 0 °C to reflux, 20 h; (c) TFA, DCM, 0 °C to RT, 2 h; (d) Et_3N, DMF, 0 °C to RT, 20 h. Note that 13 and thereby also 14-16 are in cis conformation.

Indeed, the final compounds with terminal amino groups were water soluble

(11a, 11b, 16a, 16b), while 12a and 12b, with a terminal succinyl group, were highly soluble in bicarbonate buffer (>200 mM). The compounds were subsequently tested in the FRET assay, apart from 20a, which still contained impurities. The assay indicated that all derivatives retained high affinity for CRBN independent of binding moiety and planarity of the substituent; a clear preference for either binding moiety was not recognizable. In soaking experiments, we obtained crystal structures with the 5-ring members 11a, 12a, 20a, and the 6-ring members 16b and 20b, all forming the canonical interactions within the aromatic cage. As expected, the 5-ring effectors form the interaction of the amide linker with N50, which is also observed in one instance for the 6-ring effector 16b. Further interactions of the protruding moieties are not observed for any of the compounds. Consequently, the prolonged extensions are less resolved in the electron density map, which is especially evident for 12a (Figure 23). As these prolonged compounds still retain high affinity, this confirms that the amidosuccinimide scaffold can serve as universal CRBN-binding moiety allowing great chemical variability on the protruding moiety.

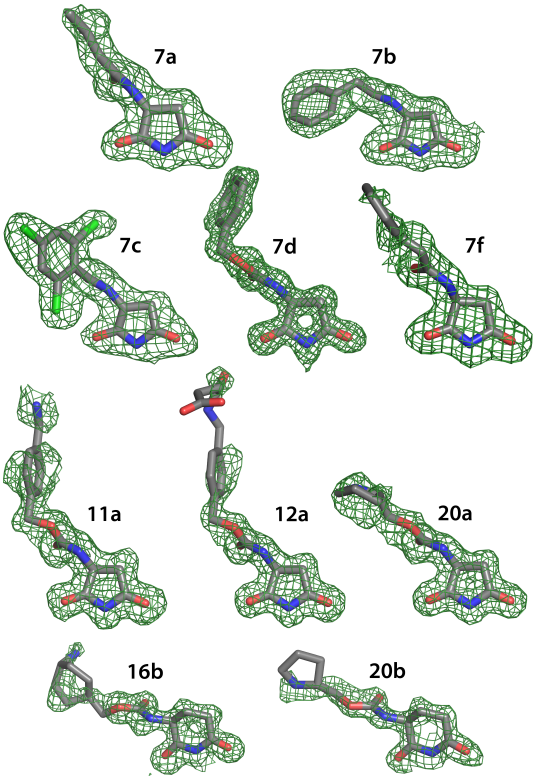

FIGURE 23: $F_O - F_C$ maps of bound compounds shown in Figure 21. All compounds are clearly defined by their electron density maps with the exception of the prolonged extension in 12a. Crystallographic structures were refined to resolutions between 1.1 Å and 1.8 Å, the maps are contoured at 2σ.

TABLE 10: Data Collection and Refinement Statistics of crystal structures with novel succinimide effectors and thalidomide hydrolysis product

	MsCl4 · 4a	MsCl4 · 4b	MsCl4 · 5a	MsCl4 · 5b	MsCl4 · 7a
Data Collection					
Space group	P212121	P212121	P212121	P212121	P212121
Unit cell					
a, b, c (Å)	56.46, 58.82, 88.23	56.75, 58.82, 88.57	56.95, 59.58, 89.05	56.66, 58.71, 88.01	56.33, 58.68, 89.27
α, β, γ (°)	90, 90, 90	90, 90, 90	90, 90, 90	90, 90, 90	90, 90, 90
Resolution range, Å	44.1 - 1.55 (1.64 - 1.55)	44.28 - 1.6 (1.7 - 1.6)	44.53 - 1.7 (1.8 - 1.7)	47.64 - 1.75 (1.85 - 1.75)	49.03 - 1.8 (1.86 - 1.8)
Redundancy	12.7 (11.8)	12.9 (12.9)	12.4 (12.8)	12.8(12.8)	12.86(12)
Completeness %	99.8 (98.9)	99.9 (99.4)	99.0 (98.2)	99.6 (97.7)	99.6 (97.6)
Rmerge %	9.0 (98.2)	5.3 (82.8)	7.3 (94.6)	6.6 (98.5)	7.2 (89.0)
CC(1/2)	99.9 (85.4)	100 (90.4)	99.9 (87.8)	100 (87.6)	100 (84.6)
I/σ(I)	15.09 (1.78)	25.88 (2.73)	20.22 (2.02)	20.47 (2.27)	22.12(2.39)
Refinement					
Number of reflections (total/test)	43370 (4254)	39841 (3904)	33803 (3354)	30301 (2985)	28122 (2771)
No. of atoms	2871	2787	2767	2709	2544
Protein	2572	2519	2504	2523	2338
Solvent	223	173	185	134	175
Ligand	76	95	78	52	31
Rwork%	0.17	0.19	0.18	0.19	0.17
Rfree%	0.20	0.22	0.23	0.23	0.22
Ligand in chain					
A	thalidomide	hydrolyzed 4b	thalidomide	5b	7a
B	4a	hydrolyzed 4b	hydrolyzed 5a	5b	7a
C	hydrolyzed 4a	hydrolyzed 4b	5a	-	-
PDB ID	6R0S	6R0V	6R0U	6R11	6R1X

	MsCI4 · 7b	MsCI4 · 7c	MsCI4 · 7d	MsCI4 · 7f	MsCI4 · 11a
Data Collection					
Space group	P212121	P212121	P21	P212121	P212121
Unit cell					
a, b, c (Å)	56.42, 58.80, 88.23	56.33, 58.68, 89.27	31.63, 52.39, 59.29	56.87, 58.55, 88.28	56.63, 59.59, 88.90
α, β, γ (°)	90, 90, 90	90, 90, 90	90.0, 95.8, 90.0	90, 90, 90	90, 90, 90
Resolution range, Å	48.93 - 1.73 (1.84 - 1.73)	49.03 - 1.85 (1.96 - 1.85)	39.2 - 1.1 (1.16 - 1.1)	44.14 - 1.65 (1.75 - 1.65)	44.45 - 1.35 (1.43 - 1.35)
Redundancy	12.5 (12.0)	12.9 (13.0)	6.3(5.3)	12.9 (13.2)	12.7 (12.4)
Completeness %	98.8 (92.4)	99.8 (98.6)	99.1 (95.1)	99.9 (99.6)	99.9 (99.3)
Rmerge %	14.2 (88.8)	6.1 (102.8)	5.3 (39.4)	6.9 (81.5)	7.4 (96.3)
CC(1/2)	99.6 (85.7)	99.9 (78.1)	99.8 (92.4)	99.9 (86.6)	99.9 (83.2)
I/σ(I)	10.55 (1.73)	21.46 (2.25)	17.67 (3.64)	20.72 (2.35)	17.62 (1.97)
Refinement					
Number of reflections (total/test)	30582 (2948)	28122 (2771)	77822 (7458)	36182 (3558)	66738 (6544)
No. of atoms	2778	2675	2082	2464	2977
Protein	2521	2468	1768	2229	2619
Solvent	187	123	276	166	281
Ligand	70	84	38	69	77
Rwork%	0.17	0.18	0.12	0.20	0.16
Rfree%	0.23	0.22	0.15	0.22	0.19
Ligand in chain					
A	thalidomide	7c		thalidomide	thalidomide
B	7b	7c	Co-crystal with 7d	7f	11a
C	thalidomide	7c		-	thalidomide
PDB ID	6R12	6R1K	6R1D	6R13	6R18

	MsCI4 · 12a	MsCI4 · 16b	MsCI4 · 20a	MsCI4 · 20b	MsCI4 · CBG
Data Collection					
Space group	P212121	P212121	P212121	P212121	P21
Unit cell					
a, b, c (Å)	56.66, 59.02, 88.59	56.53, 59.44, 88.36	56.56, 59.23, 88.43	56.56, 59.3, 88.0	61.7, 59.1, 61.7
α, β, γ (°)	90, 90, 90	90, 90, 90	90, 90, 90	90, 90, 90	90, 105.6, 90
Resolution range, Å	49.12 - 1.5 (1.59 - 1.5)	47.62 - 1.35 (1.43 - 1.35)	49.21 - 1.45 (1.50 - 1.45)	49.18 – 1.54 (1.64-1.54)	49.17 - 1.50 (1.59 – 1.50)
Redundancy	12.6 (12.6)	12.6 (12.7)	12.8 (12.9)	12.6 (12.1)	3.4(3.1)
Completeness %	99.5 (97.2)	99.8 (99.1)	99.8 (98.5)	99.5 (96.7)	99.0 (97.5)
Rmerge %	11.4 (78.6)	7.9 (98.8)	9.5 (89.4)	13.1 (81.5)	8.0 (88.0)
CC(1/2)	99.8 (86.5)	99.9 (84.0)	99.8 (86.2)	99.7 (83.8)	99.8 (55.6)
I/σ(I)	14.29 (2.32)	16.63 (1.85)	14.83 (2.11)	10.28 (1.71)	9.70(1.15)
Refinement					
Number of reflections (total/test)	48282 (4739)	66083 (6516)	53344 (5211)	44026 (4112)	68399 (6707)
No. of atoms	2995	3057	3074	2928	3985
Protein	2665	2638	2634	2617	3480
Solvent	252	338	339	232	421
Ligand	78	81	101	79	84
Rwork%	0.21	0.16	0.17	0.18	0.16
Rfree%	0.24	0.20	0.20	0.21	0.20
Ligand in chain					
A	thalidomide	thalidomide	thalidomide	thalidomide	
B	12a	16b	20a	thalidomide	Co-crystal with CBG
C	thalidomide	16b	thalidomide	20b	
PDB ID	6R1C	6R1W	6R19	6R1A	6R0Q

4.5 Displacement of endogenous substrates

After assessing the biophysical and structural parameters of our designs, we tested their potential for the displacement of endogenous substrates. By using on-chip ubiquitination, Fischer et al [50] identified several possible endogenous substrates of CRBN. Treatment of M059J cells (previously found to have high expression levels of MEIS2) with IMiDs and proteasome inhibitors showed increased steady-state levels. We hypothesized that endogenous substrates of CRBN, independent from the nature of the ligand, should be displaced from the E3-complex and thereby protected from proteasomal degradation. Having confirmed high affinity binding of several 5- and 6-ring analogs, we aimed to test their potential to displace various endogenous CRBN-substrates. To this end, M059J cells were cultured in our lab and subjected to increasing concentrations of

small molecules and proteasome inhibitors. Antibody test blots were performed and initially showed good intra-blot variability (CV<5%)

Cells were incubated with different concentrations of diluent (DMSO), proteasome inhibitor (bortezomib), classical IMiDs and compounds 7a, 7b and aminosuccinimide (Figure 20). After incubation, cells were lysed and subjected to gel electrophoresis and transferred onto membranes. After overnight incubation with primary antibody, blots were either subjected to HRP-conjugated secondary antibodies and developed using ECL-substrate, or IR-labeled (800 nm) secondary antibodies. Blots using ECL (upper panel Figure 24) showed sufficient resolution and transfer of endogenous MEIS2 protein. However, detection limits of MEIS2 appeared to be much higher than for actin. Although this is to be expected for housekeeping proteins, the detection limit for MEIS2 appeared to be too high for reliable read-out. Chemiluminescence detection in western blots only has very narrow linear ranges which makes them not suitable for quantitative immunoassays. Here, detection based on fluorescently labeled secondary antibodies is usually the method of choice which shows improved read-out stability and linear range for target protein and normalization signal. As expected, MEIS2 immunoblots using IR fluorescence showed improved linear range and signal-to-noise (bottom panel Figure 24).

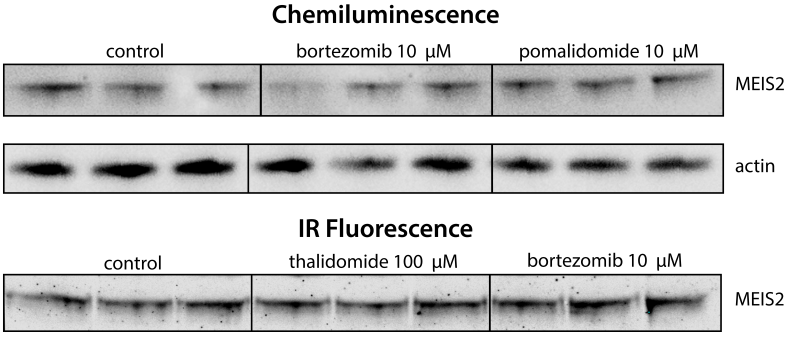

FIGURE 24: Densiometric analysis of endogenous MEIS2 levels of M059J cells upon treatment with the indicated compounds

However, quantitative analysis showed only minor changes of MEIS2 levels independent of compounds treatment (Figure 25). Significant changes were seen for

7a and 10 µM thalidomide, however in a negative manner. In this assay, compound treatment did not seem to protect MEIS2 from proteasomal degradation.

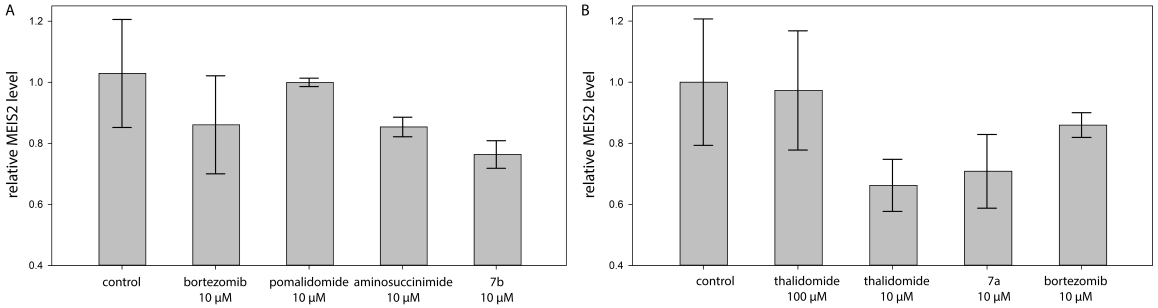

FIGURE 25: Relative MEIS2 levels of M059J cells upon treatment with proteasome inhibitor and small molecule effectors, detected via (A) chemiluminescence and (B) IR-detection

These finding can be due to several reasons. Due to the nature of cell-based assays, standard deviations are usually higher than in other in-vitro experiments. However, control measurements performed with DMSO in this assay are in acceptable ranges and comparable to previously reported data [50]. Comparing published data with our initial results indicates that the low expression of MEIS2 seems to be of general difficulty. Even in M059J cells, which were characterized to have high levels of MEIS2 messenger RNA [50], detection of endogenous MEIS2 was rather difficult. Comparison of different antibodies (monoclonal and polyclonal) only showed the detection of additional protein bands, but did not lead to lower detection limits for MEIS2. Western blot workflow in the lab and in general has since been improved by the usage of pre-made stacks for the transfer of protein to membrane, the usage of cross-adsorbed IR-labeled secondary antibodies, and the usage of total protein loading control and will be repeated in future experiments. However, for this study the scientific impact did not justify longer assay development. In the meantime, further studies showed that MM-derived cell lines show altered expression levels of MEIS2 upon IMiD treatment [1], suggesting a more complex interplay in MEIS2 turnover than previously thought.

4.6 Degradation of neo-substrates

After testing our designs for the displacement of endogeneous substrates, we tested their potential for the degradation of neo-substrates in the MM-derived human cell line OPM-2. To this end, we have selected the established neo-substrates IKZF3, which is targeted via a variety of IMiDs [92, 93, 113, 162], and CK1α, which is so far only targeted via lenalidomide [91], as two complementary targets. We therefore treated OPM-2 cells for 24 h with the different compounds and assayed for the endogenous levels of both neo-substrates; for comparison, the classical IMiDs thalidomide, lenalidomide and pomalidomide were included in the test set. As anticipated, the results for the two neo-substrates were very different. None of the marketed IMiDs apart from lenalidomide was able to reduce the levels of CK1α significantly [91], but also none of our compounds showed any effect on CK1α. This indicates that our compounds could neither supersede nor sufficiently mimic the interface for CK1α recruitment formed by lenalidomide, substantiating the notion of a very narrow specificity window for this substrate [91]. However, the situation was completely different for IKZF3. Here, in addition to all classical IMiDs, multiple of our designs were successful: Significant effects were observed for 5a, 7d and 7f, which are all compounds with a rather compact structure from our first and second panel (Figure 26). The only successful compound from the first, phthaloyl-based panel, 5a, represents a direct succinimide analog of pomalidomide. It reduced IKZF3 levels by almost 40%. Comparison of its structural binding mode to that of thalidomide or pomalidomide already suggested that it may be a possible functional substitute for pomalidomide. The fact that the other compounds of that panel did not show similar effects indicate that substitutions larger than an amino group in the R^2 position of the phthaloyl moiety, as for 4a and 4c, or any substitution in R^1, as for 4b, 4d, and 5b, abolish IKZF3 recruitment.

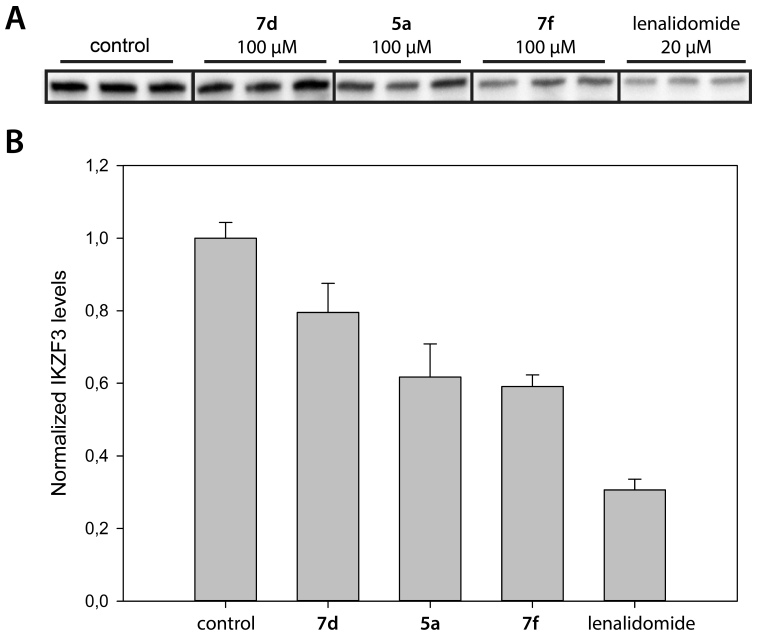

FIGURE 26: Compound-mediated IKFZ3 degradation in vitro.
(A) Immunoblot analysis of IKZF3 levels in OPM-2 cells after treatment with indicated compounds (100 µM) for 24 h, compared to DMSO (control) and lenalidomide (20 µM) (n=3). Lenalidomide at 100 µM reduced IKFZ3 levels effectively by 100% (not shown). (B) Averaged IKZF3 levels from the three independent experiments, normalized against total protein loading control (see supplementary [65]). The significance of the data was tested comparing IKZF3 levels in the presence of the compounds and DMSO ($p > 0.05$).

Most interesting is the analysis of the successful compounds of the second panel, 7d and 7f, which are not derived from classical IMiDs, but from the hydrolysis products of the first panel. 7d, which is also the highest-affinity binder in this study, reduced IKZF3 levels by about 20%. Moreover, the analogous 7f, which is a weaker binder that only differs from 7d in one heavy atom in the linker, reduced IKZF3 levels by even 40%. Both compounds are more flexible and elongated than 5a, so it appears impossible that their protruding moieties adopt a conformation mimicking the classical IMiDs at the interface between CRBN and IKZF3. Their terminal benzyl groups inevitably project further away from the thalidomide binding pocket, requiring another mode of interaction with the zinc finger motif than characterized for classical IMiDs [175]. This interaction mode is also very sensitive to chemical changes: Shortening of the linker by only one atom, as for 7b, further modifications on the benzyl group, as for 11a or 12a, or any other

variant we designed in the second or third panel abolished IKZF3 recruitment, which is indicative for a highly specific interaction. Therefore, 7d and 7f are the first representatives of a novel type of CRBN effectors with a recognition mode that is clearly distinct from that of the classical thalidomide-based IMiDs.

4.7 Conclusions

The development of novel CRBN effectors is a rapidly growing field, with ever expanding therapeutic areas. For both main thrusts of this field, IMiDs and PROTACS, novel compounds are reported frequently. To date, essentially all of these CRBN effectors are based on the classical thalidomide scaffold, which significantly restrains the chemical space available for the recruitment of neo-substrates. Here, following on from our previous characterization of CRBN-binding moieties, we have probed the chemical space for the linking and protruding moiety, taking advantage of the structural binding modes of hydrolyzed metabolites. Although not in the focus of this work, the apparent specificity of CRBN for these hydrolysis products, especially for the major thalidomide metabolite CBG, may inspire further research towards the understanding of their pharmacological relevance. As a consensus from the binding modes of our initial designs and their hydrolysis products, we derived an amidosuccinimide scaffold as a minimal binding and linking moiety. 3-amidosuccinimide can be used to mount almost arbitrary chemistry as the protruding moiety, while retaining affinities to CRBN in the range of classical IMiDs, rendering it an attractive CRBN-binding moiety for future PROTACs. However, the most relevant aspect of our study concerns the versatility of the 3-amidosuccinimide scaffold for the design of IMiD-like CRBN effectors. As a minimal binding and linking moiety, it does not restrain the chemical space of protruding moieties, allowing for the design of substrate-recruiting motifs that cannot be realized on a classical IMiD scaffold. In our attempt to probe the effect of different protruding moieties mounted on the amidosuccinimide scaffold, two out of twelve compounds were able to recruit the neo-substrate IKZF3 without further optimization. Although we do not have structural insight into the

IKZF3 recognition mode of these effectors, it is clearly incompatible with that of the classical IMiDs, which points at a large unexplored chemical space for the recruitment of neo-substrates. For the ongoing characterization of the proteome druggable via the IMiD approach, novel CRBN effectors are needed both for probing the space of neo-substrates, as well as for future pharmacological exploitation. With this work, we contribute first steps towards the rational design of a post-thalidomide generation of such effectors, towards unlocking the full potential of the IMiD approach.

Chapter 5

On the anti-angiogenic properties of thalidomide and its analogs

5.1 Introduction

The exact MOAs of IMiDs remain far from being fully characterized. Their pleiotropic effects, including anti-inflammatory, anti-fibrotic, anti-angiogenesis, and immune regulation effects however are appreciated in many clinical settings [15, 76, 79, 95, 207]. Effects observed in MM include co-stimulation of T and NK cells, and the inhibition of inflammatory cytokines TNFα and IL-6 [147, 191]. One of the main drivers of efficacy, however, seems to be the inhibition of vascular endothelial growth factor (VEGF) [102, 146]. VEGF plays a major role in the physiological process of new blood vessel formation, which is called angiogenesis. This process is tightly controlled by the interplay of chemical signals and proteins like VEGF and essential for growth and healing [48]. However, in many pathological conditions and especially cancer, this process is miss-regulated. Solid tumors have an abnormally high demand of blood supply [150] that can only be met by releasing angiogenesis signaling molecules and even healthy surrounding cells can be stimulated to do so [170]. With enough supply of oxygen and nutrients, the newly formed blood vessels allow the growing tumor to move and form

metastases. Inhibiting angiogenesis as a form of cancer therapy was proposed in the early 1970s [51], with the first FDA approval for bevacizumab, an antibody against VEGF, in 2004 [122]. Since then, many molecular targets have been identified and treatment with anti-angiogenic small molecules has shown to lock cancers in a static state.

Thalidomide and its analogues have been demonstrated to have anti-angiogenic properties. In-vitro experiments and patient data suggest that it is the formation of an active metabolite rather than thalidomide itself that exerts these properties [11]. The structural characterization of one such metabolite (CBG), that shows higher TNFα-inhibitory activity than thalidomide itself, was shown in the preceding chapter. Earlier research also suggests that tetrafluorinated thalidomide analogues have improved anti-angiogenic properties, which operate via a different mechanism than cereblon modulation [101]. Based on these observations, we set out to characterize the anti-angiogenic properties of thalidomide analogues and whether their efficacy is dependent on CRBN-binding. To this end, we use two cell-based assays and an in vitro binding assay. A rat aortic ring angiogenesis assay and an endothelial cell tube formation assay allow us to quantify the impact of compound treatment on the vascular outgrow and cell formation. A third assay is used to determine binding of these compounds to CRBN. We have developed an alternative to the previously used FRET-assay, because measurements of the IMiDs iberdomide and avadomide showed high autofluorescence. This interfered with the read-out wavelength, to a point where affinities could not be determined. In order to circumvent problems with autofluorescence in our test compounds, we establish a binding assay based on MST. In this assay, fluorescently labeled MsCI4 is used to quantify the binding of our compound designs. Our results support the hypothesis that anti-angiogenic properties of thalidomide analogs do not rely on the binding to CRBN.

5.2 Design of compounds

To study the influence of CRBN-binding and tetrafluorination on anti-angiogenic properties, we designed a set of fluorinated and un-fluorinated compounds (Table 14). Our designs are based on two scaffolds: The first scaffold is based on canonical IMiDs (Table 14 A), in which a phtaloyl-based moiety is linked directly to glutarimide. A second scaffold is inspired by hydrolysis products like CBG and features a benzyl-based scaffold that is linked to glutarimide via an amide linker (Figure 14 B). Furthermore, we introduced three chemical substitutions for each scaffold, leading to a test set of 8 compounds. The un-fluorinated parent molecules (thalidomide, Gue3408) which should be able to bind to CRBN, an N-isopropyl and keto substitution at positions R^1 and R^2 (Gu991, Gu3407), respectively, which should obstruct binding to CRBN due to steric clashes, and tetrafluorination at R^4 for these designs (Gu3041, Gu3364, Gu993, Gu1032). This set of compounds should allow us to delineate the contribution of tetrafluorination on (i) CRBN-binding and (ii) inhibition of angiogenesis, and demonstrate possible correlations between (i) and (ii).

5.3 Development of an MST based assay

In order to assay for the affinity of test compounds, and to avoid problems with auto-fluorescence as seen for the novel IMiDs iberdomide and avadomide, an assay based on MST was developed. A small molecule dye (<1kDa, exact structure proprietary to Nanotemper Technologies) was covalently linked to MsCI4 protein via amine-reactive crosslinking. Measurements are performed by inducing a temperature change with an IR-laser and recording variations of fluorescence. For this labeled MsCI4 assay, fluorescence variations based on TRIC were used to assess affinities.

In order to verify the suitability of this approach for MsCI4, we performed reference measurements with known binders that were previously characterized in

orthogonal assays. A general complication of MsCI4-based assays is the involuntary binding of DMSO, which is often the only solvent able to dissolve small molecules. Therefore, the impact of DMSO had to be studied. For this, affinities of water-soluble compounds thiohydantoin, N-methylhydantoin, uridine and succiminide dissolved in water (Figure 27 A), and dissolved in DMSO (Figure 27 B) were assessed. Affinities determined in water can be considered K_D values, whereas measurements performed in DMSO lead to IC_{50} values, due to the competition of small molecule and DMSO for the same binding site. When comparing K_D (H_2O) and IC_{50} values (0.5% DMSO), a constant ratio for these compounds can be seen, which will be referred to as F (Table 11). This factor allows for correction of MST measurements that are performed in the presence of 0.5% DMSO, and calculate their respective affinities, which we termed K_i^*.

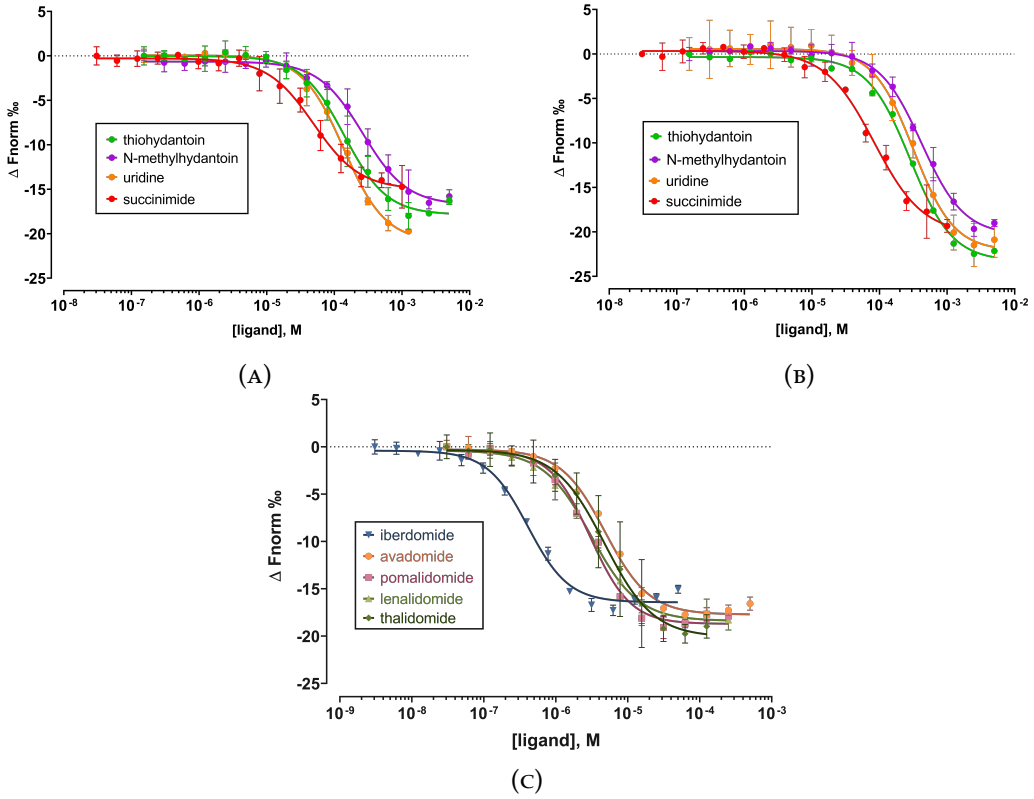

FIGURE 27: MST dose-response curves for water soluble compounds, which were used to quantify the influence of DMSO. (A) compounds dissolved in water. (B) water-soluble compounds dissolved in DMSO. (C) MST dose-response curves for reference compounds. All measurements were performed in triplicates.

With this setup and correction factor in place, measurements of reference compounds were performed to further validate this assay. The canonical binders avadomide, iberdomide, pomalidomide, lenalidomide and thalidomide were chosen and assayed for their affinity (Figure 27 C). Overall, measurements showed high signal-to-noise ratios and data was fitted, leading to IC_{50} values. IC_{50} and their corrected K_i^* values (Table 11) are in accordance with previously published data for single domain TBDs, using ITC, FRET, and TR-FRET [2, 19, 121].

TABLE 11: Binding affinities of reference compounds measured by labeled MST. (Top Table) Binding affinities of water soluble compounds shown in Figure 27 A, 27 B and the calculated correction factor F are shown. (Bottom Table) Binding affinities of canonical binders

compound	thiohydantoin	N-methylhydantoin	uridine	succinimide	mean
K_D[µM]	146 ± 12	262 ± 21	137 ± 12	49.2 ± 4.8	
IC_{50}[µM]	283 ± 15	417 ± 28	319 ± 16	83.2 ± 8.8	
F	0.515	0.628	0.430	0.592	0.541

compound	IC_{50} [µM]	K_i^* [µM]
avadomide	4.85 ± 0.3	2.63
iberdomide	0.41 ± 0.03	0.22
pomalidomide	3.02 ± 0.2	1.64
lenalidomide	3.08 ± 0.2	1.67
thalidomide	4.75 ± 0.6	2.57

5.4 Characterization of Gu compounds

Having confirmed the applicability of this labeled MST assay setup for DMSO-soluble compounds, we set out to determine IC_{50} and calculate K_i^* values of our thalidomide analogues, and tested for their anti-angiogenic potential in an endothelial cell tube formation assay (tube formation, lattice assay) and rat aortic ring assay (RAR assay). Representative pictures and results for the tube formation assay are shown in Figure 29. Results and representative pictures for the RAR assay, for compounds tested at their highest assay concentrations, are shown in Figure 30. Table 14 summarizes IC_{50} values for binding affinities and angiogenic assays.

Evaluation of MST experiments shows that several of our thalidomide analogues bind to MsCI4 (Figure 28), with thalidomide showing the highest affinity (K_i^* = 2.57 µM). Tetrafluorination of thalidomide, Gu3041, lowered its affinity almost 18-fold to 45.7 µM. Compounds based on scaffold B showed overall lower affinities compared to A, however tetrafluorination further decreased affinities, as seen for Gu3408 and Gu3364 with K_i^* values of 42.7 and 103 µM, respectively. As expected, N-isopropylation of the barbituric acid moiety rendered compounds unable to bind to MsCI4, independent of fluorination (Gu991, Gu993, Gu3407, Gu1032). This is due to steric constrains, which we have previously established for barbiturates [20].

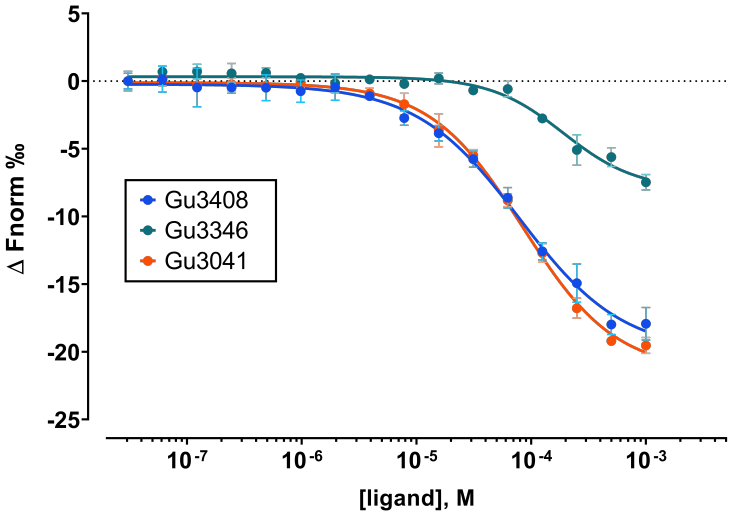

FIGURE 28: MST binding curves for thalidomide analogues Gu3408, Gu3346, Gu3041 (Table 14), which were found to bind to MsCI4 (n=3). Compounds Gu991, Gu993, Gu3407 and Gu1032 did not show detectable binding and are omitted.

In the tube formation assay, anti-angiogenic potency of a compound is measured by its ability to inhibit endothelial cells from forming tubelike structures. Compared to vehicle (0.5% DMSO), thalidomide did not show any potency at a maximum assay concentration of 100 µM (Figure 29 A), which is quantitatively evaluated as the mean lattice area (Figure 29 B). Our compounds were initially assayed at a concentration of 10 µM, prior to concentration-dependent testing. Here, high potency was shown for both tetrafluorinated versions of scaffold A (Gu3041, Gu993) to inhibit cell-outgrowth. Comparison with vehicle (0.5% DMSO) showed inhibitions of 83% and 88% at an assay concentration of 10 µM, which is comparable to the positive control CPS49 (c = 30 µM) with 89%. Gu3041 and Gu993 further showed concentration-dependent inhibition of tube formation in the concentration range of 0.1 - 10 µM. No other designs, including the tetrafluorinated counterparts of scaffold B, were able to inhibit this tube formation of endothelial cells.

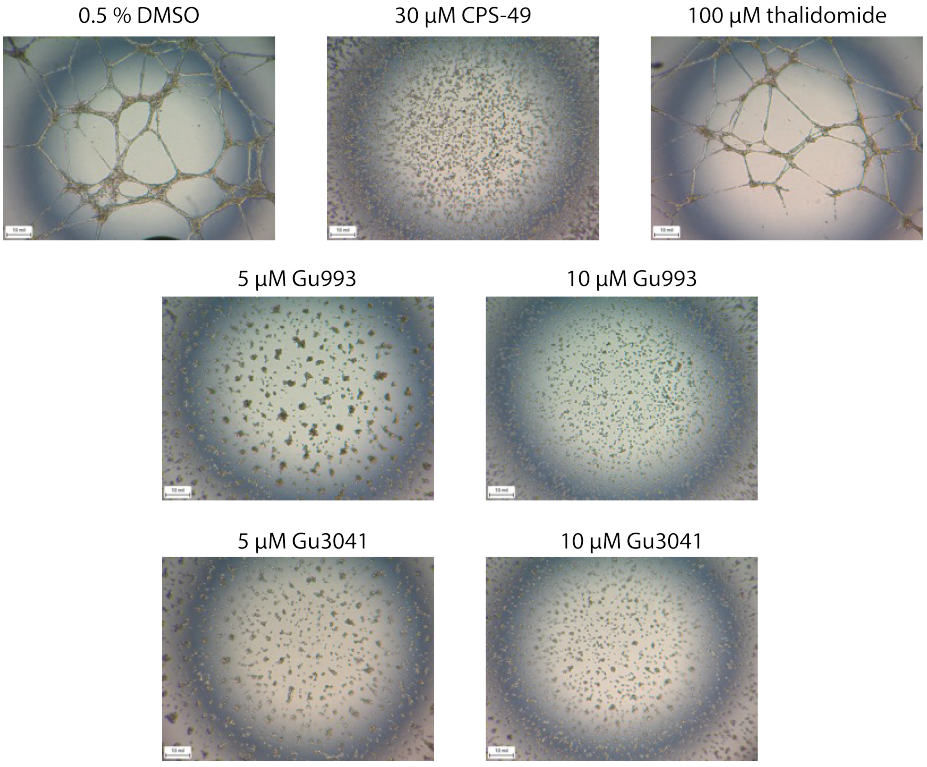

(A)

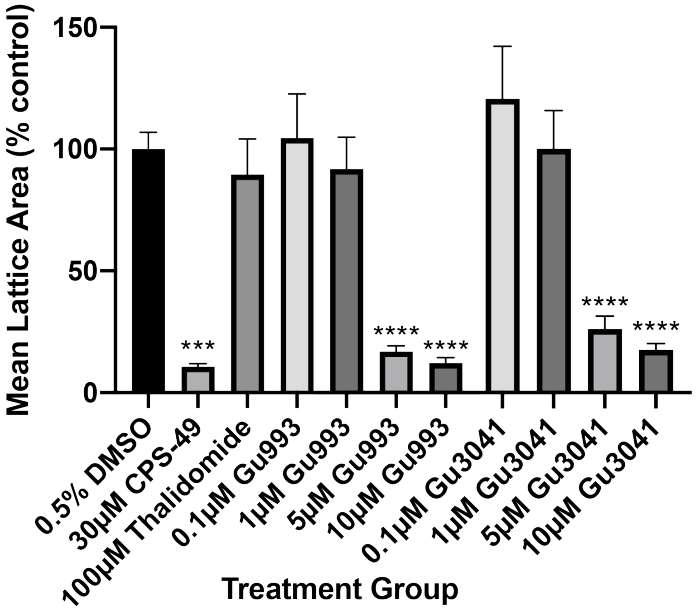

(B)

FIGURE 29: Results for endothelial cell tube formation assay. Vehicle and treatment with thalidomide showed no anti-angiogenic effects, while positive control (CPS-49), Gu993 and Gu3041 showed strong inhibition of tube formation at the indicated concentrations. (A) Representative tube formation images for vehicle (DMSO), positive control (CPS-49), thalidomide, Gu993 and Gu3041. (B) Mean lattice area for vehicle, positive control, and increasing concentrations of Gu993 and 3041 (n=3)

In the rat aortic ring assay (RAR assay), compounds were tested for their ability to inhibit vascular outgrowth at initial screening doses of 50 µM. Compounds that demonstrated >50% inhibition were selected for further testing at concentrations between 5 - 100 µM. Similar to the tube formation assay, thalidomide did not display significant effects on the outgrowth of microvessels, even at concentrations of 100 µM. Several of our analogues showed inhibition to varying degrees (Figure 30 A). Compounds Gu3041 and Gu993, which also showed potency in the other angiogenesis assay, inhibited cell outgrowth with IC_{50} values of 70 and 50 µM, respectively. Compared to the positive controls TNP-470 (92%) and CAI (95%), Gu3041 and Gu993 showed a reduction of cell outgrowth by 61% and 94% at 100 µM concentrations (Figure 30 B). The un-fluorinated version of Gu993, Gu991, showed no significant inhibition. The also un-fluorinated compounds Gu3407 and Gu3408 showed lower potency to inhibit microvessel outgrowth, with reduction by 41% and 65% at assay concentrations of 100 µM. The respective IC_{50} value for Gu3407 is therefore above the tested concentrations (>100 µM). Interestingly, tetrafluorination of this compound, Gu1032, was found to be the strongest inhibitor of angiogenesis in this assay, with an IC_{50} value of 25 µM. Concentration-dependent inhibition of outgrowth for this analogue was also shown (up to 88% at 50 µM).

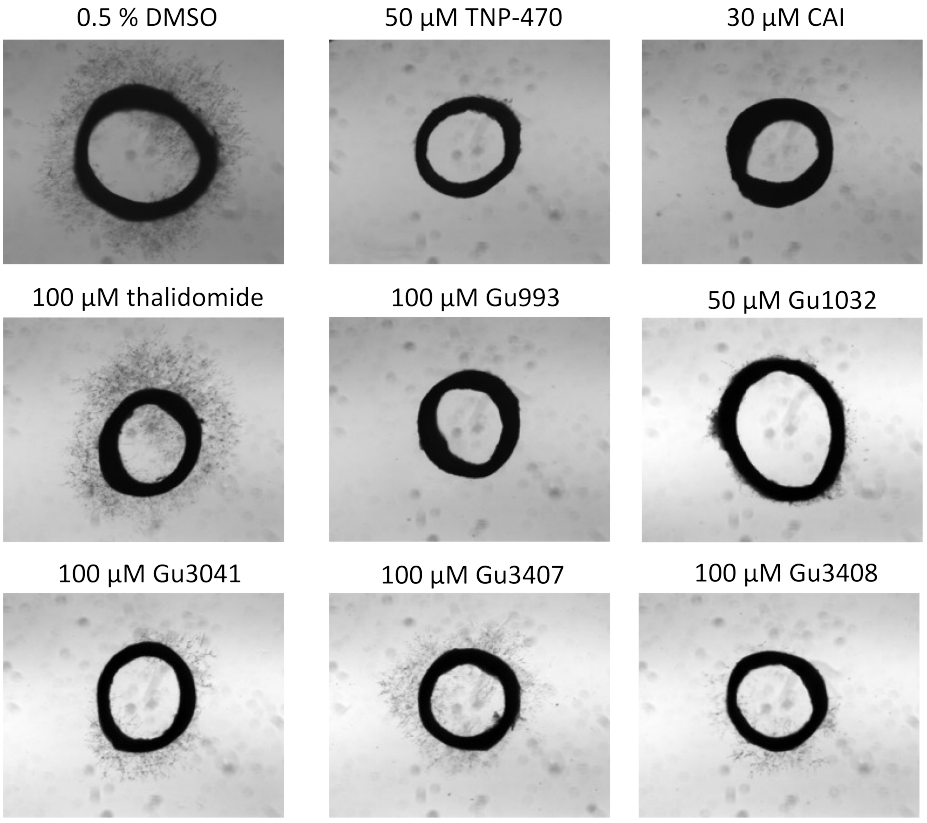

(A)

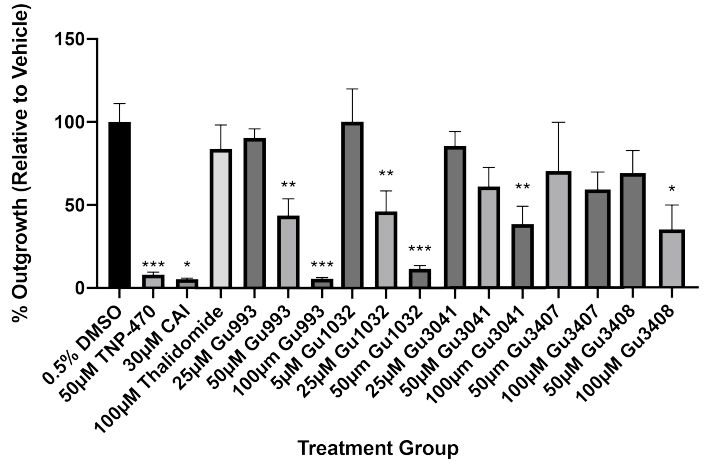

(B)

FIGURE 30: Results for rat aortic ring assay. Relative outgrowth Vehicle and treatment with thalidomide showed no anti-angiogenic effects, while positive controls (TNP-470 and CAI), Gu993, Gu1032, Gu3041, Gu3407 and Gu3408 showed inhibition of outgrowth at the indicated concentrations. (A) Exemplary pictures of outgrowth for vehicle (DMSO), positive controls (TNP-470 and CAI), and Gu993, Gu1032, Gu3041, Gu3407, Gu3408 at the highest tested assay concentrations. (B) Relative outgrowth for vehicle (DMSO), positive controls (TNP-470 and CAI) and Gu compounds (n=3)

TABLE 14: Markush structures of thalidomide analogues, their affinities to MsCI4 and anti-angiogenic potential. (A) chemical structure of scaffold A. (B) chemical structure of scaffold B. (C) Affinities of Gu compounds to MsCI4 and their anti-angiogenic effects in tube formation and RAR assay.
n.b. no binding; n.i. no inhibition.

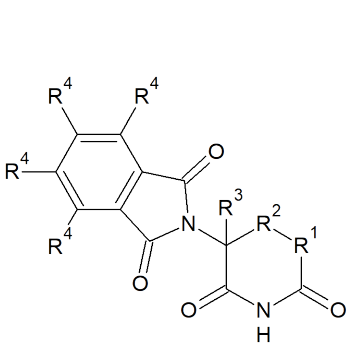

(A)

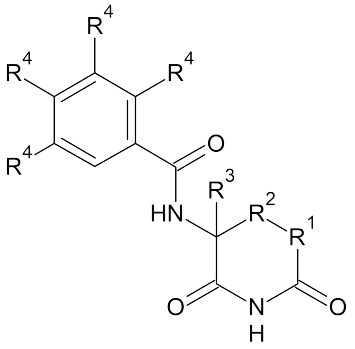

(B)

Compound	Scaffold	R^1	R^2	R^3	R^4	MST		Tube formation	RAR assay
						K_i^* [µM]	IC_{50} [µM]	[µM]	[µM]
Thalidomide	A	CH	CH	H	H	2.57	4.75 ± 0.6	n.i.	n.i.
Gu3041		CH	CH	H	F	45.7	84.4 ± 5.6	3	70
Gu991		N-$CH(CH_3)_2$	C=O	CH_3	H		n.b.	n.i.	n.i.
Gu993		N-$CH(CH_3)_2$	C=O	CH_3	F		n.b.	3	50
Gu3408	B	CH	CH	H	H	42.7	78.9 ± 7.9	n.i.	70
Gu3364		CH	CH	H	F	103	191 ± 50	n.i.	n.i.
Gu3407		N-$CH(CH_3)_2$	C=O	CH_3	H		n.b.	n.i.	>100
Gu1032		N-$CH(CH_3)_2$	C=O	CH_3	F		n.b.	n.i.	25

(C)

5.5 Conclusions

Inhibiting angiogenesis has become a standard therapy for various forms of cancer [212] by "starving" tumors of their high demand in blood and nutrients. However, limitations in efficacy and lack of understanding for their MOA fuels the need for novel and potent agents with less side-effects. Thalidomide has been used in MM for many decades now, however, research has predominantly shown that metabolites rather than thalidomide itself mediate anti-angiogenic effects in

MM [144]. Based on thalidomide metabolites, N-substituted and fluorinated analogues have been investigated and shown to possess high potency to inhibit angiogenesis [13, 127]. Several thalidomide analogues in our test set showed affinity to MsCI4 and inhibited angiogenesis in two assays. The most potent inhibitors in this test set are the tetrafluorinated analogues Gu3041 and Gu993. They showed similar high inhibition in tube formation and rat aortic ring assay. Moreover, these compounds show tendency for higher potency than previously reported analogues [101, 128]. Similar to previous reports [26, 43, 127, 133], thalidomide did not show any anti-angiogenic potency in our assays at concentrations of up to 100 µM. While Gu3041 showed rather low affinities to MsCI4, Gu993 did not show any binding. This suggest a CRBN-independent MOA for the inhibition of angiogenesis. This is further supported by our finding that besides Gu993, the tetrafluorinated compounds Gu3041 and Gu1032 also showed effects in the RAR assay, albeit not showing detectable binding to MsCI4. Tetrafluorination only showed effects in the tube formation assay when the phthalimido group (scaffold A), but not the phenyl-ring (scaffold B) was substituted. In return, tetrafluorination of the latter in Gu1032 showed the highest potency in the rat aortic assay. Although CRBN-binding was reduced or impaired for compounds in our test set, anti-angiogenic properties were significantly enhanced compared to thalidomide. These effects could partially be mediated by the bioavailability of compounds, as carbon–fluorine bonds are more hydrophobic than carbon–hydrogen bonds, which increases their lipophilicity as well as potentially strengthening the binding with their target molecules [133]. Moreover, differences in potency seen for the tube formation and RAR assay show that the compound susceptibility differs between cell types and assay set-ups. For these reasons, multiple assays should be considered when assessing efficacy, but also potential side effects of agents in preclinical development.

MOA of thalidomide and analogues have not been elucidated fully yet. The identification of downstream targets of Gu993 and Gu1032 might be useful here in order to elucidate the mechanisms by which such analogues mediate their effects. It was shown that for TNFα-inhibition, fluorinated and non-fluorinated

compounds exert their effects through different pathways [133]. Inhibition of angiogenesis was therefore suggested to be mediated through TNFα-independent pathways [101]. Another possible pathway is via selective inhibition of Cyclooxygenase (COX) enzymes, most prominently known to be inhibited by non-steroidal anti-inflammatory drugs (NSAIDs). COX-2 promotes angiogenesis and inflammation, and has been associated with various tumors. Thalidomide was found to be a weak COX-2 inhibitor while other analogues where highly specific and potent [135]. The exact contributions coming from TNF-α, COX-2 inhibition, or even other unidentified downstream targets will have to be investigated. In this study, we demonstrate that several analogues exert significant anti-angiogenic effects *in-vitro*. The most potent compound, Gu993 did not bind to MsCI4, which highlights that CRBN-binding is most likely not a prerequisite to mediate anti-angiogenic effects.

Chapter 6

Novel binding motifs for cereblon and assays for their characterization

6.1 Introduction

We have previously probed the ligand space of CRBN and established chemical requirements for CRBN binding [20]. Based on a test set of imides and lactams of different size and chemical modifications, we have outlined a set of rules using a pharmacophore-based nomenclature with up to six positions a-f (Figure 31) for 5- and 6-membered rings. Position a is generally branched to the protruding moiety in canonical IMiDs. Positions b, c, and d correspond to the distant carbonyl, the secondary amine and the inward-oriented carbonyl group, respectively. We have established that at least one carbonyl group at position d is required for binding, while a second carbonyl at b increases affinity. Additional heteroatoms within the ring lowered affinities to MsCI4. Polar groups at position e and larger substitutions at position f abolished binding.

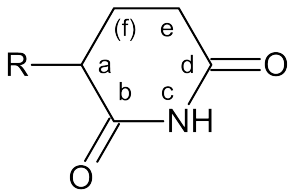

FIGURE 31: Previously established pharmacophore-based nomenclature for CRBN-binding

Inspired by these findings, we also wondered if there are other, chemically distant moieties that could also bind to the aromatic cage of CRBN. To explore this on a broad scale, we resorted to a high throughput approach. Enabled by the MsCI4 FRET assay, a high throughput screening (HTS) based on this FRET assay was initiated. Due to interference of compound absorption with FRET read-out wavelength, initial hits from the HTS were filtered manually and a complementary assay based on MST was developed and employed to validate these hits. By designing a fluorescent MST-reporter, we established a competitive MST-assay that ensures compound specificity for the tri-Trp pocket of MsCI4. Moreover, a reliable MST-based assay using the hTBD was developed using the same reporter. By using X-ray crystallography, we then characterized the binding mode of several novel motifs and rationalize their binding affinities. Surprisingly, several of these moieties did not comply with our previously established rules for CRBN binding.

6.2 Affinities and structural characterization of HTS hits

The HTS was based on the displacement of the ligand UMANT (Figure 7), which builds a FRET pair with tryptophans inside the binding pocket of MsCI4. The bound complex is excited at the protein tryptophan fluorescence and shows an emission maximum at around 430 nm. This signal is decreased when the UMANT is displaced by a ligand. Approximately 40.000 compounds on 122

384-well plates were screened and analyzed, resulting in about 373 initial hits. Because of the nature of the FRET assay, compounds which absorb around the FRET emission spectra can show up as positive binders. These potentially false positives were filtered out manually, and in a first round, a total five individual compounds and the class of glucocorticoids were selected for further experiments (Figure 32).

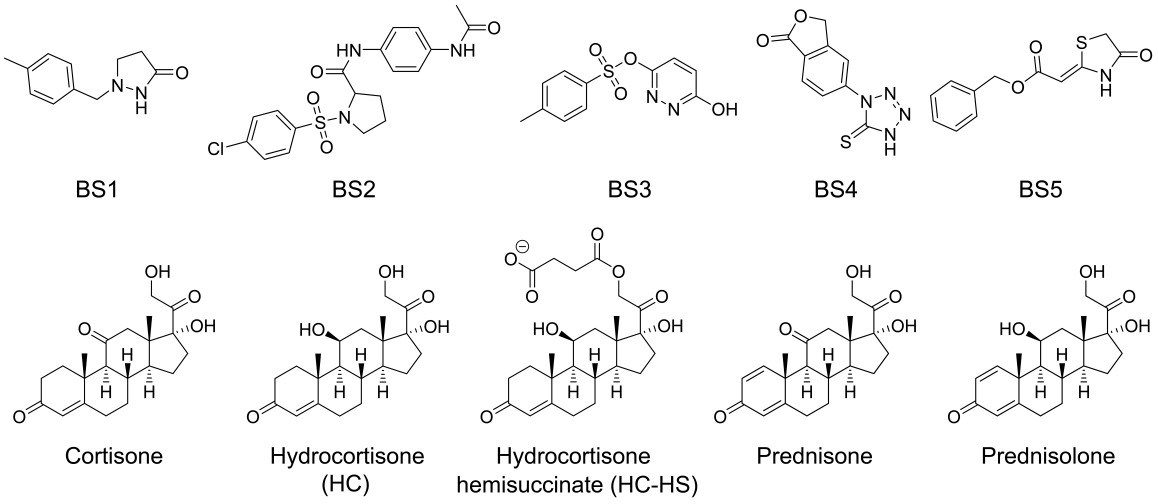

FIGURE 32: Chemical structures of HTS hits. Compounds were used as identified in the HTS with exception of BS4, which originally had an additional dioxabicyclooctanone moiety (FMPD library ID 209819), and additional glucocorticoid derivatives.

The previously established MST assay based on NHS-labeled MsCI4 (Chapter 5) was used as an orthogonal assay to validate these hits from the HTS and quantify binding affinities. IC_{50} values were determined from their respective binding curves and converted to K_i^* values for MsCI4 WT by employing the empirical correction factor (F=0.541; Table 11) that compensates for DMSO. This correction was not necessary for the Y101F mutant, which is used to create a chemically equivalent aromatic cage of MsCI4 to human CRBN. In this construct, DMSO affinity was significantly decreased, similar to hCRBN [19].

MST data shows that all tested compounds bind to MsCI4 WT protein with high affinities, confirming the initial hits from the HTS. IC_{50} values and their respective K_i^* values were in the low micromolar range, with the exception of BS5 (K_i^* = 628 nM), which shows one the highest affinities reported to date. Second highest

affinity was observed for BS4 (K_i^* = 7.8 µM), which is in the same range as thalidomide. BS1, BS2 and BS3 show lower affinities (K_i^* = 29.3, 41.7, 20.7 µM, respectively). Affinities to the MsCI4 Y101F mutant are reduced for all compounds and no binding was detected for BS2 (Table 15).

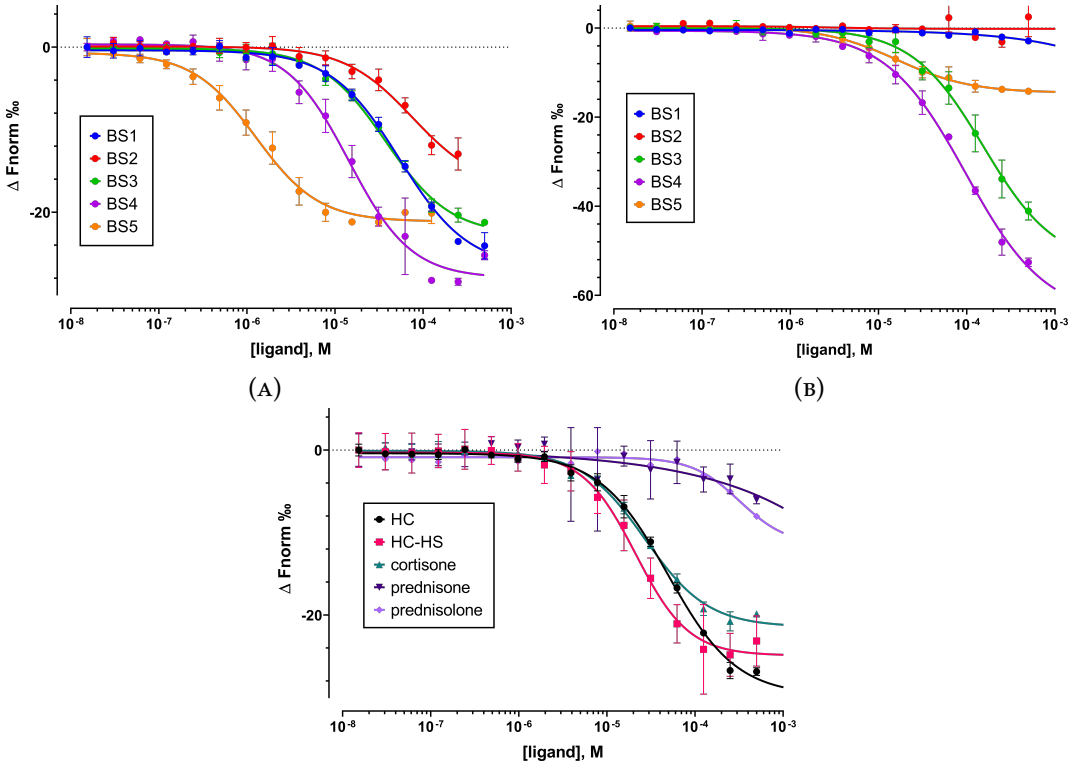

(A) (B) (C)

FIGURE 33: Labeled MST experiments of identified compounds in the HTS. (A) MST binding curves for compounds BS1-5 to MsCI4 (n=3). (B) MST binding curves for compounds BS3-5 (n=3), BS1 (n=1), BS2 (n=2) to MsCI4 Y101F. (C) MST binding curves for hydrocortisone (HC), hydrocortisone hemisuccinate (HC-HS), cortisone, prednisone and prednisolone to MsCI4.

TABLE 15: Affinities determined by labeled MST assay for BS1-5 and glucocorticoids and their respective K_i^* values

	compound	BS1	BS2	BS3	BS4	BS5
MsCI4 WT	IC_{50} [µM]	54.1 ± 8.4	77.1 ± 24	38.2 ± 2.8	14.4 ± 1.4	1.26 ± 0.12
	K_i^* [µM]	29.3	41.7	20.7	7.80	0.682
MsCI4 Y101F	K_i [µM]	>1000	n.b.	155 ± 35	98.0 ± 11	14.8 ± 2.2
	compound	cortisone	HC	HC-HS	prednisone	prednisolone
MsCI4 WT	IC_{50} [µM]	27.0 ± 1.9	49.1 ± 2.9	21.2 ± 1.4	>1000	321 ± 228
	K_i^* [µM]	14.6	26.6	21.2	-	174

Examination of the structures of compounds BS2, BS3, BS4 and the class of glucocorticoids showed no obvious similarities with canonical binders and previously established rules for CRBN-binding. It was therefore highly desirable to investigate their binding at a molecular level. By employing our MsCI4 crystal-soaking system, we successfully captured the binding modes for all compounds (Figure 35). Compounds were clearly resolved in at least on chain of the ASU, which is reflected by their respective F_O-F_C omit maps (Figure 34).

BS1 represents the most compact compound of this screen. The crystal structure (Figure 35 A) shows the 5-membered ring bound within the aromatic cage, engaging in hydrogen bonding with Y101 and the amide backbone, similar to canonical binders like thalidomide. However, due to its branching at the b position, the protruding moiety exits the binding pocket at a different exit vector. Overall, the 5-ring binding moiety is tilted upwards towards W99 in order to allow the branching of the methylbenzoyl group. This protruding moiety however does not engage in interactions with the protein, which explains the moderate affinity to MsCI4 (K_i^* = 29.3 µM). BS5, which exhibits a similar binding moiety to BS1, also engages in similar binding interactions (Figure 35 E) within the binding pocket. However, the ester carbonyl-group of the protruding moiety interacts with two water molecules which engage themselves in hydrogen bonding with the secondary amine of W99 and the amide of N50. Additionally, the terminal benzyl group engages in $\pi-\pi$ stacking with F77, which bends outwards to enable

this interaction. Taken together, these interactions most likely contribute largely to the sub-micromolar affinity seen for BS5 (Table 15), which supersedes first and second generation IMiDs. The crystal structure of BS2 (Figure 35 B) shows that the compound, which lacks an intact ring system for binding, engages in the canonical interactions within the tri-tryptophan pocket through the acetamide group. The protruding moiety branches out in the b position. Even though the distal acetamido group shows hydrogen bonding with a water molecule and the sulfonyl-group engages in additional interactions with the species-conserved N50, the affinity to MsCI4 is rather low. For BS3, it is seen that the hydroxyl group most likely tautomerizes with the neighboring imine to form a carbonyl group and a secondary amine group. Here, the classical interactions with Y101 and the amide of the protein backbone are formed. Additionally, the sulfonyl group engages in an interaction with N50, contributing to the affinity of K_i^* = 20.7 µM. For BS4, the binding mode was highly unexpected. It has to be noted, that BS4 was not the compound that was identified in the HTS. The identified hit featured an additional bulky moiety attached to the unbranched nitrogen next to the sulfur. According to our previously established CRBN-binding rules, using the pharmacophore-based nomenclature (Figure 31), no chemical moiety within this parent compound would have qualified for binding. We therefore expected BS4 to interact through the now accessible tetrazole-thione group. To our surprise, the crystal structure showed the bulky phthalide moiety inside the binding pocket. The carbonyl group in the lactone ring engages in H-bonding with the backbone and the ether group engages with the hydrogen of Y101. Y101 slightly moves aside in order to facilitate optimal binding geometry.

As for BS4, the class of glucocorticoids seemed incompatible with previously established binding rules. However, cortisone, hydrocortisone and hydrocortisone hemisuccinate (HC-HS) bound with good affinities. Their K_i^* values of 14.6 µM, 26.6 µM and 21.2 µM, respectively, are comparable to uracil and similar compounds measured via the FRET assay.

The crystal structures of cortisone and hydrocortisone hemisuccinate (Figure 35 F and G) show that corticosteroids bind via ring A to the binding cage, which

is comparable to canonical binders, albeit lacking a nitrogen in position C. The carbonyl group here occupies position d, and the double bond is found between positions b and c. Binding seems to rely almost exclusively on the interaction between this carbonyl group in ring A and Y101 and the backbone. The second canonical backbone interaction cannot be formed here due to the missing nitrogen in position C. This binding mode contradicts the rules previously established [20], where the minimal binding moiety was determined to be lactams. Additional interaction with W99 were seen for the keto group of cortisone while hydrocortisone hemisuccinate interacts with W99 via a bridging water. This difference might be part of the reason why cortisone showed a 2-fold higher affinity than hydrocortisone. The additional double bond in prednisone and prednisolone greatly decreased binding to a point where data could not be fitted for prednisolone. This could be due to the change in geometry of the ring A, which is more planar for these two synthetic corticosteroids. Affinities for hydrocortisone and HC-HS are very alike, which is easily explained when examining the crystal structure. The terminal hemisuccinate group is solvent exposed and does not engage in additional interactions. This again, shows the applicability of the correction factor F: The water-soluble HC-HS shows a comparable K_i value to the DMSO corrected K_i^* value of hydrocortisone.

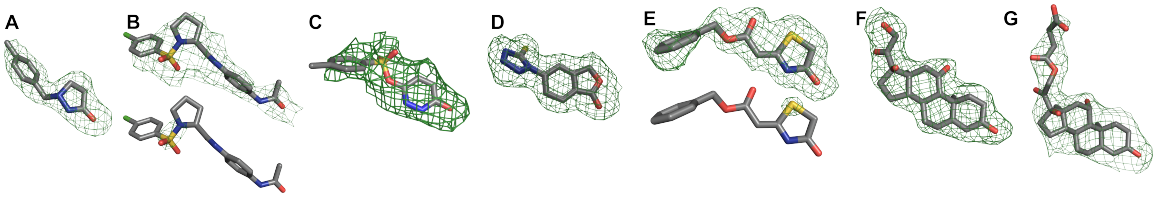

FIGURE 34: $F_O - F_C$ omit maps of HTS hits. Additional contour levels clearly locate sulfur atoms. (A) compound BS1 (2.0 σ), (B) compound BS2 (1.0 and 5.0 σ), (C) BS3 (1.5 σ), (D) BS4 (2 σ), (E) compound BS5 (1.5 and 5.0 σ), (F) cortisone (2.0 σ), (G) HC-HS (2.0 σ).

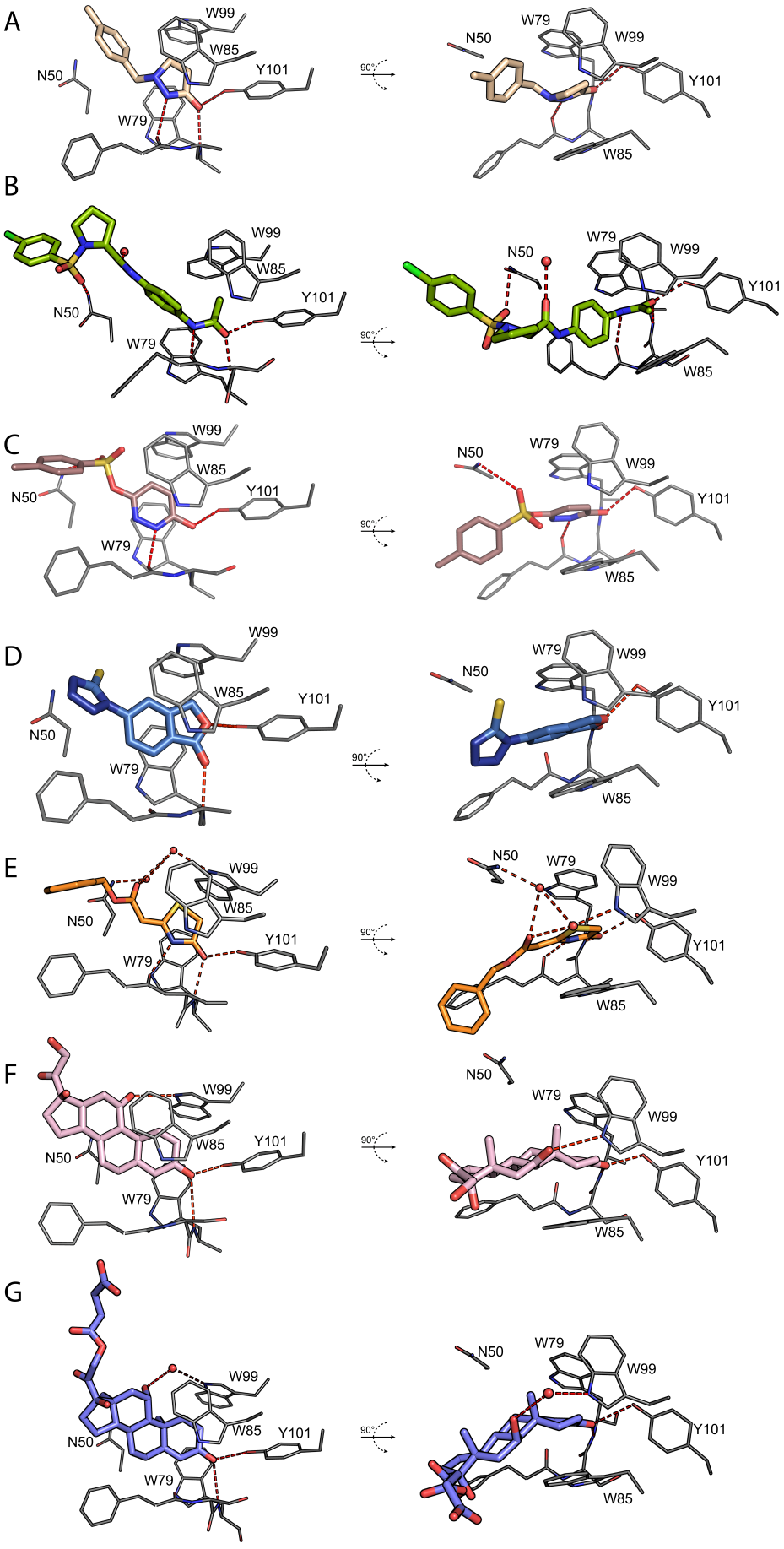

FIGURE 35: Binding mode of HTS hits. (A) BS1, (B) BS2, (C) BS3, (D) BS4, (E) BS5, (F) cortisone, (G) HC-HS.

TABLE 16: Data collection and refinement statistics of crystal structures of MsCI4 and HTS hits

	MsCI4 · BS1	MsCI4 · BS2	MsCI4 · BS3	MsCI4 · BS4
Data Collection				
Space group	P212121	P212121	P212121	P212121
Unit cell				
a, b, c (Å)	56.95 59.93 87.97	56.35 59.75 88.02	57.15 59.52 88.06	57.01 60.33 88.38
α, β, γ (°)	90, 90, 90	90, 90, 90	90, 90, 90	90, 90, 90
Resolution range, Å	47.8 - 2.28 (2.42 - 2.28)	49.43 - 2.79 (2.96 - 2.79)	47.94 - 2.69 (2.85 - 2.69)	41.43 - 2.0 (2.07 - 1.95)
Redundancy	13.1 (13.6)	12.9 (13.6)	13 (13.5)	6.87 (6.04)
Completeness %	99.8 (98.6)	99.9 (99.7)	99.94 (99.52)	99.9 (99.7)
Rmerge %	12.0 (95.3)	18.5 (100.09)	13.5 (99.9)	6.9 (104.0)
CC(1/2)	99.9 (84.0)	99.7 (92.5)	99.8 (79.2)	99.9 (74.3)
I/σ(I)	16.27 (2.54)	12.29 (2.08)	15.48 (2.43)	14.24 (1.26)
Refinement				
Number of reflections (total/test)	14188 (1370)	7816 (756)	8767 (837)	21229 (2096)
No. of atoms	2809	2574	2652	2644
Protein	2557	2521	2557	2479
Solvent	222	23	57	130
Ligand	30	30	38	35
Rwork%	0.18	0.20	0.17	0.19
Rfree%	0.25	0.26	0.25	0.24
Ligand in chain				
A	BS1	BS2	BS3	BS4
B	BS1	BS2	BS3	BS4
C	-	BS2	-	-

	MsCI4 · BS5	MsCI4 · Cortisone	MsCI4 · HC-HS
Data Collection			
Space group	P212121	P212121	P212121
Unit cell			
a, b, c (Å)	56.25 59.52 88.11	57.52 61.09 88.11	57.57 60.82 87.76
α, β, γ (°)	90, 90, 90	90, 90, 90	90, 90, 90
Resolution range, Å	44.05 - 1.8 (1.91 - 1.8)	30.35 - 2.24 (2.37 - 2.24)	48.14 - 2.59 (2.75 - 2.59)
Redundancy	6.9 (6.9)	13.00 (13.35)	12.9 (13.2)
Completeness %	99.9 (99.1)	98.4 (90.6)	99.8 (98.6)
Rmerge %	10.3 (84.9)	7.2 (71.5)	11.2 (98.6)
CC(1/2)	99.8 (80.9)	100 (93.7)	99.9 (87.4)
I/σ(I)	10.67 (1.62)	22.76 (3.37)	17.46 (2.46)
Refinement			
Number of reflections (total/test)	28082 (2755)	14325 (1417)	10033 (953)
No. of atoms	2761	2345	2532
Protein	2551	2199	2416
Solvent	169	91	47
Ligand	41	55	69
Rwork%	0.18	0.19	0.18
Rfree%	0.22	0.26	0.26
Ligand in chain			
A	BS5	CO	HC-HS
B	BS5	CO	HC-HS
C	-	-	-

6.3 Development of a competitive MST assay for CRBN variants

We have successfully used the labeled MST assay to detect and quantify binding of anti-angiogenic compounds (Chapter 5) and to validate HTS hits (Section 6.2). This assay was found to be generally applicable and highly reproducible. However, in order to ensure specificity to the aromatic binding cage, we developed a competitive MST-based assay. To this end, a reporter molecule based on uracil and the fluorescent BODIPY 493/503 was designed, which will be referred to as BU (Figure 8). This reporter should be applicable for all binding assays using MsCI4 and hCRBN, without the need for further labeling. For the assay itself, the reporter is pre-incubated with protein, here MsCI4, hTBD or DDB1-CRBN. Compounds in question then compete for the same binding site and ensure specificity for the thalidomide binding pocket.

6.3.1 Establishment of the competitive MST assay based on MsCI4

In a first step, we determined the affinity of the reporter BU. The reporter was kept at a constant concentration while the native MsCI4 protein was titrated. Reporter affinity was determined from this experiment by assessing the initial fluorescence which was quenched depending on the protein concentration (Figure 37 B). The affinity of the reporter BU was 3.8 µM, and thus almost identical to that of the MANT-uracil reporter [19] employed in the FRET assay (3.3 µM). Again, as in previous assays, the influence of DMSO on the measurements had to be determined. A 2:1 serial dilution series shows the displacement of BU reporter, leading to a DMSO affinity that agrees well with previous assays. Furthermore, IC_{50} value for succinimide is also in good agreement with the FRET assay and measurements performed using the labeled MST assay. Moreover, this set-up showed a strong advantage over the labeled assay: Displacement of the small reporter ligand from MsCI4 led to a reversion in thermophoretic behavior (Figure

36 A,C,E), which leads to a superior signal-to-noise ratio compared to the labeled assay. However, evaluation of affinities for MsCI4 in this assay were difficult because of the competition between labeled reporter, test compound, and DMSO, hampering the determination of a simple experimental conversion factor as for the labeled MST assay.

TABLE 17: Results of competitive MST measurements for MsCI4. IC_{50} values were determined from their respective MST curves.

Compound	IC_{50} [µM]
BU	3.76 ± 0.3
DMSO	$(1.61 \pm 0.2) \cdot 10^4$
succinimide	1.72 ± 0.36

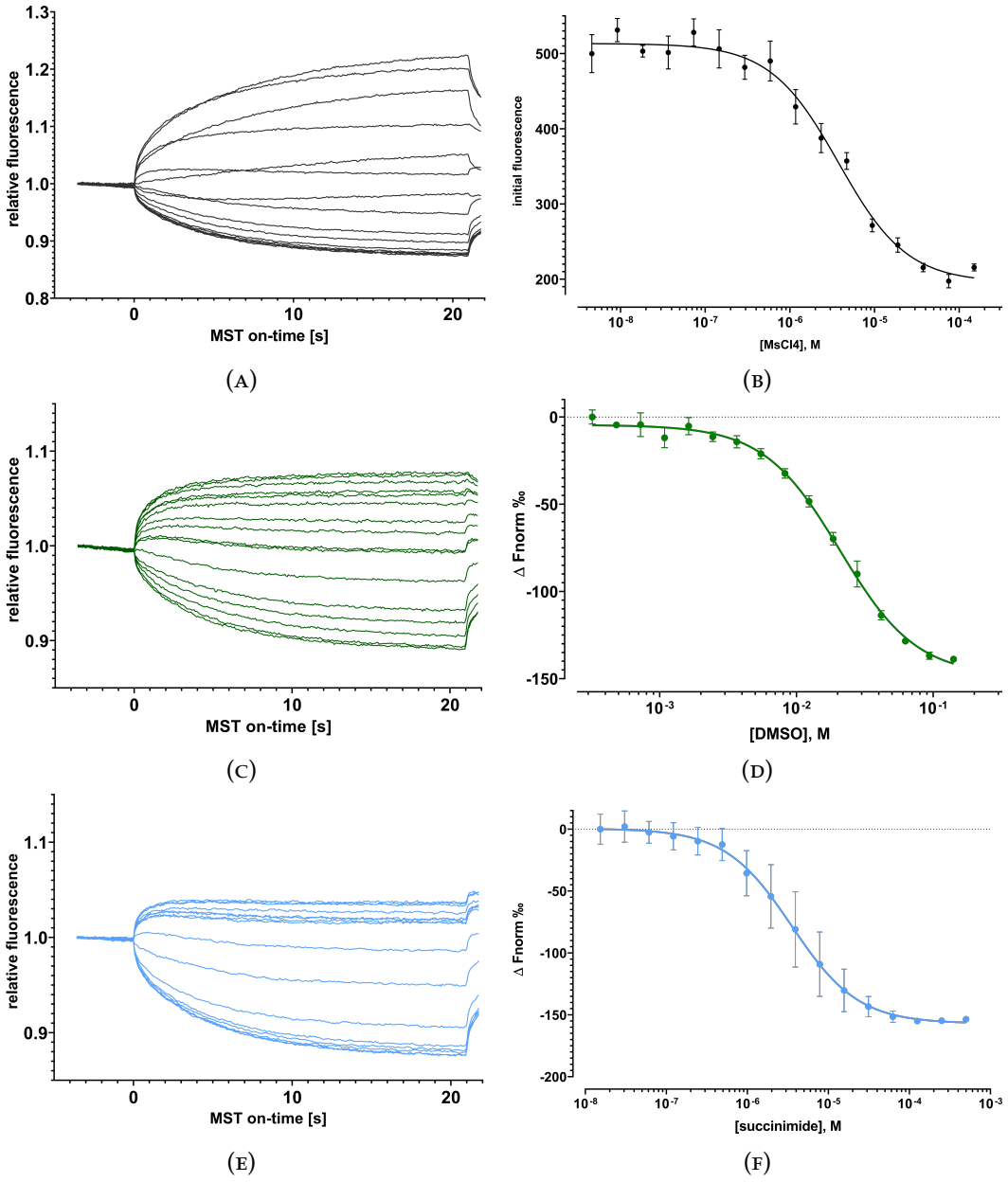

FIGURE 36: Fluorescence and MST data of competitive MsCI4 assay. (A) Representative MST traces of BODIPY-uracil upon binding to MsCI4. (B) Initial fluorescence of BODIPY-uracil upon binding to MsCI4 (n=6). (C) Representative MST traces of DMSO replacing BU. (D) Competitive MST displacement of reporter BODIPY-uracil by DMSO in a 2:1 serial dilution (n=3). (E) Competitive MST displacement of reporter BU by succinimide. (F) Representative MST traces of succinimide replacing BU.

6.4 Establishing the competitive MST assay based on human CRBN

We set out to establish the competitive MST assay for human CRBN also, which potentially holds several advantages. Affinities to human CRBN are directly relevant in a human context without the need for humanized constructs. Measurements via FRET have previously shown much lower affinities of DMSO [19], potentially eliminating the need for correction factors. We used the reporter BU, which was successfully used for MsCI4, to establish this competitive assay.
First, the DDB1-CRBN construct was assessed: Serial dilution of BU against DDB1-CRBN showed significant changes in MST behavior and evaluation of binding showed a $K_i \sim 500$nM. This 7.5-fold increase in affinity compared to MsCI4 was expected, based on previous reports for canonical binders. Full length CRBN constructs in complex with DDB1 showed up to 10-fold higher affinities for small molecules as their single domain TBDs [2, 121]. Initial measurements, using thalidomide to displace BU from the complex, however, did not lead to significant changes in MST behavior, such that the experiment could not be evaluated properly. To exclude problems with this combination of protein construct and reporter, an additional reporter based on thalidomide and Cy5 as a fluorophore was designed and will be used in future experiments.

To circumvent the problems encountered for the DDB1-CRBN construct, we tried to establish the competitive MST assay for hTBD. First, the affinity of reporter to protein was determined, like previously via change in initial fluorescence upon protein titration (Figure 37 A). Affinity of the reporter ($K_D = 10.9 \pm 1.2$ µM) was in the expected range and comparable to that observed for the MsCI4 constructs. Moreover, the reversion in MST behavior seen for BU in the bound and unbound state with MsCI4 was also observed here (data not shown). This led to similarly high signal-to-noise ratios. Assessing the binding of DMSO to hTBD showed much weaker affinities than those observed for MsCI4 (Figure 37 B). Lower DMSO

affinities to hCRBN constructs were previously shown [19] and result in the possibility to directly convert IC_{50} values determined via MST to K_i values, without accounting for DMSO. The lower affinity of DMSO (K_i = 0.24 ± 0.02 M) resulted in no significant change in MST behavior at the concentrations used in our assay (typically 0.5% DMSO).

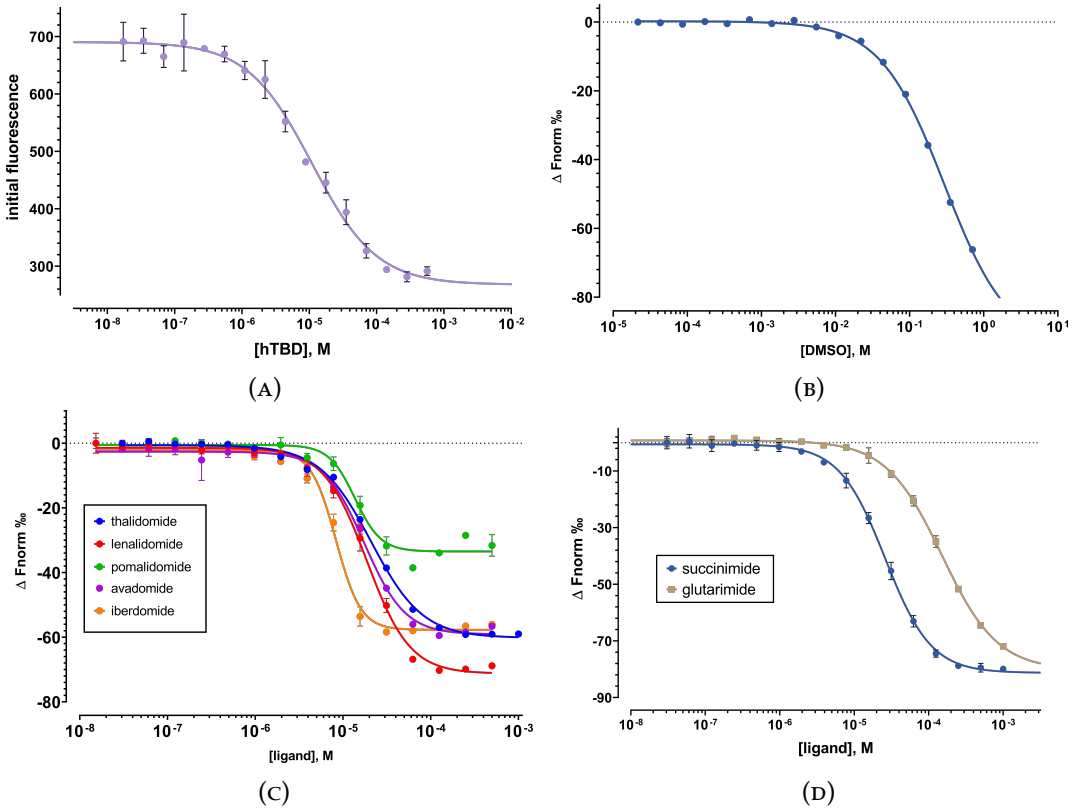

FIGURE 37: Binding curves for competitive MST assays with hTBD. (A) Initial fluorescence of BODIPY-uracil (n=3). (B) MST binding curve for DMSO (K_i = 0.24 ± 0.02 M, corresponds to 1.7% DMSO. (C) MST binding curves for marketed IMiDs (n=3). (D) MST binding curves for water soluble compounds glutarimide and succinimide (n=3).

Next, we tested this assay using classical IMiDs (Figure 37 C). We were so far unable to determine the affinities of avadomide and iberdomide because of autofluorescence of these compounds in the FRET assay. In this MST assay, however, measurements could be performed with excellent signal to noise ratios. Binding affinities for all canonical binders are in accordance with MsCI4 and previous studies done via ITC [2]. Moreover, it was clearly seen that newer generations of

Table 18: Affinities of commercially available IMiDs and minimal binders to hTBD

compound	IC_{50} ± SEM	K_i [µM]
thalidomide	20.9 ± 1.0	7.47
lenalidomide	18.7 ± 1.0	6.32
pomalidomide	13.7 ± 0.9	3.71
avadomide	17.5 ± 0.8	5.70
iberdomide	8.31 ± 0.3	0.920
succinimide	26.1 ± 1.1	10.8
glutarimide	150 ± 8.1	74.8

IMiDs also increase in affinity (Table 18). Interestingly, the significant difference in affinity between succinimide and glutarimide to MsCI4, that inspired experiments presented in Chapter 4, was also seen for hTBD (Figure 37 D). These data show the accuracy and reliability of this assay in determining the specific binding of compounds to the aromatic cage of hTBD.

Unexpectedly, the robustness of the competitive MST assay was used to identify a false positive binder. Nitrofurantoin, which is commercially marketed as an antibiotic medication to treat bladder and kidney infections previously yielded a binding curve indicative for considerable affinity in the FRET assay. Nitrofurantoin also showed effects in the thermophoretic behavior in the labeled MsCI4 MST assay with low signal-to-noise ratio. This was already indicative that binding might be non-specific, as all other binders were evaluated through changes in TRIC and not thermophoresis. In this competitive assay, no displacement of the reporter was seen for MsCI4 or hTBD, meaning that nitrofurantoin is probably able to bind to CRBN, however not into the binding pocket directly.

6.5 Affinities of HTS hits to hCRBN

This competitive approach was then used to verify the HTS hits found in the bacterial homologue MsCI4, in the human protein hTBD. We assessed the affinities of

BS1-BS5 and corticosteroids by measuring the displacement of BU. Interestingly, almost all compounds bound to the human protein (Table 20). BS5 was again the tightest binder tested in this panel; the IC_{50} value (6.26 µM) exceeded the reporter affinity considerably, to a point where the K_i conversion model (Equation 1) is no longer applicable. We reason that most interactions seen for BS5 and the bacterial protein are conserved for hTBD. The keto and amide group of thiazolidin probably interact only with the amide backbone, since Y101 in MsCI4 is here a phenylalanine. Of the secondary interactions, only the carbonyl-group with two water molecules could be formed here, because the π-π stacking of the terminal benzyl group relies on F77, which corresponds to a histidine in hCRBN. BS4 showed good affinities (K_i = 25.9 µM), which is slightly lower compared to MsCI4 (K_i = 7.8 µM). The crystal structure of BS4 with MsCI4 previously showed the bulky phthalide moiety inside the binding pocket. Of the two interactions formed, we expect the H-bond between the ether group and the hydrogen of Y101 not be present here as the corresponding residue is F402 in hCRBN. BS2, which only showed weak binding to MsCI4, did not show measurable binding to hTBD. This is not surprising, because the corresponding residue present in human CRBN (F402) abolished binding for the MsCI4 Y101F mutant. BS1 and BS3, showed lower but considerable affinities.

Finally, we were surprised by the affinity data of the corticosteroids. In contrary to MsCI4 Y101F, hTBD bound cortisone, hydrocortisone and HC-HS with good affinities (20). These affinities are even comparable to MsCI4. Analysis via X-ray crystallography suggested that glucocorticoid binding strongly relies on the interaction of the keto group of ring A with Y101, of which the latter is not present in the human protein. Further crystallographic studies are needed to determine whether binding is reinforced through interactions with distant residues that differ between MsCI4 and hTBD.

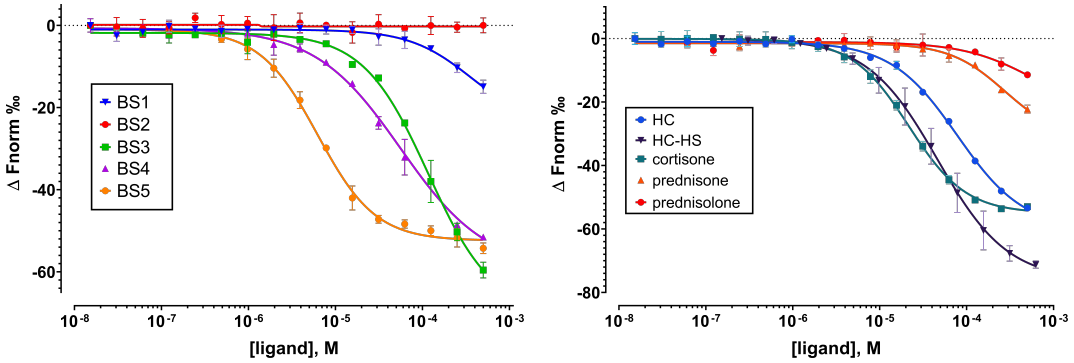

(A) (B)

FIGURE 38: Binding curves of HTS hits with hTBD. A MST binding curves for compounds BS1-5 to hTBD (n=3). B MST binding curves for glucocorticoids to hTBD (n=3).

TABLE 20: Affinities determined by competitive MST assay for BS1-5 and glucocorticoids and their respective K_i values to hTBD.

	compound	BS1	BS2	BS3	BS4	BS5
hTBD	IC_{50} [µM]	365 ± 279	n.b.	145 ± 29	56.2 ± 8.2	6.26 ± 0.27
	K_i [µM]	187 ± 145	n.b.	72.0 ± 15	25.9 ± 4.3	<< 10*
	compound	cortisone	HC	HC-HS	prednisone	prednisolone
hTBD	IC_{50} [µM]	21 ± 0.9	78.2 ± 4.4	46.2 ± 4.6	275 ± 78	595 ± 1339
	K_i [µM]	7.84 ± 0.5	37.3 ± 2.3	20.6 ± 2.4	140 ± 41	-

*IC_{50} value of BS5 was significantly higher than the BU reporter, which would lead to negative K_i values using Equation 1.

6.6 Conclusions

We have used our labeled MST assay to verify binders from the HTS. Even though several compounds deviated from previously established rules for CRBN binding, all hits were confirmed to bind to MsCI4. The labeled MST-based assay has proven to be a reliable assay here as well. By employing an empirical correction factor, affinities of a reference set of DMSO-soluble compounds could be determined which are consistent with literature data. Furthermore, we have established a competitive MST assay, that showed superior signal-to-noise ratios, while

ensuring specificity for the tri-Trp cage. With this assay, we show that the BU reporter is usable across different CRBN constructs. The reversion of MST behavior in the bound and unbound state of BU resulted in high amplitudes of binding events and allows for reproducible and highly sensitive binding assays. This was again confirmed in the competitive MST assay for hTBD, which has proven to be a reliable and well-suited assay for the identification of CRBN-binders. Here, due to the lower affinity of DMSO, no correction for the solvent had to be done and K_i values could be calculated directly. In high-resolution crystal structures, we show the binding of novel, non-canonical binders. Foremost, the high affinity of BS5 for MsCI4 and hCRBN shows the potential to use this binding moiety for the design of next generation molecular glues and PROTACs. In contrast to our previous work on novel binders (Chapter 4), BS5 ranked among the tightest binders that we have assayed so far, which could have advantages in regards to e.g. dosing of compound and potential side effects. Albeit not adhering to our previously established rules for CRBN-binding, BS2, BS3, BS4 and several corticosteroids were found to bind to MsCI4 and human CRBN. This shows that the ligand space of CRBN might be much broader than previously thought, which is not only of interest for the development of new E3-binders, but could also play a role for identification of natural and universal ligands.

Chapter 7

Investigation of possible endogenous substrates and recognition motifs

7.1 Introduction

The inadvertent binding of IMiDs to CRBN, that leads to the degradation of neo-substrates clearly has not evolved naturally. A long-standing question has been what the natural substrates of the $CRL4^{CRBN}$ ligase complex are. Moreover, given the conservation of the aromatic cage of CRBN, it seems likely that its target recruitment is also conserved throughout species. Some endogenous substrates of the hCRBN have been identified, like GS, MEIS2 and APP (Section 1.6), however their mechanism of binding remains elusive so far. Possible scenarios include binding of natural small molecules that mediate binding of endogenous substrate, similar to molecular glues (Section 1.5). Possible also seems the recognition of post-translational modifications (PTMs) through the aromatic cage of CRBN. DDB1 was first described in complex with another DCAF, DDB2, which plays an important role in the recognition and repair of UV-induced DNA damage. Based on this, we hypothesized that the DCAF CRBN could also recognize DNA-related small molecules. Indeed, we were able to show that uracil binds to CRBN, forming the canonical interactions with the tri-Trp cage. However, even though uracil

showed teratogenic effects *in vivo* [63], a biological implication for this recognition could not be shown. Aromatic cages in other proteins were generally found to bind methylated ammonium or guanidinium groups through interactions of the cationic ligand and π systems of the aromatic cages [111]. This suggested cationic ligands such as methylated lysine and arginine, which function as readout states for e.g. histone tails, directly influencing chromatin structure and gene expression. However, previous studies investigating the binding of such PTMs were ambiguous, showing no significant binding of cationic ligands such as betaines, carnitines, cholines and modified residues, including arginines or lysines [20, 25, 63]. Unexpectedly, a chemically identical motif to acetyl modification was found to bind to the aromatic cage of MsCI4 during this work. Compound BS2 was shown to form the canonical IMiD H-bonds between the acetamide group and the binding pocket of MsCI4 (Figure 35). However, binding affinities were rather low for MsCI4 and undetectable for hTBD. This suggests that the secondary interactions formed through BS2 contribute substantially to the binding. Interestingly, it was shown that the binding of the endogenous substrate GS is dependent on the acetylation of two lysine residues (K11 and K14). However, this interaction seems to be enhanced by treatment with IMiDs, which contradicts a direct recognition of this PTM by the aromatic cage. In contrast, the binding of MEIS2 and IMiDs was found to be mutually exclusive, thereby protecting MEIS2 from proteasomal degradation upon IMiD treatment. For other proteins like AMPK and APP, interacting domains or sequence sections have been identified, however structural characterization is still lacking. In this chapter, we examine the recruitment of APP. We present results on identifying important residues for binding to MsCI4 via affinity and structural characterization, and uncover a potentially universal recognition motif.

7.2 Structure and functions of amyloid precursor protein

The amyloid precursor protein (APP) is best known for its role as a precursor of Aβ, whose accumulation plays a major role in the formation of Alzheimer's disease [55, 169]. APP consists of a number of largely independently-folding domains (Figure 39). The E1- and E2-domains, which are connected by an extension domain (ED) and a highly flexible acidic domain (AcD). The E1 domain consists of a growth factor-like domain (GFLD) [158] and a copper binding domain (CuBD) [89] which are connected by an ordered linker. The E2 domain consists of two coiled-coils connected through a continuous helix [40, 203]. Positively charged amino acid residues within this domain build a charged patch that allows heparin to bind, which is potentially involved in the dimerization of this domain in APP. APP_{695} is the most abundant isoform in neurons, whereas the long isoform APP_{770}, with a Kunitz-protease inhibitor (KPI) domain and an OX-2 domain inserted between AcD and E2, is ubiquitously expressed [73]. The flexible juxtamembrane region (JMR) connects E2 to the single transmembrane helix. Located inside the cell is the amyloid precursor protein intracellular domain (AICD) [90]. AICD has also been implicated to contribute to Alzheimer's (reviewed [138]). Cutting by γ-secretase releases the AICD, which can translocate to the nucleus and act as a transcriptional regulator. Over 20 gene targets have been proposed, related to lipid metabolism [56], cell cycling and signaling [164] and protein metabolism [22]. It was also suggested that APP gets recognized by CRBN through this C-terminal domain. Using a proteomics approach and validation via pull-down experiments, the AICD was found to be directly interacting with CRBN, DDB1 and Cul4a [33]. These pull-down experiments showed that the 12 C-terminal residues are sufficient as bait to retain full binding activity. Most recently, it was confirmed through immunoprecipitation experiments that CRBN interacts with APP via its C-terminal region, and that Lys751 of APP_{770} in SH-SY5Y cells is being ubiquitinated [94].

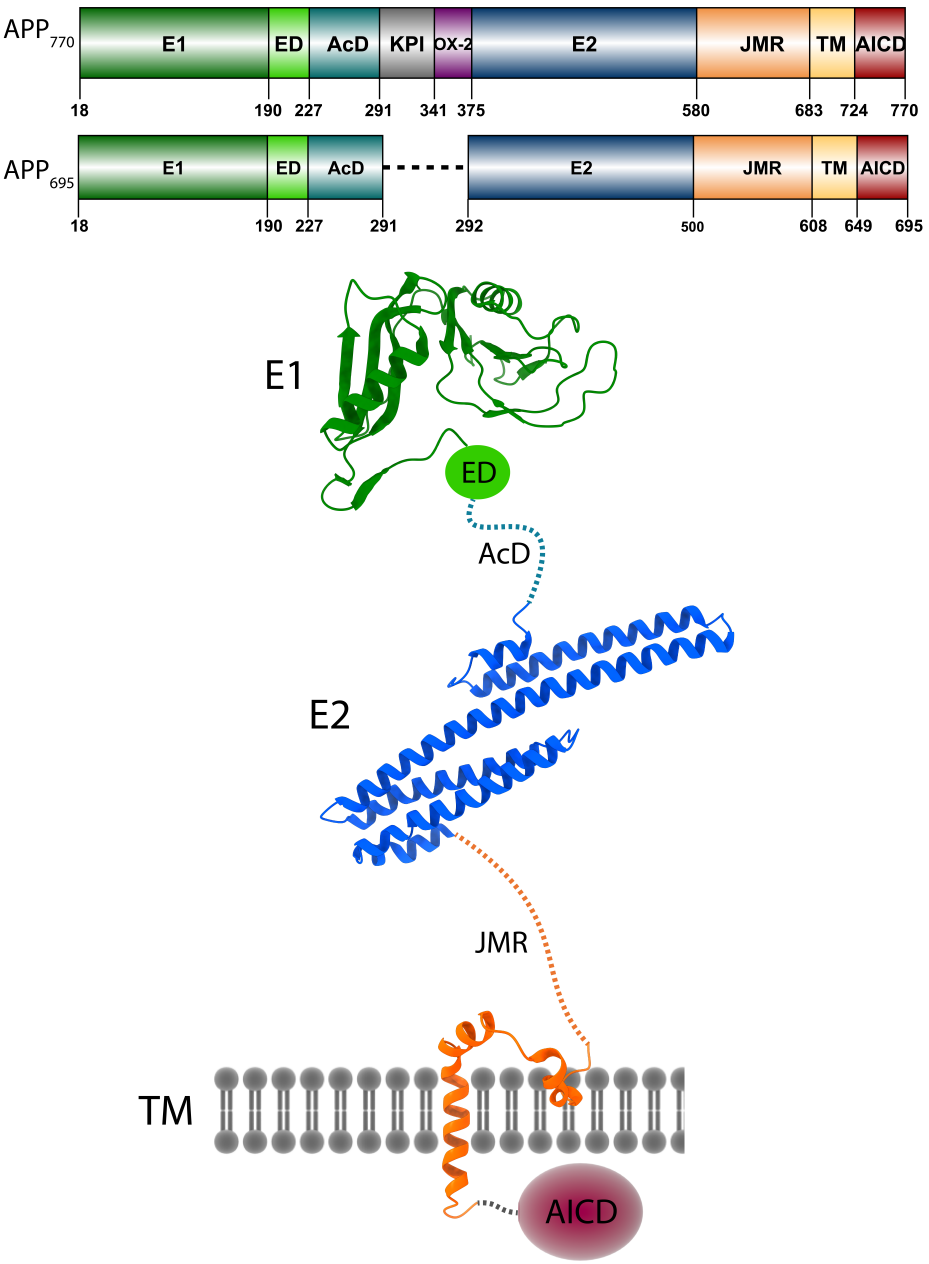

FIGURE 39: Domain organization and overall structure of APP protein. Domain organization of APP_{695}, which shows neuron-specific distribution, and the full-length isoform APP_{770}, consisting of an additional KPI and OX2 which is ubiquitously expressed. The overall structure of APP shows the E1-domain (PDB 3KTM), E2-domain (PDB 3NYL), extension domain (ED), highly flexible acidic domain (AcD), flexible juxtamembrane region (JMR), single transmembrane helix (PDB 2LP1) and the amyloid precursor protein intracellular domain (AICD).

7.3 Affinities and structural characterization of truncated APP peptides

The goal of this study was to narrow down residues of APP that are required for CRBN-recognition. With our previously established assays for the identification and characterization of CRBN substrates, we set out to further characterize the binding of APP. For this, N-terminally truncated peptides of the COOH-terminus of APP were synthesized by solid-phase peptide synthesis (SPPS) (Table 21), assayed for their affinity via MST and characterization of their binding was attempted via X-ray crystallography.

TABLE 21: Sequences of peptides resembling the C-terminus of APP and their respective affinities to MsCI4 as determined by labeled MST assay. Underlined is Lys751, previously found to be ubiquitinated by $CRL4^{CRBN}$

construct	sequence	MsCI4 affinity [µM]
4mer	QMQN	428 ± 93
8mer	KFFEQMQN	85.2 ± 24
12mer	ENPTYKFFEQMQN	24.1 ± 4.6
$12mer^{N-I}$	ENPTYKFFEQMQI	n.b.
31mer	AAVTPEERHLS<u>K</u>MQQNGYENPTYKFFEQMQN	25.8 ± 5.9

Surprisingly, the tetra peptide (QMQN) already showed clear binding to MsCI4 in the labeled MST assay, however with low affinity. The affinity increased significantly when adding four residues N-terminally. The 8mer peptide already shows affinities in the range of previously tested small molecules. Finally, the 12mer and the 31mer show the highest affinities to MsCI4. Affinities of 12mer and 31mer are almost identical, suggesting that no additional interactions between peptide and MsCI4 are formed beyond 12 residues. The 12mer peptide with the C-terminal mutation N-I, which is present in the functionally redundant

homologue amyloid-precursor like protein 2 (ALPL2), did not show any binding. This suggests the essential need for an asparagine at the C terminus to mediate binding.

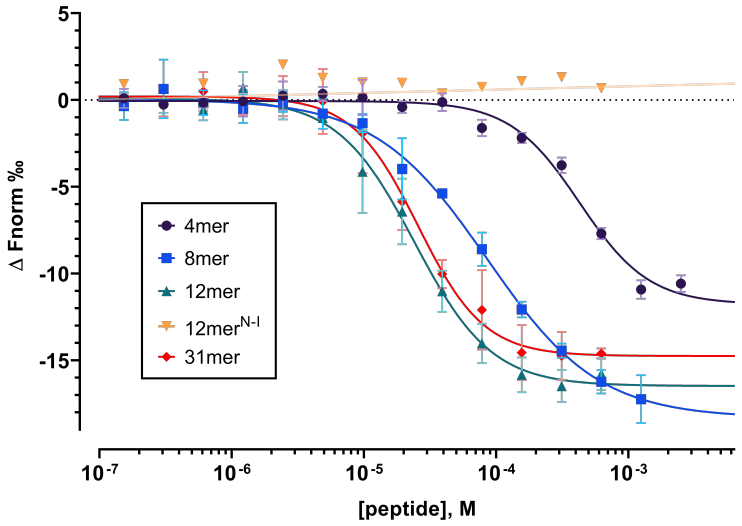

FIGURE 40: MST binding curves of N-terminally truncated APP COOH-terminal petides (n=3)

Having confirmed the binding of these peptides, the next step was to characterize their binding modes. While we were not able to obtain co-crystal structures, soaking trials using our established MsCI4 system led to a high-resolution structure. Soaking was performed using the 4mer, 8mer, 12mer and 31mer, however only the 4mer showed successful out-competition of thalidomide. This crystal diffracted to 1.85 Å and showed a distinctly different electron density at the binding pocket.

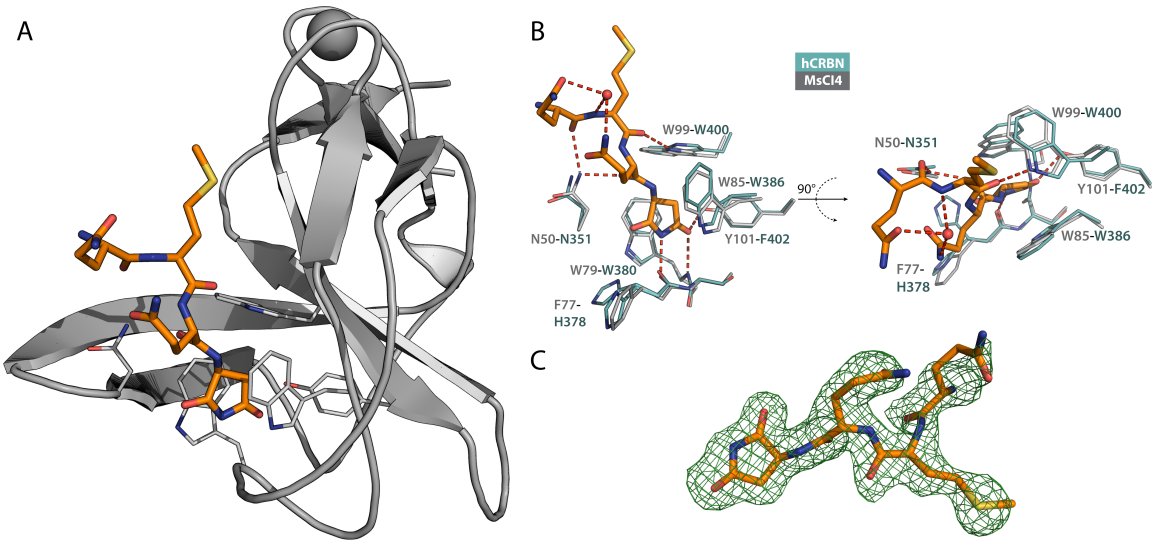

FIGURE 41: Crystal structure of MsCI4 in complex with quad peptide (QMQN) containing a C-terminally cyclized Asn. (A) Overall structure of the peptide with MsCI4. (B) Basal interactions between the cyclized asparagine and the aromatic cage of MsCI4 are identical to previous succinimide-based compounds. Additional interactions are seen for the main-chain carbonyl of Q1 and Q3 with N50. The main-chain carbonyl of M2 engages in hydrogen bonding with W99. Residues involved in binding of this modified peptide are conserved in hCRBN, which is superimposed in cyan. (C) F_O-F_C omit map of the $QMQN_{cyc}$ peptide in the MsCI4 binding pocket at a contour level of 2σ.

Modeling of the tetra peptide QMQN into this density revealed that not the designed peptide, but a modified form was bound (Figure 41). It appeared that the C-terminal Asn had internally cyclized and bound to MsCI4, forming the same basal interactions that were seen for other succinimide-based compounds (Chapter 4). The peptide will therefore be referred to as $QMQN_{cyc}$. Additional interactions of $QMQN_{cyc}$ are exclusively formed with the peptide backbone and MsCI4. The carbonyls of the two Gln engage in H-bonds with N50, and Met interacts with W99 via H-bonds. These interactions are sequence independent and should be possible for all peptides with a cyclized asparagine or glutamine at the terminus. Interestingly, pull-down experiments also showed binding of APP peptides containing Q instead of N at the terminus [33]. These observations inspired our hypothesis that is discussed in the succeeding section.

TABLE 22: Data collection and refinement statistics for MsCI4 · $QMQN_{cyc}$

	MsCI4 · QMQN
Data Collection	
Space group	P212121
Unit cell	
a, b, c (Å)	56.98 59.04 88.68
α, β, γ (°)	90, 90, 90
Resolution range, Å	44.34 - 1.85 (1.96 -1.85)
Redundancy	12.8 (13.1)
Completeness %	99.9 (99.5)
Rmerge %	6.5 (80.8)
CC(1/2)	100 (90.1)
I/σ(I)	24.12 (2.89)
Refinement	
Number of reflections (total/test)	26206 (2585)
No. of atoms	2495
Protein	2331
Solvent	141
Ligand	23
Rwork%	0.19
Rfree%	0.23
Ligand in chain	
A	$QMQN_{cyc}$
B	$QMQN_{cyc}$
C	-

7.4 A degron for CRBN-recognition?

The presented crystal structure of the APP C terminus in complex with MsCI4 bears multiple biological implications for CRBN. Besides the PTMs already described in the preceding section, further enzyme-catalyzed modifications are used in nature to extent the chemical space beyond the limit of the 20 standard amino acids. Moreover, spontaneous non-enzymatic modifications can occur to Asn, Asp, Gln and Ser and include the racemization, deamidation and cleavage, which can lead to irreversible modifications or breakdown of proteins [52]. Asn residues

can undergo slow cyclization to amidosuccinimide, which often results in deamidation of the side chain or its conversion to e.g. isoAsp. Alternatively, the 'β-amide nitrogen of asparagine can attack the peptide bond carbonyl, which results in peptide bond breakage and the release of a C-terminal succinimide moiety (Figure 42 B). This spontaneous peptide bond cleavage has been shown for Asn and Gln, whereas the latter appeared to be much slower [156]. This process is dependent on many factors such as the flanking residues, pH, or temperature. It was found that especially long-lived proteins, such as α-crystallin can undergo spontaneous peptide bond cleavage [200], which releases two peptides whereby one carries a C terminal succinimide ring (Figure 42 B). Most recently, a similar mechanism has been shown to lead to spontaneous cross-linking in aging proteins [52].

Protein splicing is an essential mechanism by which proteins can be modulated to yield a sequence that is not linear with the corresponding gene. This process is self-catalyzed and involves an intervening peptide, the intein, which excises itself from precursor proteins with the flanking C- and N-terminal external proteins, the exteins. There are three classes of inteins based on sequence and splicing mechanisms, with class 1 being the most abundant. This mechanism is dependent on an Asn at the C-terminus of the intein, and occurs through four distinct steps [142, 209]: 1) Reversible transition of the amino end of intein and extein into an ester or thioester bond (N to S/O acyl shift). 2) The side-chain of the C-terminal intein attacks the ester or thioester at the end of the intein (trans-(thio)esterification). 3) The amide nitrogen atom of the Asn side chain cleaves apart the peptide bond between intein and extein. This results in a free intein with a terminal succinimide that slowly hydrolyzes to regenerate Asn or Iso-Asn (Figure 42). 4) A second acyl shift occurs, which leads to the formation of an amide bond between the two exteins. In rare cases, inteins were shown to have Gln as their carboxy ends. Here, the same reaction proceeds through Gln cyclization into a glutarimide ring [5].

The above described mechanisms lead to C-terminal succinimide or glutarimide

motifs, and have been found in prokaryotic and eukaryotic organisms. As especially the peptide bond breakage often results in damaged or non-functioning proteins, recognition of these motifs could be a conceivable physiological function of CRBN.

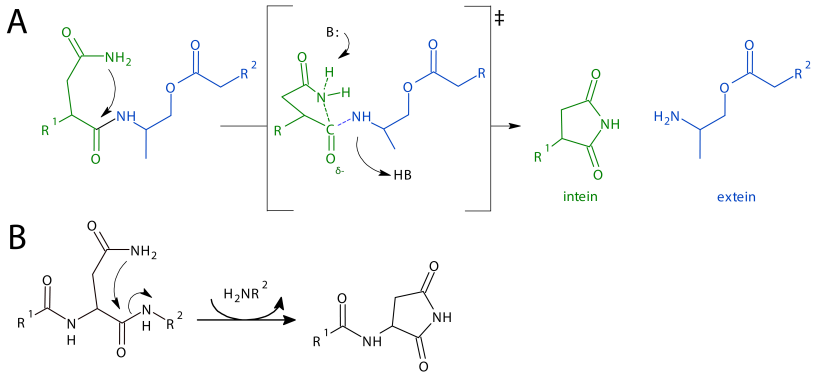

FIGURE 42: Schematic mechanisms leading to C-terminal succinimide motifs. (A) The third step of protein splicing is shown. After N to S/O acyl shift and trans-(thio)esterification, the amide nitrogen atom of the side chain cleaves apart the peptide bond between the intein (green) and the extein (blue). (B) Spontaneous peptide bond breakage through attack of the side chain amide nitrogen

Strikingly, sequence comparison of previously reported endogenous substrates of CRBN shows that APP and GS have a C-terminal asparagine, and AMPK and MEIS2 a C-terminal glutamine (Table 23). Having found the APP peptide to be cyclized C-terminally and bound to MsCI4, led us to hypothesize that CRBN potentially recognizes aged proteins which contain cyclized C-termini. To this end, genes encoding for the endogenous substrates APP, GS and MEIS2 were subcloned and used to transfect HEK293 cells. This was done for the wild-type constructs and for variants carrying a C-terminal Ala mutation (APP^{N-A}, GS^{N-A} and $MEIS2^{Q-A}$). The goal was to follow the ubiquitination of these proteins in cell culture. Potential differences for wild-type and mutant constructs, and accumulation of both proteins upon treatment with proteasome inhibitors would indicate that their cyclized moieties is recognized by CRBN.

TABLE 23: Sequence comparison of C-terminal amino acids of the endogenous CRBN-substrates APP, GS, AMPK and MEIS2

APP	...TYKFFEQMQN 770
GS	...TGDEPFQYKN 373
AMPK	...MCANLIKILAQ 559
MEIS2	...GGQVMDIHAQ 477

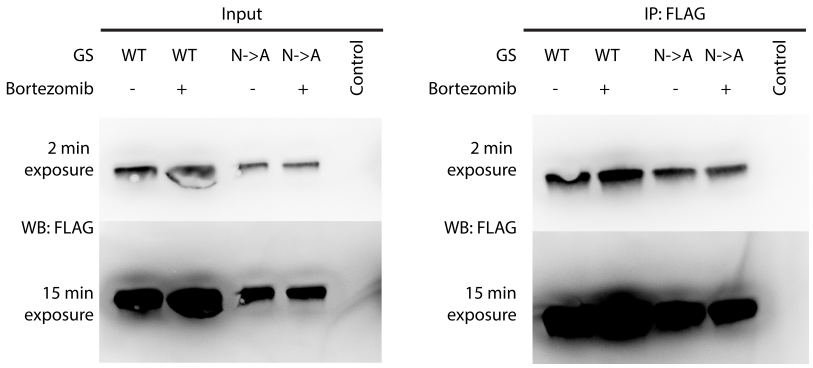

FIGURE 43: Initial GS pull-down experiment. HEK293 cells were co-transfected with GS WT and C-terminal N-A mutation. GS constructs carried a FLAG Tag that was used to pull down the protein. Chemiluminescent detection of protein bands showed clear expression and enrichment after the IP. However, no higher molecular bands were detected that would correspond to ubiquitination.

Initial experiments showed clear expression levels of GS and GS^{N-A}. However, no ubiquitination ladder was seen for either construct (Figure 43). This is potentially due to the high expression of the proteins, for which not enough E3 ligase machinery is available, or the time-frame of the experiment was too short for the formation of cyclic residues. Detection of ubiquitin did not show prominent bands, besides two faint bands which most likely correspond to IgG antibodies which were stripped off the beads used for pull-down experiments (not shown). These initial results do not show an effect of C-terminal amino acid mutations from asparagine or glutamine to alanine. We can therefore not make any statements about the potential influence of terminal amino acid cyclization on the recognition of substrates through CRBN. However, we also did not observe any detectable ubiquitination of wild-type GS (Figure 43). Here, careful optimization

is required in follow-up experiments. Since ubiquitin antibodies were found to have high detection limits, a possible solution is to resort to HA-tagged ubiquitin that can be co-transfected in HEK293 cells. Subsequently, HA-antibodies coupled with fluorescence detection can be used in future experiments to quantitatively evaluate protein levels, and study the influence of the C-termini of endogenous CRBN substrates.

7.5 Conclusions

Targeting unwanted proteins and removing them by proteasomal degradation has been developed to a useful tool that is investigated in many clinical settings. IMiDs, and most recently PROTACs, are utilizing the E3 ligase $CRL4^{CRBN}$ for this purpose. However, besides the identification of a handful of endogenous substrates, little is still known about the function of $CRL4^{CRBN}$ in absence of artificial ligands. Furthermore, no conclusive structural information on the binding of endogenous substrates has been presented. In this study, we show a high-resolution crystal structure of MsCI4, which selectively bound a modified form of an APP peptide. The peptide showed a cyclized Asn at the C-terminus, which formed similar interactions to previously characterized succinimide moieties. We found that APP peptides bound to MsCI4, as long as they carry an Asn at the C-terminus. The sequence of preceding residues seems to be unimportant as all interactions are exclusively formed via the peptide backbone. While the tetra peptide showed weak affinities to MsCI4 (K_D= 428 µM), they considerably improved for the 8mer (K_D= 85.2 µM), and peaked for the 12mer (K_D= 24.1 µM) and 31mer (K_D= 25.8 µM). Observed interactions between the tetra peptide and MsCI4 are expected to be similar for human CRBN, as all residues involved in the binding are conserved. Binding is also expected for peptides carrying a cyclized Gln at the N-terminus, which would correspond to an aminoglutarimide moiety that could form the conserved IMiD-interactions. Recognition of such cyclized motifs by an E3 substrate receptor could be physiologically relevant. Aging proteins were shown to be susceptible to spontaneous peptide bond cleavage, which can not

only lead to the formation of non-functioning and potentially toxic proteins, but Asn residues were also implicated as sites of protein cross-linking in long-lived proteins. These reactions could potentially be intercepted by the recognition of cyclized residues by an E3 ligase. It must be noted, that the terminal cyclization of the synthesized peptide is possibly an artifact of the SPPS. Imide formation during SPPS has been shown to occur within a peptide chain and methods for its prevention have been described [117, 125]. However, APP was originally identified as an interactor of $CRL4^{CRBN}$ through an unbiased proteomics approach, and most recently confirmed by cellular expression and immunoprecipitation of APP and CRBN [94]. This makes it seem unlikely that in all these cases, cyclization of Asn was introduced artificially. As a consequence, APP is either recognized by an alternative motif in the cellular context, or the observed cyclization indeed occurs naturally. The potential influence of aging, cellular context, or whether the TBD can actually promote cyclization remains to be investigated.

Chapter 8

Concluding Remarks

The discovery, that IMiDs work as molecular glues for the $CRL4^{CRBN}$ ligase complex has opened new frontiers in developing novel therapeutics, including the development of CRBN-directed PROTACs. The repurposing of E3 ligases for therapeutic applications has been proven to be a game changing technology and attracted attention from academia and the pharmaceutical industry. Disease-related proteins lacking classical active sites, such as transcription factors, non-enzymatic and scaffolding proteins, which were not accessible to treatment with conventional small-molecule therapeutics, can be targeted using molecular glues or PROTACs. Particularly for PROTACS, a major perspective for PROTACs is the increasing problem of drug resistance, especially in cancers, caused by high concentrations of classical inhibitors. The unique characteristic of efficient degradation at only catalytic amounts instead of inhibition with higher doses of classical inhibitors makes PROTACs powerful therapeutic tools. Their clinical safety is currently tested in clinical trials, but they are already used in academia as an alternative to the RNAi approach or gene editing via CRISPR. However, PROTAC development is currently empirical and limited by the availability of only a few sufficiently characterized E3 ligases and E3 binders.

Within this work, we have shown that the substrate receptor of $CRL4^{CRBN}$ can bind more motifs than previously characterized. We identified additional, chemically more distant binders in an HTS, and designed more minimalistic CRBN effectors in a rational and modular approach guided by hydrolysis products of thalidomide and its analogs. Thereby, we have established a novel amidosuccinimide motif as a minimal scaffold and showed its applicability in molecular glues that led to degradation of neo-substrates. Further, several HTS hits could be validated in a customized complementary MST affinity assay and in X-ray crystal structures. We found that our previously established rules for CRBN binding were insufficient to describe the binding of some of these novel binders, which shows that the substrate spectrum of CRBN is much broader than previously thought. Interestingly, some of the newly identified moieties are more compact than thalidomide, were found to bind with exceptionally high affinity, and revealed previously not described exit vectors. All these properties can aid the development of potentially more potent molecular glues and PROTACs with improved physicochemical properties.

The thalidomide binding pocket of CRBN is not only of high interest for pharmaceutical development, but also from an evolutionary point of view. The high sequence conservation of CRBN between species makes a common ligand very likely and a final proof of such a ligand is still missing. The binding modes of some non-canonical compounds identified in this study could be a hint that natural ligands might be more chemically distant from thalidomide than previously suggested natural ligands. Within this work, we uncover cyclized forms of the amino acids Asn and Gln as potential natural degrons for CRBN. The formation of these cyclized residues can occur upon peptide bond breakage after Asn and Gln residues. This was reported to be especially prominent in long-lived proteins such as α-crystallin. We have observed this motif in a crystal structure of MsCI4 in complex with a peptide that resembles the C terminus of the natural substrate APP. Its C-terminal Asn was found to be cyclized to an amidosuccinimide motif, which formed the same basal interactions with MsCI4 as the minimal IMiD

analogs that we designed. We found that the affinities of longer APP peptides were comparable to those of classical IMiDs, supporting the idea of a similar mode of interaction. However, not much is known about the incidence of terminal succinimide motifs beyond long-live proteins and the physiological relevance of their recognition through $CRL4^{CRBN}$ therefore remains to be determined.

Chapter 9

Contributions

The work of this PhD thesis was conducted in the department of Protein Evolution in the group of Dr. Marcus Hartmann, who initiated the project and supervised this study. I performed all experiments unless otherwise specified.

3 Design and characterization of bacterial and human CRBN constructs
I performed the analysis of conserved residues between human and bacterial CRBN, designed the humanized construct, performed cloning and expression in *E. coli* and cloning and expression of DDB1-CRBN in insect cells. I also designed and performed PCR reactions for MsCI4 truncations, humanized α and β constructs. Construct MsCI4 humanized σ was designed and cloned by Samuel Maiwald under my supervision. I performed nanoDSF measurements of MsCI4, humanized constructs and of DDB1-CRBN. I designed the construct for hTBD, which was cloned, expressed and purified by Dr. Reinhard Albrecht and Maxim Drömer.

4 *De-novo* design of cereblon (CRBN) effectors guided by natural hydrolysis products of thalidomide derivatives
MsCI4 protein was expressed by myself and by Kerstin Bär, who also performed FRET experiments. Evaluation of FRET data was performed by Dr. Birte Hernandez. Compounds were designed in collaboration with the lab of Prof. Dr. A. Giannis who synthesized the compounds. Crystallographic set-ups were done by

Kerstin Bär, Dr. Reinhard Albrecht and myself. I performed all crystallography, including soaking experiments, crystallographic measurements, structure solution and figure preparation. I performed all cell culture experiments and western blots with initial help from Dr. Birte Hernandez.

5 On the anti-angiogenic properties of thalidomide and its analogs
The project was initiated by Prof. Dr. Michael Gütschow and his lab at the Pharmaceutical Institute, University of Bonn, who synthesized the compounds. MST experiments were performed by Samuel Maiwald under my supervision. I evaluated the data and prepared all figures. Angiogenesis experiments and figures thereof were performed by the lab of Dr. William D. Figg from the Center for Cancer Research, National Cancer Institute, NIH, USA.

6 Novel binding motifs for cereblon and assays for their characterization The project was initiated by Dr. Marcus Hartmann. The HTS screen was established and performed by Dr. Jens Peter von Kries and Screening Unit at the Leibniz-Forschungsinstitut für Molekulare Pharmakologie (FMP). I assessed the hit list and designed follow-up experiments. MST experiments, crystallization set-ups, soaking experiments and structure solution were done by Samuel Maiwald and me.

7 Investigation of possible endogenous substrates and recognition motifs All experiments in this Chapter were performed by me with support in MST measurements by Samuel Maiwald.

Acknowledgments

A big thank you to everyone who made this PhD possible, in one way or another. Firstly, I would like to thank Dr. Marcus Hartmann for his support and trust. The balance between guidance and freedom to pursue my own ideas during my PhD have allowed me to grow, both personally and professionally.
I would like to thank Prof. Dr. Andrei Lupas for the funding and support of this project, as well as scientific guidance. Besides my advisors, I would like to thank the rest of my TAC committee, Prof. Dr. Karl Forchhammer and Dr. Oliver Weichenrieder for their insightful comments and encouragement.
My sincere thanks also goes to the group members, especially Dr. Reinhard Albrecht for the constant help, discussions, and over 35 trips to beamlines. I would like to thank Dr. Birte Hernandez Alvarez for the discussions, help with cell culture, lab work and general questions and concerns. Thanks to Samuel Maiwald for his help in several aspects of this project.
I thank all past and present labmates for the help in the lab, stimulating discussions, and providing an enjoyable work atmosphere. Especially the people who contributed to a smooth daily work, Emilija Basina, Kerstin Bär, Karin Lehmann, Melanie Maier, Astrid Ursinus, and everyone else. A sincere thank you to John Weir and his lab members, especially Dorota Rousova, who have always welcomed and supported me in their lab at various occasions.
Thank you to all my friends who have supported me over the years, especially Timo and Zach.
Ganz besonders bedanken möchte ich mich bei meiner Mutter und meinem Bruder, die mich ermuntert, bestätigt und immer an mich geglaubt haben.

Bibliography

[1] Maria Pia Abruzzese, Maria Teresa Bilotta, Cinzia Fionda, Alessandra Zingoni, Alessandra Soriani, Maria Teresa Petrucci, Maria Rosaria Ricciardi, Rosa Molfetta, Rossella Paolini, Angela Santoni, and Marco Cippitelli. The homeobox transcription factor meis2 is a regulator of cancer cell survival and imids activity in multiple myeloma: modulation by bromodomain and extra-terminal (bet) protein inhibitors. *Cell death & disease*, 10:324, April 2019.

[2] A. A. Akuffo, A. Y. Alontaga, R. Metcalf, M. S. Beatty, A. Becker, J. M. McDaniel, R. S. Hesterberg, W. E. Goodheart, S. Gunawan, M. Ayaz, Y. Yang, M. R. Karim, M. E. Orobello, K. Daniel, W. Guida, J. A. Yoder, A. M. Rajadhyaksha, E. Schonbrunn, H. R. Lawrence, N. J. Lawrence, and P. K. Epling-Burnette. Ligand-mediated protein degradation reveals functional conservation among sequence variants of the cul4-type e3 ligase substrate receptor cereblon. *J Biol Chem*, 293(16):6187–6200, 2018.

[3] Daniel Alcolea, Pablo Martínez-Lage, Pascual Sánchez-Juan, Javier Olazarán, Carmen Antúnez, Andrea Izagirre, Mirian Ecay-Torres, Ainara Estanga, Montserrat Clerigué, Maria Concepción Guisasola, Domingo Sánchez Ruiz, Juan Marín Muñoz, Miguel Calero, Rafael Blesa, Jordi Clarimón, María Carmona-Iragui, Estrella Morenas-Rodríguez, Eloy Rodríguez-Rodríguez, José Luis Vázquez Higuera, Juan Fortea, and Alberto Lleó. Amyloid precursor protein metabolism and inflammation markers in preclinical alzheimer disease. *Neurology*, 85:626–633, August 2015.

[4] Michael Amatangelo, Chad C. Bjorklund, Jian Kang, Ann Polonskaia, Sridevi Viswanatha, and Anjan Thakurta. Iberdomide (CC-220) has synergistic anti-tumor and immunostimulatory activity against multiple myeloma in combination with both bortezomib and dexamethasone, or in combination with daratumumab in vitro. *Blood*, 132(Supplement 1):1935–1935, November 2018.

[5] Gil Amitai, Bareket Dassa, and Shmuel Pietrokovski. Protein splicing of inteins with atypical glutamine and aspartate c-terminal residues. *Journal of Biological Chemistry*, 279(5):3121–3131, oct 2003.

[6] Hideki Ando, Tomomi Sato, Takumi Ito, Junichi Yamamoto, Satoshi Sakamoto, Nobuhiro Nitta, Tomoko Asatsuma-Okumura, Nobuyuki Shimizu, Ryota Mizushima, Ichio Aoki, Takeshi Imai, Yuki Yamaguchi, Arnold J. Berk, and Hiroshi Handa. Cereblon control of zebrafish brain size by regulation of neural stem cell proliferation. *iScience*, 15:95–108, may 2019.

[7] R. Baird, R. N. van Zyl-Smit, A. Iveson, J. Duddy, and S. M. Rassam. Thalidomide is highly effective in a patient with meningeal acute myeloid leukaemia. *Leuk Lymphoma*, 45(1):179–81, 2004.

[8] B. Barlogie. Thalidomide and cc-5013 in multiple myeloma: the university of arkansas experience. *Semin Hematol*, 40(4 Suppl 4):33–8, 2003.

[9] J. B. Bartlett, K. Dredge, and A. G. Dalgleish. The evolution of thalidomide and its imid derivatives as anticancer agents. *Nat Rev Cancer*, 4(4):314–22, 2004.

[10] J. B. Bartlett, A. Michael, I. A. Clarke, K. Dredge, S. Nicholson, H. Kristeleit, A. Polychronis, H. Pandha, G. W. Muller, D. I. Stirling, J. Zeldis, and A. G. Dalgleish. Phase i study to determine the safety, tolerability and immunostimulatory activity of thalidomide analogue cc-5013 in patients with metastatic malignant melanoma and other advanced cancers. *Br J Cancer*, 90(5):955–61, 2004.

[11] Kenneth S Bauer, Shannon C Dixon, and William D Figg. Inhibition of angiogenesis by thalidomide requires metabolic activation, which is species-dependent. *Biochemical Pharmacology*, 55(11):1827–1834, jun 1998.

[12] R. Beckmann. Ueber das verhalten von thalidomid im organismus. *Arzneimittel-Forschung*, 13:185–191, 1963.

[13] S. L. Beedie, C. J. Peer, S. Pisle, E. R. Gardner, C. Mahony, S. Barnett, A. Ambrozak, M. Gutschow, C. H. Chau, N. Vargesson, and W. D. Figg. Anticancer properties of a novel class of tetrafluorinated thalidomide analogues. *Molecular Cancer Therapeutics*, 14(10):2228–2237, aug 2015.

[14] Saoussen Ben Halima, Sabyashachi Mishra, K. Muruga Poopathi Raja, Michael Willem, Antonio Baici, Kai Simons, Oliver Brüstle, Philipp Koch, Christian Haass, Amedeo Caflisch, and Lawrence Rajendran. Specific inhibition of β-secretase processing of the alzheimer disease amyloid precursor protein. *Cell reports*, 14:2127–2141, March 2016.

[15] F. Bertolini, W. Mingrone, A. Alietti, P. F. Ferrucci, E. Cocorocchio, F. Peccatori, S. Cinieri, P. Mancuso, C. Corsini, A. Burlini, E. Zucca, and G. Martinelli. Thalidomide in multiple myeloma, myelodysplastic syndromes and histiocytosis. analysis of clinical results and of surrogate angiogenesis markers. *Ann Oncol*, 12(7):987–90, 2001.

[16] J. Bian, J. Ren, Y. Li, J. Wang, X. Xu, Y. Feng, H. Tang, Y. Wang, and Z. Li. Discovery of wogonin-based protacs against cdk9 and capable of achieving antitumor activity. *Bioorg Chem*, 81:373–381, 2018.

[17] Andrew J. Billnitzer, Irina Barskaya, Cailing Yin, and Ruth G. Perez. App independent and dependent effects on neurite outgrowth are modulated by the receptor associated protein (rap). *Journal of neurochemistry*, 124:123–132, January 2013.

[18] Chad C. Bjorklund, Jian Kang, Michael Amatangelo, Ann Polonskaia, Mark Katz, Hsiling Chiu, Suzana Couto, Maria Wang, Yan Ren, Maria Ortiz, Fadi

Towfic, J. Erin Flynt, William Pierceall, and Anjan Thakurta. Iberdomide (cc-220) is a potent cereblon e3 ligase modulator with antitumor and immunostimulatory activities in lenalidomide- and pomalidomide-resistant multiple myeloma cells with dysregulated crbn. *Leukemia*, 34:1197–1201, April 2020.

[19] I. Boichenko, S. Deiss, K. Bar, M. D. Hartmann, and B. Hernandez Alvarez. A fret-based assay for the identification and characterization of cereblon ligands. *J Med Chem*, 59(2):770–4, 2016.

[20] Iuliia Boichenko, Kerstin Bär, Silvia Deiss, Christopher Heim, Reinhard Albrecht, Andrei N. Lupas, Birte Hernandez Alvarez, and Marcus D. Hartmann. Chemical ligand space of cereblon. *ACS Omega*, 3(9):11163–11171, 2018.

[21] Emil Bulatov, Almaz Zagidullin, Aygul Valiullina, Regina Sayarova, and Albert Rizvanov. Small molecule modulators of ring-type e3 ligases: Mdm and cullin families as targets. *Frontiers in pharmacology*, 9:450, 2018.

[22] Erica Buoso, Cristina Lanni, Gennaro Schettini, Stefano Govoni, and Marco Racchi. beta amyloid precursor protein metabolism: focus on the functions and degradation of its intracellular domain. *Pharmacological Research*, 62(4):308–317, oct 2010.

[23] G. M. Burslem, P. Ottis, S. Jaime-Figueroa, A. Morgan, P. M. Cromm, M. Toure, and C. M. Crews. Efficient synthesis of immunomodulatory drug analogues enables exploration of structure-degradation relationships. *ChemMedChem*, 2018.

[24] Cecilia Carpio, Reda Bouabdallah, Loïc Ysebaert, Juan-Manuel Sancho, Gilles Andre Salles, Raul Cordoba, Antonio Pinto, Mecide Gharibo, Drew Rasco, Carlos Panizo, Jose A Lopez-Martin, Armando Santoro, Antonio Salar, Silvia Damian, Alejandro Martin Garcia-Sancho, Gregor Verhoef, Eric W Van Den Neste, Maria Wang, Suzana Couto, Soraya Carrancio, Andrew Weng, Xuehai Wang, Frank Schmitz, Xin Wei, Kristen M Hege, Matthew

William Burnell Trotter, Alberto Risueno, Tonia Buchholz, Patrick Ryan Hagner, Anita Krithivas Gandhi, Michael Pourdehnad, and Vincent Ribrag. Avadomide monotherapy in relapsed/refractory DLBCL: Safety, efficacy, and a predictive gene classifier. *Blood*, jan 2020.

[25] P. P. Chamberlain, A. Lopez-Girona, K. Miller, G. Carmel, B. Pagarigan, B. Chie-Leon, E. Rychak, L. G. Corral, Y. J. Ren, M. Wang, M. Riley, S. L. Delker, T. Ito, H. Ando, T. Mori, Y. Hirano, H. Handa, T. Hakoshima, T. O. Daniel, and B. E. Cathers. Structure of the human cereblon-ddb1-lenalidomide complex reveals basis for responsiveness to thalidomide analogs. *Nat Struct Mol Biol*, 21(9):803–9, 2014.

[26] C. Chaulet, C. Croix, D. Alagille, S. Normand, A. Delwail, L. Favot, J. C. Lecron, and M. C. Viaud-Massuard. Design, synthesis and biological evaluation of new thalidomide analogues as tnf-alpha and il-6 production inhibitors. *Bioorg Med Chem Lett*, 21(3):1019–22, 2011.

[27] T. L. Chen, G. B. Vogelsang, B. G. Petty, R. B. Brundrett, D. A. Noe, G. W. Santos, and O. M. Colvin. Plasma pharmacokinetics and urinary excretion of thalidomide after oral dosing in healthy male volunteers. *Drug Metab Dispos*, 17(4):402–5, 1989.

[28] T. T. Chu, N. Gao, Q. Q. Li, P. G. Chen, X. F. Yang, Y. X. Chen, Y. F. Zhao, and Y. M. Li. Specific knockdown of endogenous tau protein by peptide-directed ubiquitin-proteasome degradation. *Cell Chem Biol*, 23(4):453–61, 2016.

[29] F. Chung, J. Lu, B. D. Palmer, P. Kestell, P. Browett, B. C. Baguley, M. Tingle, and L. M. Ching. Thalidomide pharmacokinetics and metabolite formation in mice, rabbits, and multiple myeloma patients. *Clin Cancer Res*, 10(17):5949–56, 2004.

[30] Marie Daval, Fabienne Foufelle, and Pascal Ferré. Functions of AMP-activated protein kinase in adipose tissue. *The Journal of Physiology*, 574(1):55–62, jun 2006.

[31] Stefanie A. H. de Poot, Geng Tian, and Daniel Finley. Meddling with fate: The proteasomal deubiquitinating enzymes. *Journal of molecular biology*, 429:3525–3545, November 2017.

[32] David A. DeGoey, Hui-Ju Chen, Philip B. Cox, and Michael D. Wendt. Beyond the rule of 5: Lessons learned from AbbVie's drugs and compound collection. *Journal of Medicinal Chemistry*, 61(7):2636–2651, sep 2017.

[33] Dolores Del Prete, Richard C. Rice, Anjali M. Rajadhyaksha, and Luciano D'Adamio. Amyloid precursor protein (app) may act as a substrate and a recognition unit for crl4(crbn) and stub1 e3 ligases facilitating ubiquitination of proteins involved in presynaptic functions and neurodegeneration. *The Journal of Biological Chemistry*, 291(33):17209–17227, 2016.

[34] M. S. Denison and J. P. Whitlock. Xenobiotic-inducible transcription of cytochrome p450 genes. *The Journal of biological chemistry*, 270:18175–18178, August 1995.

[35] Raymond J. Deshaies and Claudio A. P. Joazeiro. Ring domain e3 ubiquitin ligases. *Annual review of biochemistry*, 78:399–434, 2009.

[36] Mario Di Napoli and Francesca Papa. The proteasome system and proteasome inhibitors in stroke: controlling the inflammatory response. *Current opinion in investigational drugs (London, England : 2000)*, 4:1333–1342, November 2003.

[37] K. A. Donovan, J. An, R. P. Nowak, J. C. Yuan, E. C. Fink, B. C. Berry, B. L. Ebert, and E. S. Fischer. Thalidomide promotes degradation of sall4, a transcription factor implicated in duane radial ray syndrome. *Elife*, 7, 2018.

[38] Katja K. Dove, Benjamin Stieglitz, Emily D. Duncan, Katrin Rittinger, and Rachel E. Klevit. Molecular insights into rbr e3 ligase ubiquitin transfer mechanisms. *EMBO reports*, 17:1221–1235, August 2016.

[39] K. Dredge, R. Horsfall, S. P. Robinson, L. H. Zhang, L. Lu, Y. Tang, M. A. Shirley, G. Muller, P. Schafer, D. Stirling, A. G. Dalgleish, and J. B. Bartlett.

Orally administered lenalidomide (cc-5013) is anti-angiogenic in vivo and inhibits endothelial cell migration and akt phosphorylation in vitro. *Microvasc Res*, 69(1-2):56–63, 2005.

[40] Irina Dulubova, Angela Ho, Iryna Huryeva, Thomas C Südhof, and Josep Rizo. Three-dimensional structure of an independently folded extracellular domain of human amyloid-β precursor protein. *Biochemistry*, 43(30):9583–9588, 2004.

[41] Scott D. Edmondson, Bin Yang, and Charlene Fallan. Proteolysis targeting chimeras (PROTACs) in 'beyond rule-of-five' chemical space: Recent progress and future challenges. *Bioorganic & Medicinal Chemistry Letters*, 29(13):1555–1564, jul 2019.

[42] Ruth Eichner, Michael Heider, Vanesa Fernández-Sáiz, Frauke van Bebber, Anne-Kathrin Garz, Simone Lemeer, Martina Rudelius, Bianca-Sabrina Targosz, Laura Jacobs, Anna-Maria Knorn, Jolanta Slawska, Uwe Platzbecker, Ulrich Germing, Christian Langer, Stefan Knop, Herrmann Einsele, Christian Peschel, Christian Haass, Ulrich Keller, Bettina Schmid, Katharina S Götze, Bernhard Kuster, and Florian Bassermann. Immunomodulatory drugs disrupt the cereblon–CD147–MCT1 axis to exert antitumor activity and teratogenicity. *Nature Medicine*, 22(7):735–743, jun 2016.

[43] Bishoy Y.A. El-Aarag, Tomonari Kasai, Magdy A.H. Zahran, Nadia I. Zakhary, Tsukasa Shigehiro, Sreeja C. Sekhar, Hussein S. Agwa, Akifumi Mizutani, Hiroshi Murakami, Hiroki Kakuta, and Masaharu Seno. In vitro anti-proliferative and anti-angiogenic activities of thalidomide dithiocarbamate analogs. *International Immunopharmacology*, 21(2):283–292, aug 2014.

[44] P. Emsley, B. Lohkamp, W. G. Scott, and K. Cowtan. Features and development of coot. *Acta Crystallogr D Biol Crystallogr*, 66(Pt 4):486–501, 2010.

[45] S. Fabro, R. L. Smith, and R. T. Williams. The fate of the hydrolysis products of thalidomide in the pregnant rabbit. *Biochem J*, 104(2):570–4, 1967.

[46] FDA. Us thalomid (thalidomide) label, July 2015.

[47] FDA. Novel drug approvals for 2019, 2020.

[48] Napoleone Ferrara, Hans-Peter Gerber, and Jennifer LeCouter. The biology of VEGF and its receptors. *Nature Medicine*, 9(6):669–676, jun 2003.

[49] Emma C. Fink, Marie McConkey, Dylan N. Adams, Saurav D. Haldar, James A. Kennedy, Andrew A. Guirguis, Namrata D. Udeshi, D. R. Mani, Michelle Chen, Brian Liddicoat, Tanya Svinkina, Andrew T. Nguyen, Steven A. Carr, and Benjamin L. Ebert. Crbni391v is sufficient to confer in vivo sensitivity to thalidomide and its derivatives in mice. *Blood*, 132:1535–1544, October 2018.

[50] E. S. Fischer, K. Bohm, J. R. Lydeard, H. Yang, M. B. Stadler, S. Cavadini, J. Nagel, F. Serluca, V. Acker, G. M. Lingaraju, R. B. Tichkule, M. Schebesta, W. C. Forrester, M. Schirle, U. Hassiepen, J. Ottl, M. Hild, R. E. Beckwith, J. W. Harper, J. L. Jenkins, and N. H. Thoma. Structure of the ddb1-crbn e3 ubiquitin ligase in complex with thalidomide. *Nature*, 512(7512):49–53, 2014.

[51] J. Folkman, E. Merler, C. Abernathy, and G. Williams. Isolation of a tumor factor responsible for angiogenesis. *The Journal of experimental medicine*, 133:275–288, February 1971.

[52] Michael G. Friedrich, Zhen Wang, Kevin L. Schey, and Roger J.W. Truscott. Mechanism of protein cleavage at asparagine leading to protein-protein crosslinks. *Biochemical Journal*, dec 2019.

[53] Fernando Galvão, Kamila Castro Grokoski, Bruno Batista da Silva, Marcelo Lazzaron Lamers, and Ionara Rodrigues Siqueira. The amyloid precursor protein (app) processing as a biological link between alzheimer's disease and cancer. *Ageing research reviews*, 49:83–91, January 2019.

[54] R. García-Sanz, T. J. González-López, L. Vázquez, G. Hermida, I. F. Graciani, and J. F. San Miguel. The combination of thalidomide, cyclophosphamide and dexamethasone is potentially useful in highly resistant hodgkin's lymphoma. *European journal of haematology*, 84:266–270, March 2010.

[55] George G. Glenner and Caine W. Wong. Alzheimer's disease: Initial report of the purification and characterization of a novel cerebrovascular amyloid protein. *Biochemical and Biophysical Research Communications*, 120(3):885–890, may 1984.

[56] Marcus OW Grimm, Tatjana L Rothhaar, and Tobias Hartmann. The role of app proteolytic processing in lipid metabolism. *Experimental brain research*, 217(3-4):365–375, 2012.

[57] F. Peter Guengerich. Cytochrome p450 and chemical toxicology. *Chemical research in toxicology*, 21:70–83, January 2008.

[58] Christian Haass and Dennis J. Selkoe. Soluble protein oligomers in neurodegeneration: lessons from the alzheimer's amyloid beta-peptide. *Nature reviews. Molecular cell biology*, 8:101–112, February 2007.

[59] Patrick R. Hagner, Hon-Wah Man, Celia Fontanillo, Maria Wang, Suzana Couto, Mike Breider, Chad Bjorklund, Courtney G. Havens, Gang Lu, Emily Rychak, Heather Raymon, Rama Krishna Narla, Leo Barnes, Gody Khambatta, Hsiling Chiu, Jolanta Kosek, Jian Kang, Michael D. Amantangelo, Michelle Waldman, Antonia Lopez-Girona, Ti Cai, Michael Pourdehnad, Matthew Trotter, Thomas O. Daniel, Peter H. Schafer, Anke Klippel, Anjan Thakurta, Rajesh Chopra, and Anita K. Gandhi. CC-122, a pleiotropic pathway modifier, mimics an interferon response and has antitumor activity in DLBCL. *Blood*, 126(6):779–789, aug 2015.

[60] X. Han, C. Wang, C. Qin, W. Xiang, E. Fernandez-Salas, C. Y. Yang, M. Wang, L. Zhao, T. Xu, K. Chinnaswamy, J. Delproposto, J. Stuckey,

and S. Wang. Discovery of ard-69 as a highly potent proteolysis targeting chimera (protac) degrader of androgen receptor (ar) for the treatment of prostate cancer. *J Med Chem*, 62(2):941–964, 2019.

[61] D. Grahame Hardie. AMP-activated/SNF1 protein kinases: conserved guardians of cellular energy. *Nature Reviews Molecular Cell Biology*, 8(10):774–785, oct 2007.

[62] M. D. Hartmann, I. Boichenko, M. Coles, A. N. Lupas, and B. Hernandez Alvarez. Structural dynamics of the cereblon ligand binding domain. *PLoS One*, 10(5):e0128342, 2015.

[63] M. D. Hartmann, I. Boichenko, M. Coles, F. Zanini, A. N. Lupas, and B. Hernandez Alvarez. Thalidomide mimics uridine binding to an aromatic cage in cereblon. *J Struct Biol*, 188(3):225–32, 2014.

[64] Noriko Hasebe, Yuki Fujita, Masaki Ueno, Kazuhiro Yoshimura, Yuji Fujino, and Toshihide Yamashita. Soluble β-amyloid precursor protein alpha binds to p75 neurotrophin receptor to promote neurite outgrowth. *PloS one*, 8:e82321, 2013.

[65] Christopher Heim, Dimanthi Pliatsika, Farnoush Mousavizadeh, Kerstin Bär, Birte Hernandez Alvarez, Athanassios Giannis, and Marcus D Hartmann. De-novo design of cereblon (crbn) effectors guided by natural hydrolysis products of thalidomide derivatives. *Journal of medicinal chemistry*, 62:6615–6629, July 2019.

[66] T. Hideshima, D. Chauhan, Y. Shima, N. Raje, F. E. Davies, Y. T. Tai, S. P. Treon, B. Lin, R. L. Schlossman, P. Richardson, G. Muller, D. I. Stirling, and K. C. Anderson. Thalidomide and its analogs overcome drug resistance of human multiple myeloma cells to conventional therapy. *Blood*, 96(9):2943–50, 2000.

[67] J. J. Higgins, J. Pucilowska, R. Q. Lombardi, and J. P. Rooney. A mutation in a novel ATP-dependent lon protease gene in a kindred with mild mental retardation. *Neurology*, 63(10):1927–1931, nov 2004.

[68] C. Hoareau, V. Borrell, E. Soriano, M. O. Krebs, A. Prochiantz, and B. Allinquant. Amyloid precursor protein cytoplasmic domain antagonizes reelin neurite outgrowth inhibition of hippocampal neurons. *Neurobiology of aging*, 29:542–553, April 2008.

[69] Jiantao Hu, Biao Hu, Mingliang Wang, Fuming Xu, Bukeyan Miao, Chao-Yie Yang, Mi Wang, Zhaomin Liu, Daniel F Hayes, Krishnapriya Chinnaswamy, James Delproposto, Jeanne Stuckey, and Shaomeng Wang. Discovery of erd-308 as a highly potent proteolysis targeting chimera (protac) degrader of estrogen receptor (er). *Journal of medicinal chemistry*, 62:1420–1442, February 2019.

[70] S. Hunter and C. Brayne. Understanding the roles of mutations in the amyloid precursor protein in alzheimer disease. *Molecular psychiatry*, 23:81–93, January 2018.

[71] Jeffrey R Infante, Suzanne F Jones, Johanna C Bendell, David R Spigel, Denise A Yardley, Colin D Weekes, Wells A Messersmith, John D Hainsworth, and Howard A Burris III. A phase i, dose-escalation study of pomalidomide (cc-4047) in combination with gemcitabine in metastatic pancreas cancer. *European journal of cancer*, 47(2):199–205, 2011.

[72] T. Ito, H. Ando, T. Suzuki, T. Ogura, K. Hotta, Y. Imamura, Y. Yamaguchi, and H. Handa. Identification of a primary target of thalidomide teratogenicity. *Science*, 327(5971):1345–50, 2010.

[73] Kristin T Jacobsen and Kerstin Iverfeldt. Amyloid precursor protein and its homologues: a family of proteolysis-dependent receptors. *Cellular and molecular life sciences*, 66(14):2299–2318, 2009.

[74] Anne-Claire Jacomin, Emmanuel Taillebourg, and Marie-Odile Fauvarque. Deubiquitinating enzymes related to autophagy: New therapeutic opportunities? *Cells*, 7, August 2018.

[75] Moran Jerabek-Willemsen, Timon André, Randy Wanner, Heide Marie Roth, Stefan Duhr, Philipp Baaske, and Dennis Breitsprecher. MicroScale

thermophoresis: Interaction analysis and beyond. *Journal of Molecular Structure*, 1077:101–113, dec 2014.

[76] R. E. Johnston and S. H. Abdalla. Thalidomide in low doses is effective for the treatment of resistant or relapsed multiple myeloma and for plasma cell leukaemia. *Leuk Lymphoma*, 43(2):351–4, 2002.

[77] W. Kabsch. Xds. *Acta Crystallogr D Biol Crystallogr*, 66(Pt 2):125–32, 2010.

[78] U. Kaiser. [thalidomide as a new treatment option in patients with multiple myeloma]. *Dtsch Med Wochenschr*, 125(50):T26–T29, 2000.

[79] V. Kale and A. F. List. Immunomodulatory drugs (imids): a new treatment option for myelodysplastic syndromes. *Curr Pharm Biotechnol*, 7(5):339–42, 2006.

[80] Robert B Kargbo. Protac-mediated degradation of estrogen receptor in the treatment of cancer. *ACS medicinal chemistry letters*, 10:1367–1369, October 2019.

[81] Robert B. Kargbo. Treatment of alzheimer's by protac-tau protein degradation. *ACS Medicinal Chemistry Letters*, 2019.

[82] Daniel B. Kassel. Applications of high-throughput adme in drug discovery. *Current opinion in chemical biology*, 8:339–345, June 2004.

[83] H. KELLER, K. U. N. Z. W, and H. MUCKTER. [n-phthalyl-glutamic acid imide; experimental studies on a new synthetic product with sedative properties]. *Arzneimittel-Forschung*, 6:426–430, August 1956.

[84] Kazunori Kikuchi, Kiwami Kidana, Takuya Tatebe, and Taisuke Tomita. Dysregulated metabolism of the amyloid-β protein and therapeutic approaches in alzheimer disease. *Journal of cellular biochemistry*, 118:4183–4190, December 2017.

[85] Kidae Kim, Dong Ho Lee, Sungryul Park, Seung-Hyun Jo, Bonsu Ku, Sung Goo Park, Byoung Chul Park, Yeong Uk Jeon, Sunjoo Ahn,

Chung Hyo Kang, Daehee Hwang, Sehyun Chae, Jae Du Ha, Sunhong Kim, Jong Yeon Hwang, and Jeong-Hoon Kim. Disordered region of cereblon is required for efficient degradation by proteolysis-targeting chimera. *Scientific Reports*, 9(1), dec 2019.

[86] Yong Deuk Kim, Kwang Min Lee, Seung-Lark Hwang, Hyeun Wook Chang, Keuk-Jun Kim, Robert A. Harris, Hueng-Sik Choi, Won-Sik Choi, Sung-Eun Lee, and Chul-Seung Park. Inhibition of cereblon by fenofibrate ameliorates alcoholic liver disease by enhancing AMPK. *Biochimica et Biophysica Acta (BBA) - Molecular Basis of Disease*, 1852(12):2662–2670, dec 2015.

[87] Y. Kishi, Y. Oki, and U. Machida. Thalidomide in multiple myeloma. *N Engl J Med*, 342(13):975; author reply 975–6, 2000.

[88] A. Kneller, P. Raanani, I. Hardan, A. Avigdor, I. Levi, M. Berkowicz, and I. Ben-Bassat. Therapy with thalidomide in refractory multiple myeloma patients - the revival of an old drug. *Br J Haematol*, 108(2):391–3, 2000.

[89] Geoffrey K-W Kong, Julian J Adams, Hugh H Harris, John F Boas, Cyril C Curtain, Denise Galatis, Colin L Masters, Kevin J Barnham, William J McKinstry, Roberto Cappai, et al. Structural studies of the alzheimer's amyloid precursor protein copper-binding domain reveal how it binds copper ions. *Journal of molecular biology*, 367(1):148–161, 2007.

[90] Christopher D Kroenke, Dorota Ziemnicka-Kotula, Jiliu Xu, Leszek Kotula, and Arthur G Palmer. Solution conformations of a peptide containing the cytoplasmic domain sequence of the β amyloid precursor protein. *Biochemistry*, 36(26):8145–8152, 1997.

[91] J. Kronke, E. C. Fink, P. W. Hollenbach, K. J. MacBeth, S. N. Hurst, N. D. Udeshi, P. P. Chamberlain, D. R. Mani, H. W. Man, A. K. Gandhi, T. Svinkina, R. K. Schneider, M. McConkey, M. Jaras, E. Griffiths, M. Wetzler, L. Bullinger, B. E. Cathers, S. A. Carr, R. Chopra, and B. L. Ebert. Lenalidomide induces ubiquitination and degradation of ck1alpha in del(5q) mds. *Nature*, 523(7559):183–188, 2015.

[92] J. Kronke, S. N. Hurst, and B. L. Ebert. Lenalidomide induces degradation of ikzf1 and ikzf3. *Oncoimmunology*, 3(7):e941742, 2014.

[93] J. Kronke, N. D. Udeshi, A. Narla, P. Grauman, S. N. Hurst, M. McConkey, T. Svinkina, D. Heckl, E. Comer, X. Li, C. Ciarlo, E. Hartman, N. Munshi, M. Schenone, S. L. Schreiber, S. A. Carr, and B. L. Ebert. Lenalidomide causes selective degradation of ikzf1 and ikzf3 in multiple myeloma cells. *Science*, 343(6168):301–5, 2014.

[94] Tomotaka Kurihara, Toru Asahi, and Naoya Sawamura. Cereblon-mediated degradation of the amyloid precursor protein via the ubiquitin-proteasome pathway. *Biochemical and biophysical research communications*, January 2020.

[95] J. Kuruvilla, K. Song, P. Mollee, T. Panzarella, J. McCrae, T. Nagy, M. Crump, and A. Keating. A phase ii study of thalidomide and vinblastine for palliative patients with hodgkin's lymphoma. *Hematology*, 11(1):25–9, 2006.

[96] R. A. Kyle and S. V. Rajkumar. Therapeutic application of thalidomide in multiple myeloma. *Semin Oncol*, 28(6):583–7, 2001.

[97] A. C. Lai and C. M. Crews. Induced protein degradation: an emerging drug discovery paradigm. *Nat Rev Drug Discov*, 16(2):101–114, 2017.

[98] M. Larkin. Low-dose thalidomide seems to be effective in multiple myeloma. *Lancet*, 354(9182):925, 1999.

[99] Jennifer Lee and Pengbo Zhou. DCAFs, the missing link of the CUL4-DDB1 ubiquitin ligase. *Molecular Cell*, 26(6):775–780, jun 2007.

[100] Widukind Lenz. A short history of thalidomide embryopathy. *Teratology*, 38(3):203–215, 1988.

[101] Erin R. Lepper, Sylvia S. W. Ng, Michael Gütschow, Michael Weiss, Sunna Hauschildt, Thomas K. Hecker, Frederick A. Luzzio, Kurt Eger, and William D. Figg. Comparative molecular field analysis and comparative

molecular similarity indices analysis of thalidomide analogues as angiogenesis inhibitors. *Journal of Medicinal Chemistry*, 47(9):2219–2227, apr 2004.

[102] Xiping Li, Xuyi Liu, Jie Wang, Zengli Wang, Wei Jiang, Eddie Reed, Yi Zhang, Yuanlin Liu, and Q. Quentin Li. Thalidomide down-regulates the expression of vegf and bfgf in cisplatin-resistant human lung carcinoma cells. *Anticancer research*, 23:2481–2487, 2003.

[103] Yuanyuan Li, Silong Zhang, Jing Zhang, Zhiye Hu, Yuan Xiao, Jian Huang, Chune Dong, Shengtang Huang, and Hai-Bing Zhou. Exploring the protac degron candidates: Obhsa with different side chains as novel selective estrogen receptor degraders (serds). *European journal of medicinal chemistry*, 172:48–61, June 2019.

[104] Yuhua Li, Qiang Meng, Mengbi Yang, Dongyang Liu, Xiangyu Hou, Lan Tang, Xin Wang, Yuanfeng Lyu, Xiaoyan Chen, Kexin Liu, et al. Current trends in drug metabolism and pharmacokinetics. *Acta Pharmaceutica Sinica B*, 9(6):1113–1144, 2019.

[105] C. A. Lipinski, F. Lombardo, B. W. Dominy, and P. J. Feeney. Experimental and computational approaches to estimate solubility and permeability in drug discovery and development settings. *Advanced drug delivery reviews*, 46:3–26, March 2001.

[106] Cui-Hua Liu, Alfred L. Goldberg, and Xiao-Bo Qiu. New insights into the role of the ubiquitin-proteasome pathway in the regulation of apoptosis. *Chang Gung medical journal*, 30:469–479, 2007.

[107] Qing Liu, Fu Shang, Weimin Guo, Marisa Hobbs, Paloma Valverde, Venkat Reddy, and Allen Taylor. Regulation of the ubiquitin proteasome pathway in human lens epithelial cells during the cell cycle. *Experimental eye research*, 78:197–205, February 2004.

[108] A Lopez-Girona, D Mendy, T Ito, K Miller, A K Gandhi, J Kang, S Karasawa, G Carmel, P Jackson, M Abbasian, A Mahmoudi, B Cathers, E Rychak,

S Gaidarova, R Chen, P H Schafer, H Handa, T O Daniel, J F Evans, and R Chopra. Cereblon is a direct protein target for immunomodulatory and antiproliferative activities of lenalidomide and pomalidomide. *Leukemia*, 26(11):2326–2335, may 2012.

[109] G. Lu, R. E. Middleton, H. Sun, M. Naniong, C. J. Ott, C. S. Mitsiades, K.-K. Wong, J. E. Bradner, and W. G. Kaelin. The myeloma drug lenalidomide promotes the cereblon-dependent destruction of ikaros proteins. *Science*, 343(6168):305–309, nov 2013.

[110] M. Lu, T. Liu, Q. Jiao, J. Ji, M. Tao, Y. Liu, Q. You, and Z. Jiang. Discovery of a keap1-dependent peptide protac to knockdown tau by ubiquitination-proteasome degradation pathway. *Eur J Med Chem*, 146:251–259, 2018.

[111] Andrei N Lupas, Hongbo Zhu, and Mateusz Korycinski. The thalidomide-binding domain of cereblon defines the cult domain family and is a new member of the β-tent fold. *PLoS computational biology*, 11(1):e1004023, 2015.

[112] Mariette Matondo, Marlène Marcellin, Karima Chaoui, Marie-Pierre Bousquet-Dubouch, Anne Gonzalez-de Peredo, Bernard Monsarrat, and Odile Burlet-Schiltz. Determination of differentially regulated proteins upon proteasome inhibition in aml cell lines by the combination of large-scale and targeted quantitative proteomics. *Proteomics*, 17, April 2017.

[113] M. E. Matyskiela, W. Zhang, H. W. Man, G. Muller, G. Khambatta, F. Baculi, M. Hickman, L. LeBrun, B. Pagarigan, G. Carmel, C. C. Lu, G. Lu, M. Riley, Y. Satoh, P. Schafer, T. O. Daniel, J. Carmichael, B. E. Cathers, and P. P. Chamberlain. A cereblon modulator (cc-220) with improved degradation of ikaros and aiolos. *J Med Chem*, 61(2):535–542, 2018.

[114] Mary E. Matyskiela, Thomas Clayton, Xinde Zheng, Christopher Mayne, Eileen Tran, Aaron Carpenter, Barbra Pagarigan, Joseph McDonald, Mark Rolfe, Lawrence G. Hamann, Gang Lu, and Philip P. Chamberlain. Crystal structure of the sall4-pomalidomide-cereblon-ddb1 complex. *Nature structural molecular biology*, 27:319–322, April 2020.

[115] Mary E. Matyskiela, Suzana Couto, Xinde Zheng, Gang Lu, Julia Hui, Katie Stamp, Clifton Drew, Yan Ren, Maria Wang, Aaron Carpenter, Chung-Wein Lee, Thomas Clayton, Wei Fang, Chin-Chun Lu, Mariko Riley, Polat Abdubek, Kate Blease, James Hartke, Gondi Kumar, Rupert Vessey, Mark Rolfe, Lawrence G. Hamann, and Philip P. Chamberlain. Sall4 mediates teratogenicity as a thalidomide-dependent cereblon substrate. *Nature Chemical Biology*, 2018.

[116] Mary E. Matyskiela, Gang Lu, Takumi Ito, Barbra Pagarigan, Chin-Chun Lu, Karen Miller, Wei Fang, Nai-Yu Wang, Derek Nguyen, Jack Houston, Gilles Carmel, Tam Tran, Mariko Riley, Lyn'Al Nosaka, Gabriel C. Lander, Svetlana Gaidarova, Shuichan Xu, Alexander L. Ruchelman, Hiroshi Handa, James Carmichael, Thomas O. Daniel, Brian E. Cathers, Antonia Lopez-Girona, and Philip P. Chamberlain. A novel cereblon modulator recruits GSPT1 to the CRL4crbn ubiquitin ligase. *Nature*, 535(7611):252–257, jun 2016.

[117] M Mergler, F Dick, B Sax, P Weiler, and Th Vorherr. The aspartimide problem in fmoc-based spps. part i. *Journal of peptide science: an official publication of the European Peptide Society*, 9(1):36–46, 2003.

[118] M. T. Miller. Thalidomide embryopathy: a model for the study of congenital incomitant horizontal strabismus. *Transactions of the American Ophthalmological Society*, 89:623–674, 1991.

[119] M. T. Miller and K. Strömland. Teratogen update: thalidomide: a review, with a focus on ocular findings and new potential uses. *Teratology*, 60:306–321, November 1999.

[120] Ashley Mooneyham and Martina Bazzaro. Targeting deubiquitinating enzymes and autophagy in cancer. *Methods in molecular biology (Clifton, N.J.)*, 1513:49–59, 2017.

[121] Tomoyuki Mori, Takumi Ito, Shujie Liu, Hideki Ando, Satoshi Sakamoto, Yuki Yamaguchi, Etsuko Tokunaga, Norio Shibata, Hiroshi Handa, and

Toshio Hakoshima. Structural basis of thalidomide enantiomer binding to cereblon. *Scientific Reports*, 8(1):1294, 2018.

[122] Mohamed Muhsin, Joanne Graham, and Peter Kirkpatrick. Bevacizumab. *Nature Reviews Drug Discovery*, 3(12):995–996, dec 2004.

[123] Garib N. Murshudov, Pavol Skubák, Andrey A. Lebedev, Navraj S. Pannu, Roberto A. Steiner, Robert A. Nicholls, Martyn D. Winn, Fei Long, and Alexei A. Vagin. REFMAC5 for the refinement of macromolecular crystal structures. *Acta Crystallographica Section D Biological Crystallography*, 67(4):355–367, mar 2011.

[124] T. Nakamura, T. Noguchi, H. Miyachi, and Y. Hashimoto. Hydrolyzed metabolites of thalidomide: synthesis and tnf-alpha production-inhibitory activity. *Chem Pharm Bull (Tokyo)*, 55(4):651–4, 2007.

[125] Kevin Neumann, Jakob Farnung, Simon Baldauf, and Jeffrey W Bode. Prevention of aspartimide formation during peptide synthesis using cyanosulfurylides as carboxylic acid-protecting groups. *Nature communications*, 11(1):1–10, 2020.

[126] C. G. Newman. Teratogen update: clinical aspects of thalidomide embryopathy–a continuing preoccupation. *Teratology*, 32(1):133–44, 1985.

[127] Sylvia S. W. Ng, Michael Gütschow, Michael Weiss, Sunna Hauschildt, Uwe Teubert, Thomas K. Hecker, Frederick A. Luzzio, Erwin A. Kruger, Kurt Eger, and William D. Figg. Antiangiogenic activity of n-substituted and tetrafluorinated thalidomide analogues. *Cancer research*, 63:3189–3194, June 2003.

[128] Sylvia S. W. Ng, Gordon R. MacPherson, Michael Gütschow, Kurt Eger, and William D. Figg. Antitumor effects of thalidomide analogs in human prostate cancer xenografts implanted in immunodeficient mice. *Clinical cancer research : an official journal of the American Association for Cancer Research*, 10:4192–4197, June 2004.

[129] T. V. Nguyen, J. E. Lee, M. J. Sweredoski, S. J. Yang, S. J. Jeon, J. S. Harrison, J. H. Yim, S. G. Lee, H. Handa, B. Kuhlman, J. S. Jeong, J. M. Reitsma, C. S. Park, S. Hess, and R. J. Deshaies. Glutamine triggers acetylation-dependent degradation of glutamine synthetase via the thalidomide receptor cereblon. *Mol Cell*, 61(6):809–20, 2016.

[130] Thang Van Nguyen, Jing Li, Chin-Chun (Jean) Lu, Jennifer L. Mamrosh, Gang Lu, Brian E. Cathers, and Raymond J. Deshaies. p97/VCP promotes degradation of CRBN substrate glutamine synthetase and neosubstrates. *Proceedings of the National Academy of Sciences*, 114(14):3565–3571, mar 2017.

[131] National Institute for Health NICE and Care Excellence. *Overview: Bortezomib and Thalidomide for the First-Line Treatment of Multiple Myeloma: Guidance.*, July 2011.

[132] Zaneta Nikolovska-Coleska, Renxiao Wang, Xueliang Fang, Hongguang Pan, York Tomita, Peng Li, Peter P Roller, Krzysztof Krajewski, Naoyuki G Saito, Jeanne A Stuckey, et al. Development and optimization of a binding assay for the xiap bir3 domain using fluorescence polarization. *Analytical biochemistry*, 332(2):261–273, 2004.

[133] Satomi Niwayama, Christine Loh, Benjamin E. Turk, Jun O. Liu, Hiroyuki Miyachi, and Yuichi Hashimoto. Enhanced potency of perfluorinated thalidomide derivatives for inhibition of LPS-induced tumor necrosis factor-alpha production is associated with a change of mechanism of action. *Bioorganic & Medicinal Chemistry Letters*, 8(9):1071–1076, may 1998.

[134] Tomomi Noguchi, Haruka Fujimoto, Hiroko Sano, Atsushi Miyajima, Hiroyuki Miyachi, and Yuichi Hashimoto. Angiogenesis inhibitors derived from thalidomide. *Bioorganic & Medicinal Chemistry Letters*, 15(24):5509–5513, dec 2005.

[135] Tomomi Noguchi, Rumiko Shimazawa, Kazuo Nagasawa, and Yuichi Hashimoto. Thalidomide and its analogues as cyclooxygenase inhibitors. *Bioorganic & Medicinal Chemistry Letters*, 12(7):1043–1046, apr 2002.

[136] Richard J. O'Brien and Philip C. Wong. Amyloid precursor protein processing and alzheimer's disease. *Annual Review of Neuroscience*, 34(1):185–204, jul 2011.

[137] Kohei Otogawa, Yosyisuki Ogino, Kazuhiko Ishikawa, Makoto Tanaka, Motoo Shiro, Tutsuya Osaka, and Toru Asahi. Structural and thermal analyses of a hydrolysis compound of thalidomide. *Acta Crystallographica Section A*, 70(a1):C113, 2014.

[138] Raphaëlle Pardossi-Piquard and Frederic Checler. The physiology of the beta amyloid precursor protein intracellular domain AICD. *Journal of Neurochemistry*, 120:109–124, nov 2011.

[139] Jinyoung Park, Jinhong Cho, Eunice EunKyeong Kim, and Eun Joo Song. Deubiquitinating enzymes: A critical regulator of mitosis. *International journal of molecular sciences*, 20, November 2019.

[140] Olavi Pelkonen, Miia Turpeinen, Jukka Hakkola, Paavo Honkakoski, Janne Hukkanen, and Hannu Raunio. Inhibition and induction of human cytochrome p450 enzymes: current status. *Archives of toxicology*, 82:667–715, October 2008.

[141] Lijie Peng, Zhensheng Zhang, Chong Lei, Shan Li, Zhang Zhang, Xiaomei Ren, Yu Chang, Yan Zhang, Yong Xu, and Ke Ding. Identification of new small-molecule inducers of estrogen-related receptor α (errα) degradation. *ACS medicinal chemistry letters*, 10:767–772, May 2019.

[142] Francine B Perler, Ming-Qun Xu, and Henry Paulus. Protein splicing and autoproteolysis mechanisms. *Current Opinion in Chemical Biology*, 1(3):292–299, oct 1997.

[143] G. Petzold, E. S. Fischer, and N. H. Thoma. Structural basis of lenalidomide-induced ck1alpha degradation by the crl4(crbn) ubiquitin ligase. *Nature*, 532(7597):127–30, 2016.

[144] Douglas K. Price, Yuichi Ando, Erwin A. Kruger, Michael Weiss, and William D. Figg. 5'-oh-thalidomide, a metabolite of thalidomide, inhibits angiogenesis. *Therapeutic drug monitoring*, 24:104–110, February 2002.

[145] Chong Qin, Yang Hu, Bing Zhou, Ester Fernandez-Salas, Chao-Yie Yang, Liu Liu, Donna McEachern, Sally Przybranowski, Mi Wang, Jeanne Stuckey, Jennifer Meagher, Longchuan Bai, Zhuo Chen, Mei Lin, Jiuling Yang, Danya N Ziazadeh, Fuming Xu, Jiantao Hu, Weiguo Xiang, Liyue Huang, Siwei Li, Bo Wen, Duxin Sun, and Shaomeng Wang. Discovery of qca570 as an exceptionally potent and efficacious proteolysis targeting chimera (protac) degrader of the bromodomain and extra-terminal (bet) proteins capable of inducing complete and durable tumor regression. *Journal of medicinal chemistry*, 61:6685–6704, August 2018.

[146] Zhen Qu, Chunping Jiang, Junhua Wu, and Yitao Ding. Lenalidomide induces apoptosis and inhibits angiogenesis via caspase-3 and VEGF in hepatocellular carcinoma cells. *Molecular Medicine Reports*, 14(5):4781–4786, oct 2016.

[147] H. Quach, D. Ritchie, A. K. Stewart, P. Neeson, S. Harrison, M. J. Smyth, and H. M. Prince. Mechanism of action of immunomodulatory drugs (imids) in multiple myeloma. *Leukemia*, 24(1):22–32, 2010.

[148] Kanak Raina, Jing Lu, Yimin Qian, Martha Altieri, Deborah Gordon, Ann Marie K Rossi, Jing Wang, Xin Chen, Hanqing Dong, Kam Siu, James D Winkler, Andrew P Crew, Craig M Crews, and Kevin G Coleman. Protac-induced bet protein degradation as a therapy for castration-resistant prostate cancer. *Proceedings of the National Academy of Sciences of the United States of America*, 113:7124–7129, June 2016.

[149] S Vincent Rajkumar, Suzanne R Hayman, Martha Q Lacy, Angela Dispenzieri, Antje Hoering, Susan M Geyer, Steven R Zeldenrust, Philip R Greipp, Rafael Fonseca, John A Lust, et al. Combination therapy with cc-5013 (lenalidomide; revlimid™) plus dexamethasone (rev/dex) for newly diagnosed myeloma (mm)., 2004.

[150] Janusz Rak and Joanne L Yu. Oncogenes and tumor angiogenesis. *Seminars in Cancer Biology*, 14(2):93–104, apr 2004.

[151] Drew W. Rasco, Kyriakos P. Papadopoulos, Michael Pourdehnad, Anita K. Gandhi, Patrick R. Hagner, Yan Li, Xin Wei, Rajesh Chopra, Kristen Hege, Jorge DiMartino, and Kent Shih. A first-in-human study of novel cereblon modulator avadomide (CC-122) in advanced malignancies. *Clinical Cancer Research*, 25(1):90–98, sep 2018.

[152] Namrata Rastogi and Durga Prasad Mishra. Therapeutic targeting of cancer cell cycle using proteasome inhibitors. *Cell division*, 7:26, December 2012.

[153] Marianne Reist, Pierre-Alain Carrupt, Eric Francotte, and Bernard Testa. Chiral inversion and hydrolysis of thalidomide: mechanisms and catalysis by bases and serum albumin, and chiral stability of teratogenic metabolites. *Chemical research in toxicology*, 11(12):1521–1528, 1998.

[154] Katherine H. Reiter and Rachel E. Klevit. Characterization of ring-between-ring e3 ubiquitin transfer mechanisms. *Methods in molecular biology (Clifton, N.J.)*, 1844:3–17, 2018.

[155] Caroline M Robb, Jacob I Contreras, Smit Kour, Margaret A Taylor, Mohammad Abid, Yogesh A Sonawane, Muhammad Zahid, Daryl J Murry, Amarnath Natarajan, and Sandeep Rana. Chemically induced degradation of cdk9 by a proteolysis targeting chimera (protac). *Chemical communications (Cambridge, England)*, 53:7577–7580, July 2017.

[156] N.E. Robinson and A.B. Robinson. Prediction of primary structure deamidation rates of asparaginyl and glutaminyl peptides through steric and catalytic effects. *Journal of Peptide Research*, 63(5):437–448, may 2004.

[157] A Rodriguez-Gonzalez, K Cyrus, M Salcius, K Kim, C M Crews, R J Deshaies, and K M Sakamoto. Targeting steroid hormone receptors for ubiquitination and degradation in breast and prostate cancer. *Oncogene*, 27:7201–7211, December 2008.

[158] Jamie Rossjohn, Roberto Cappai, Susanne C Feil, Anna Henry, William J McKinstry, Denise Galatis, Lars Hesse, Gerd Multhaup, Konrad Beyreuther, Colin L Masters, et al. Crystal structure of the n-terminal, growth factor-like domain of alzheimer amyloid precursor protein. *Nature structural biology*, 6(4):327–331, 1999.

[159] Kathleen M. Sakamoto, Kyung B. Kim, Akiko Kumagai, Frank Mercurio, Craig M. Crews, and Raymond J. Deshaies. Protacs: Chimeric molecules that target proteins to the skp1–cullin–f box complex for ubiquitination and degradation. *Proceedings of the National Academy of Sciences*, 98(15):8554–8559, 2001.

[160] Kathleen M Sakamoto, Kyung B Kim, Rati Verma, Andy Ransick, Bernd Stein, Craig M Crews, and Raymond J Deshaies. Development of protacs to target cancer-promoting proteins for ubiquitination and degradation. *Molecular & cellular proteomics : MCP*, 2:1350–1358, December 2003.

[161] Tomo Saric, Claudia I. Graef, and Alfred L. Goldberg. Pathway for degradation of peptides generated by proteasomes. *Journal of Biological Chemistry*, 279(45):46723–46732, aug 2004.

[162] Peter H Schafer, Ying Ye, Lei Wu, Jolanta Kosek, Garth Ringheim, Zhihong Yang, Liangang Liu, Michael Thomas, Maria Palmisano, and Rajesh Chopra. Cereblon modulator iberdomide induces degradation of the transcription factors ikaros and aiolos: immunomodulation in healthy volunteers and relevance to systemic lupus erythematosus. *Annals of the Rheumatic Diseases*, 77(10):1516–1523, 2018.

[163] Matthieu Schapira, Matthew F. Calabrese, Alex N. Bullock, and Craig M. Crews. Targeted protein degradation: expanding the toolbox. *Nature reviews. Drug discovery*, 18:949–963, December 2019.

[164] Gennaro Schettini, Stefano Govoni, Marco Racchi, and Guido Rodriguez. Phosphorylation of app-ctf-aicd domains and interaction with adaptor

proteins: signal transduction and/or transcriptional role–relevance for alzheimer pathology. *Journal of neurochemistry*, 115(6):1299–1308, 2010.

[165] LLC Schrodinger. The pymol molecular graphics system, version 2.2.1, 2018.

[166] Dorothea Schulte and Dirk Geerts. MEIS transcription factors in development and disease. *Development*, 146(16):dev174706, aug 2019.

[167] H Schumacher, RL Smith, and RT Williams. The metabolism of thalidomide: the fate of thalidomide and some of its hydrolysis products in various species. *British journal of pharmacology and chemotherapy*, 25(2):338, 1965.

[168] David C Seldin, Elie B Choufani, Laura M Dember, Janice F Wiesman, John L Berk, Rodney H Falk, Carl O'Hara, Salli Fennessey, Kathleen T Finn, Daniel G Wright, et al. Tolerability and efficacy of thalidomide for the treatment of patients with light chain–associated (al) amyloidosis. *Clinical lymphoma*, 3(4):241–246, 2003.

[169] Dennis J Selkoe. The cell biology of β-amyloid precursor protein and presenilin in alzheimer's disease. *Trends in cell biology*, 8(11):447–453, 1998.

[170] R. Sever and J. S. Brugge. Signal transduction in cancer. *Cold Spring Harbor Perspectives in Medicine*, 5(4):a006098–a006098, apr 2015.

[171] Ganesh M. Shankar, Shaomin Li, Tapan H. Mehta, Amaya Garcia-Munoz, Nina E. Shepardson, Imelda Smith, Francesca M. Brett, Michael A. Farrell, Michael J. Rowan, Cynthia A. Lemere, Ciaran M. Regan, Dominic M. Walsh, Bernardo L. Sabatini, and Dennis J. Selkoe. Amyloid-beta protein dimers isolated directly from alzheimer's brains impair synaptic plasticity and memory. *Nature medicine*, 14:837–842, August 2008.

[172] J. Sheskin. Thalidomide in the treatment of lepra reactions. *Clinical Pharmacology & Therapeutics*, 6(3):303–306, may 1965.

[173] Chengcheng Shi, Huapeng Zhang, Penglei Wang, Kai Wang, Denghui Xu, Haitao Wang, Li Yin, Shuijun Zhang, and Yi Zhang. Protac induced-bet

protein degradation exhibits potent anti-osteosarcoma activity by triggering apoptosis. *Cell death & disease*, 10:815, October 2019.

[174] Yun-Feng Shi, Yue-Qing Tang, Xiao-Wen Sun, Dian-Jun Yu, Bang-Min Han, Yan Hong, and Shu-Jie Xia. [targeted degradation of androgen receptors in androgen-independent prostate cancer cells: an experimental study]. *Zhonghua nan ke xue = National journal of andrology*, 15:1059–1063, December 2009.

[175] Q. L. Sievers, G. Petzold, R. D. Bunker, A. Renneville, M. Slabicki, B. J. Liddicoat, W. Abdulrahman, T. Mikkelsen, B. L. Ebert, and N. H. Thoma. Defining the human c2h2 zinc finger degrome targeted by thalidomide analogs through crbn. *Science*, 362(6414), 2018.

[176] S. Singhal, J. Mehta, R. Desikan, D. Ayers, P. Roberson, P. Eddlemon, N. Munshi, E. Anaissie, C. Wilson, M. Dhodapkar, J. Zeddis, and B. Barlogie. Antitumor activity of thalidomide in refractory multiple myeloma. *N Engl J Med*, 341(21):1565–71, 1999.

[177] Jasper Sluimer and Ben Distel. Regulating the human hect e3 ligases. *Cellular and molecular life sciences : CMLS*, 75:3121–3141, September 2018.

[178] B. E. Smith, S. L. Wang, S. Jaime-Figueroa, A. Harbin, J. Wang, B. D. Hamman, and C. M. Crews. Differential protac substrate specificity dictated by orientation of recruited e3 ligase. *Nat Commun*, 10(1):131, 2019.

[179] R. W. Smithells and C. G. Newman. Recognition of thalidomide defects. *Journal of medical genetics*, 29:716–723, October 1992.

[180] G. F. SOMERS. PHARMACOLOGICAL PROPERTIES OF THALIDOMIDE, a NEW SEDATIVE HYPNOTIC DRUG. *British Journal of Pharmacology and Chemotherapy*, 15(1):111–116, mar 1960.

[181] G. S. Somers. Thalidomide and congenital abnormalities. *Lancet*, 1(7235):912–3, 1962.

[182] Katherine A. Southam, Fiona Stennard, Cassandra Pavez, and David H. Small. Knockout of amyloid β protein precursor (app) expression alters synaptogenesis, neurite branching and axonal morphology of hippocampal neurons. *Neurochemical research*, 44:1346–1355, June 2019.

[183] Donald E. Spratt, Helen Walden, and Gary S. Shaw. Rbr e3 ubiquitin ligases: new structures, new insights, new questions. *The Biochemical journal*, 458:421–437, March 2014.

[184] Wilfred Stein. *Transport and diffusion across cell membranes*. Elsevier, 2012.

[185] Gregory R. Steinberg and Bruce E. Kemp. AMPK in health and disease. *Physiological Reviews*, 89(3):1025–1078, jul 2009.

[186] Christian Steinebach, Hannes Kehm, Stefanie Lindner, Lan Phuong Vu, Simon Koepff, Alvaro Lopez Marmol, Corinna Weiler, Karl G. Wagner, Michaela Reichenzeller, Jan Kroenke, and Michael Guetschow. Protac-mediated crosstalk between e3 ligases. *Chemical Communications*, 55(12):1821–1824, 2019.

[187] Trent D Stephens, Carolyn J.W Bunde, and Bradley J Fillmore. Mechanism of action in thalidomide teratogenesis. *Biochemical Pharmacology*, 59(12):1489–1499, jun 2000.

[188] Ayalew Tefferi, Ruben A Mesa, William J Hogan, Trudy A Shaw, Gayle E Reyes, Jacob B Allred, Cynthia X Ma, Grace K Dy, Alexandra P Wolanskyj, Mark L Litzow, et al. Lenalidomide (cc-5013) treatment for anemia associated with myelofibrosis with myeloid metaplasia., 2005.

[189] S. K. Teo, W. A. Colburn, W. G. Tracewell, K. A. Kook, D. I. Stirling, M. S. Jaworsky, M. A. Scheffler, S. D. Thomas, and O. L. Laskin. Clinical pharmacokinetics of thalidomide. *Clin Pharmacokinet*, 43(5):311–27, 2004.

[190] D. A. Thomas, E. Estey, F. J. Giles, S. Faderl, J. Cortes, M. Keating, S. O'Brien, M. Albitar, and H. Kantarjian. Single agent thalidomide in patients with relapsed or refractory acute myeloid leukaemia. *Br J Haematol*, 123(3):436–41, 2003.

[191] Tanyifor M. Tohnya and II William Figg. Immunomodulation of multiple myeloma. *Cancer Biology & Therapy*, 3(11):1060–1061, nov 2004.

[192] Yaqin Tu, Cai Chen, Junru Pan, Junfa Xu, Zhi-Guang Zhou, and Cong-Yi Wang. The ubiquitin proteasome pathway (upp) in the regulation of cell cycle control and dna damage repair and its implication in tumorigenesis. *International journal of clinical and experimental pathology*, 5:726–738, 2012.

[193] Chiharu Uchida and Masatoshi Kitagawa. Ring-, hect-, and rbr-type e3 ubiquitin ligases: Involvement in human cancer. *Current cancer drug targets*, 16:157–174, 2016.

[194] A. Vagin and A. Teplyakov. Molecular replacement with molrep. *Acta Crystallogr D Biol Crystallogr*, 66(Pt 1):22–5, 2010.

[195] N. Vargesson. Thalidomide-induced limb defects: resolving a 50-year-old puzzle. *Bioessays*, 31(12):1327–36, 2009.

[196] Neil Vargesson. Thalidomide embryopathy: An enigmatic challenge. *ISRN Developmental Biology*, 2013:1–18, 2013.

[197] Neil Vargesson. Thalidomide-induced teratogenesis: History and mechanisms. *Birth Defects Research Part C: Embryo Today: Reviews*, 105(2):140–156, jun 2015.

[198] various authors. Thalidomide shows promising results in patients with multiple myeloma. *Oncology (Williston Park)*, 13(5):744, 1999.

[199] R. Vassar. Beta-secretase cleavage of alzheimer's amyloid precursor protein by the transmembrane aspartic protease BACE. *Science*, 286(5440):735–741, oct 1999.

[200] CE Voorter, Willeke A de Haard-Hoekman, PJ Van Den Oetelaar, Hans Bloemendal, and Wilfried W de Jong. Spontaneous peptide bond cleavage in aging alpha-crystallin through a succinimide intermediate. *Journal of Biological Chemistry*, 263(35):19020–19023, 1988.

[201] Linyan Wang, Qinghuang Tang, Jue Xu, Hua Li, Tianfang Yang, Liwen Li, Ondrej Machon, Tao Hu, and YiPing Chen. The transcriptional regulator MEIS2 sets up the ground state for palatal osteogenesis in mice. *Journal of Biological Chemistry*, 295(16):5449–5460, mar 2020.

[202] Yaya Wang, Diana Argiles-Castillo, Emma I. Kane, Anning Zhou, and Donald E. Spratt. Hect e3 ubiquitin ligases - emerging insights into their biological roles and disease relevance. *Journal of cell science*, 133, April 2020.

[203] Yongcheng Wang and Ya Ha. The x-ray structure of an antiparallel dimer of the human amyloid precursor protein e2 domain. *Molecular Cell*, 15(3):343–353, aug 2004.

[204] Tasaduq H. Wani, Anindita Chakrabarty, Norio Shibata, Hiroshi Yamazaki, F. Peter Guengerich, and Goutam Chowdhury. The dihydroxy metabolite of the teratogen thalidomide causes oxidative dna damage. *Chemical research in toxicology*, 30:1622–1628, August 2017.

[205] Janine Weber, Simona Polo, and Elena Maspero. Hect e3 ligases: A tale with multiple facets. *Frontiers in physiology*, 10:370, 2019.

[206] G. E. Winter, D. L. Buckley, J. Paulk, J. M. Roberts, A. Souza, S. Dhe-Paganon, and J. E. Bradner. Phthalimide conjugation as a strategy for in vivo target protein degradation. *Science*, 348(6241):1376–1381, 2015.

[207] H. Wu, C. Zhao, K. Gu, Y. Jiao, J. Hao, and G. Sun. Thalidomide plus chemotherapy exhibit enhanced efficacy in the clinical treatment of t-cell non-hodgkin's lymphoma: A prospective study of 46 cases. *Mol Clin Oncol*, 2(5):695–700, 2014.

[208] Wang Xin, Ni Xiaohua, Chen Peilin, Chen Xin, Sun Yaqiong, and Wu Qihan. Primary function analysis of human mental retardation related gene CRBN. *Molecular Biology Reports*, 35(2):251–256, mar 2007.

[209] M. Q. Xu and F. B. Perler. The mechanism of protein splicing and its modulation by mutation. *The EMBO journal*, 15:5146–5153, October 1996.

[210] Yan Yan, X. Zhou, H. Xu, and Karsten Melcher. Structure and physiological regulation of AMPK. *International Journal of Molecular Sciences*, 19(11):3534, nov 2018.

[211] Chao-Yie Yang, Chong Qin, Longchuan Bai, and Shaomeng Wang. Small-molecule protac degraders of the bromodomain and extra terminal (bet) proteins—a review. *Drug Discovery Today: Technologies*, 2019.

[212] Wen-Hui Yang, Jun Xu, Jian-Bing Mu, and Jun Xie. Revision of the concept of anti-angiogenesis and its applications in tumor treatment. *Chronic Diseases and Translational Medicine*, 3(1):33–40, mar 2017.

[213] Y. X. Zhu, K. M. Kortuem, and A. K. Stewart. Molecular mechanism of action of immune-modulatory drugs thalidomide, lenalidomide and pomalidomide in multiple myeloma. *Leuk Lymphoma*, 54(4):683–7, 2013.

[214] Yuan Xiao Zhu, Esteban Braggio, Chang-Xin Shi, Laura A. Bruins, Jessica E. Schmidt, Scott Van Wier, Xiu-Bao Chang, Chad C. Bjorklund, Rafael Fonseca, P. Leif Bergsagel, Robert Z. Orlowski, and A. Keith Stewart. Cereblon expression is required for the antimyeloma activity of lenalidomide and pomalidomide. *Blood*, 118(18):4771–4779, nov 2011.

[215] Yuan Xiao Zhu, Chang-Xin Shi, Laura A. Bruins, Xuewei Wang, Daniel L. Riggs, Brooke Porter, Jonathan M. Ahmann, Cecilia Bonolo de Campos, Esteban Braggio, P. Leif Bergsagel, and A. Keith Stewart. Identification of lenalidomide resistance pathways in myeloma and targeted resensitization using cereblon replacement, inhibition of stat3 or targeting of irf4. *Blood cancer journal*, 9:19, February 2019.